PHYSICAL CHEMICAL STUDIES OF (I) A PHOSPHATASE FROM PIG, (II) CYTOCHROME P450 FROM *Pseudomonas putida*, AND (III) ELECTRONIC QUENCHING OF Al AND Ga ATOMS IN RARE GAS MATRICES

By

DAVID CARL SCHLOSNAGLE

A DISSERTATION PRESENTED TO THE GRADUATE COUNCIL OF
THE UNIVERSITY OF FLORIDA
IN PARTIAL FULFILLMENT OF THE REQUIREMENTS OF THE
DEGREE OF DOCTOR OF PHILOSOPHY.

UNIVERSITY OF FLORIDA

1974

To my parents and my wife, Sara

ACKNOWLEDGEMENTS

I would like to thank the following:

Dr. J. H. Ammeter for his assistance on the Al/Ga project.

Dr. F. W. Bazer and Dr. R. M. Roberts for crude allantoic fluid and the invitation to work on the phosphatase.

Dr. J. C. M. Tsibris and Dr. W. Weltner, Jr. for their support and encouragement in this entire undertaking.

The many others who have helped in various ways during the last four years.

TABLE OF CONTENTS

LIST OF TABLES

LIST OF FIGURES

ABBREVIATIONS AND SYMBOLS

A	absorbance
A250	absorbance at 250 nm
AMP	adenosine monophosphate
apoPP	PP without metal cofactor
ATP	adenosine triphosphate
cam	camphor
CD	circular dichroism
ESR	electron spin resonance
x g	times gravity
g_{11}	g parallel
$g_{\perp}$	g perpendicular
Hb	hemoglobin
IR	infrared
Km	Michaelis constant
2-ME	2-mercaptoethanol
Pi	inorganic phosphate
pI	isoelectric point
pMB	p-mercuribenzoate
pNP	p-nitrophenol
pNPP	p-nitrophenylphosphate
PP	progesterone-induced, iron-containing phosphate
PPi	pyrophosphate

SDS	sodium dodecylsulfate
SH	sulfhydryl group
TPTZ	tripyridyl-S-triazine
Δ	crystal field splitting parameter
ζ	spin-orbit coupling constant

Abstract of Dissertation Presented to the Graduate Council of the University of Florida in Partial Fulfillment of the Requirements for the Degree of Doctor of Philosophy

PHYSICAL CHEMICAL STUDIES OF (I) A PHOSPHATASE FROM PIG, (II) CYTOCHROME P450 FROM Pseudomonas putida, AND (III) ELECTRONIC QUENCHING OF Al AND Ga ATOMS IN RARE GAS MATRICES

By

David Carl Schlosnagle

December, 1974

Chairman: William Weltner, Jr.
Major Department: Chemistry

A progesterone-induced, iron-containing protein from the allantoic fluid of pigs has been purified to homogeneity. There was found to be 1 mole of iron per mole of protein. The absorption maximum of the protein (PP) varies from 500 to 550 nm but the molar extinction coefficient (2200) is independent of wavelength. Reducing and oxidizing agents were found to shift the spectrum of PP to higher and lower energy respectively. ESR studies at liquid nitrogen temperatures have indicated that the iron is present as high-spin ferric. Testing for physiological function demonstrated that PP is an acid phosphatase with maximal activity at pH 4.9. Of number of substrates tested, PP was most active toward p-nitrophenylphosphate. The average value of Km was found to be 2.2 mM at 30° and 2.8 mM at 0°. The apparent energy of activation was found to be +11.1 kcal/mole. Under optimum conditions the greatest specific activity obtained was 170 micromoles/min/mg. This corresponds to a turnover number of 5400 molecules of substrate/min/molecule of enzyme. The rate of hydrolysis was found to be greatly inhibited by mercuric ion, fluoride and molybdate. Generally activity was increased

by reducing agents such as 2-mercaptoethanol. The amount of enhancement was variable but could be as much as 2- to 4-fold with no change in Km. The iron could be removed from the protein under reducing conditions with concomitant loss of enzymatic activity; activity could be restored by addition of ferric or cupric ions.

The complexes of nitric oxide with cytochrome P450 and P420 from P. putida were studied by optical and liquid nitrogen electron spin resonance (ESR) spectroscopy. Oxidized P450-NO has an absorption spectrum of a low-spin ferrihemoprotein and no ESR signal. The ESR spectrum of reduced P450-NO indicates a paramagnetic center of rhombic symmetry with g values of 2.08, 2.004 and 1.97. The well-resolved triplet at g = 2.004 with hfs of 20 G. gave rise to a doublet with hfs of 28 G. upon isotopic substitution with ^{15}NO. A difference in the spectra was noted depending upon the presence or absence of substrate camphor. ^{57}Fe-enriched P450 was also studied. The heme group of P420 was found to be weakly bound to the protein. Reduced P420-NO exhibits an axially symmetric ESR spectrum with g values of 2.08 and 2.01.

Aluminum and gallium atoms have been trapped in Ne, Ar, Kr and Xe matrices and studied by optical and ESR spectroscopy at liquid helium temperatures. The results indicate that both metal atoms occupy axially distorted sites in all rare gas lattices. The $^2S \leftarrow ^2P$ electronic transitions are shifted by about +1000 cm^{-1} (in Xe) to about +6000 cm^{-1} (in Ne) relative to the free metal atom values. Increasing the matrix temperature slightly causes a reversible red shift in these transitions. The ESR spectra exhibit axial symmetry and show effects of preferential orientation. While the g values of

the free Group III atoms in their Kramers degenerate $^2P_{1/2}$ ground level are approximately equal to 2/3, the observed g values of matrix-isolated Al and Ga are near free spin, i.e., almost complete quenching of the free atom angular momentum. The dependence of the g values on the matrix and on temperature can be described by a simple crystal field splitting parameter. The splittings of the aluminum and gallium p shells are very similar for both atoms and range from about 1000 to 3000 cm^{-1} and increase from light to heavy rare gas atom.

I. PROPERTIES OF A PROGESTERONE-INDUCED, IRON-CONTAINING PHOSPHATASE FROM THE ALLANTOIC FLUID OF PIGS

Introduction

It has been found that protein levels in the uterine secretions of pigs change both quantitatively and qualitatively during the normal estrous cycle. There is a slow increase in protein concentration during the first 9 days after estrous followed by a rapid change after day 10.[1] After reaching a maximum of 50 mg per gilt on day 15, the values decrease markedly. This decline occurs at a time when the corpora lutea regress and progesterone levels in plasma fall. Two new protein fractions isolated via Sephadex G-200 chromatography were not present before day 9 or after day 16 of the normal cycle. These were called Fractions IV and V, the latter having at least six components with an estimated average molecular weight of 20,000 as shown by polyacrylamide gel electrophoresis.

Fraction IV has a characteristic purple color and a somewhat higher molecular weight than the proteins of Fraction V.[2] It could be resolved into a single band which moved toward the cathode at pH 8.0 on gel electrophoresis, indicating that the protein is basic. Treatment with periodic acid - Schiff stain for carbohydrates gave a positive reaction, showing that Fraction V is a glycoprotein.

Gilts were ovariectomized on day 4 after onset of estrous and administered progesterone (12.2 mg/kg) and estrogen (1.1 µg/kg)

daily until day 15 at which stage the uterine lumen was flushed with 0.33 M sodium chloride.[2] The yield of total protein was twice that obtained from gilts given only progesterone and nearly four times that of untreated animals. In each set of experiments, the basic purple protein was found. By contrast, ovariectomized control gilts produced only small amounts of protein and no protein containing a net basic charge at pH 7.0. The purple protein was not found in the serum of pigs in any of the above experimental groups. Thus the purple protein appears to be progesterone-induced.

Properties

PP was purified from uterine flushings via ion-exchange and gel filtration chromatography.[2] Isoelectric focusing experiments gave a pI of around 9.7. SDS gel electrophoresis and equilibrium ultracentrifugation gave a molecular weight of 32,000. Amino acid analysis, Table I-1, showed a high content of basic amino acids as expected from the very basic nature of the protein. Ten half-cystine residues were found via treatment with performic acid, but the oxidation states of these were not determined. Four neutral sugars were identified by gas-liquid chromatography: fucose, mannose, glucose and galactose in a ratio of 2:5:4:4. Sialic acid could not be detected. The protein was found to contain eight moles of glucosamine and one mole of galactosamine per mole protein. Thus, each molecule of PP contains fifteen residues of neutral sugar and nine residues of amino sugar. On this basis, the total carbohydrate content would be about 12% by weight.

Partially purified protein was subjected to arc emission analysis[3] which indicated the presence of iron, about a tenth as much copper and

Table I-1. Amino acid analysis of purified Fraction IV protein from pig uterus.[a]

	moles/mg protein	Residues/32,000 mol wt[b]
Lysine	0.58	19
Histidine	0.27	9
Arginine	0.39	13
Aspartic acid	0.70	23
Threonine	0.46	15
Serine	0.47	15
Glutamic acid	0.56	19
Proline	0.37	12
Glycine	0.58	19
Alanine	0.58	19
Cysteine[c]	0.30	10
Valine	0.43	14
Methionine[c]	0.12	4
Isoleucine	0.28	9
Leucine	0.64	21
Tyrosine	0.17	6
Phenylalanine	0.39	13
Tryptophan	0.23	8
Glucosamine	0.24	8
Galactosamine	0.03	1

[a] From Ref. 2

[b] Calculated to the nearest whole number.

[c] Results of analyses on performic acid-oxidized protein.

a trace of zinc. No manganese was found. The uterine protein had an absorption maximum at 545 nm and the color was stable to prolonged dialysis against EDTA. The allantoic fluid from pregnant animals also contained the purple basic glycoprotein having the same molecular weight as the uterine protein as determined by electrophoresis.

A female lamb was immunized by injection with the purple uterine protein and the presence of antibody was verified in the serum.[2] The basic protein from allantoic fluid was found to be immunologically identical to the uterine protein. The antiserum (anti-IV) did not cross react with any of the acidic proteins obtained from the uterine flushings nor with extracts from tissues of the following organs: heart, lung, stomach, intestine, liver, spleen, kidney and oviduct tissue. Further, no reaction occurred with the serum of a pig obtained on day 15 of estrous. Sheep anti-IV was administered to gilts several times early in pregnancy and the embryos and placentae later were examined.[4] There was a significant reduction in placental and fetal crown-rump length. Between days 8 and 16 of gestation, when the purple protein is present in large amounts, rapid elongation of the blastocyst occurs. It is during this period that the major portion of embryonic deaths occur.[5]

Only two other progesterone-induced proteins have been purified to homogeneity: avidin from chick[6] and blastokinin from rabbit.[7] The purple glycoprotein from pig (PP) has been found in both the uterine flushings and the allantoic fluid, but in no other tissue. Further, this protein appears to be necessary to the growth and development of the fetus. This work was undertaken to determine the biological function of this purple protein and study the role of the iron.

Materials and Methods

Purification from Allantoic Fluid

Brown allantoic fluid from day 45 was received after having been passed through a Millipore filter to remove bacteria. The following purification was carried out in the cold. The crude solution was dialyzed against 10 mM sodium acetate for 6 hours with two changes. The dialyzed fluid was centrifuged for 30 minutes at 27,000 x g and the pellets discarded. A column (1 x 12 cm) of CM-cellulose was prepared using Whatman CM 52 treated according to manufacturer's instructions. The column was washed with several volumes of 10 mM sodium acetate and the allantoic fluid was added. Proteins having a net positive charge at pH 7.5 will be retarded by this column. The effluent was light yellow-brown and was later lyophylized and stored at $-20^{o}C$. The CM column soon took on color, as a brown protein present began to accumulate on the resin.

After the last of the allantoic solution was added, the column was washed with 2 volumes of 10 mM sodium acetate followed by 0.1 M and 0.2 M acetate which eluted the brown protein. The visible absorption spectrum was taken of an aliquot of this fraction and was found to be typical of hemoproteins with alpha, beta and Soret bands. No attempt was made at identification. At one point a narrow single band of pink-orange coloration was seen moving down the column nearly free of any other visible bands. The optical spectrum of this fraction resembled the reduced form of cytochrome c. 1 M sodium acetate was used to elute the violet-colored band still remaining on the column. An aliquot of this fraction was scanned in the visible region and found to have a

broad absorption at 505 nm, a weak peak from contaminating hemoprotein and a shoulder around 320 nm. Part of the more dilute violet fractions were lyophilized and stored at -20^{o} for later use. The remaining fractions were pooled and concentrated via vacuum dialysis.

Half of this protein solution was placed on a room-temperature column (2 x 100 cm) of Sephadex G-100, previously prepared and equilibrated with 0.1 M sodium acetate. The Sephadex beads serve to separate molecules according to size. The transmission at 280 nm was continuously and automatically monitored. The second aliquot of the purple protein was passed through the same Sephadex G-100 column, this time equilibrated with 0.1 M (Na^{+}, H^{+}) acetate buffer, pH 4.8. The two elution patterns are shown in Figure I-1. In the first case, there are three bands, two of which are colored. The first fraction is pink and the second purple with absorption maxima of 505 nm and 535 nm respectively. In the second fractionation, only one colored band was obtained. The leading shoulder on this band was from an impurity. SDS polyacrylamide gel electrophoresis was used to determine purity.

Protein Concentration

Protein concentration was determined by a number of ways. Pure PP could be quantitated by optical absorption where an optical density of 1.0 at 280 nm corresponds to 1.0 mg protein/ml. A molar extinction coefficient of 2200 at 550 nm was also used to calculate PP concentration.

Two common analytical procedures in use are the Lowry[8] and the biuret methods. The Lowry is at least twenty times more sensitive than the biuret, but suffers from non-linearity at higher protein concentrations. A good relationship was found between PP dry weight and the Lowry method. The biuret method is quicker but requires more protein.

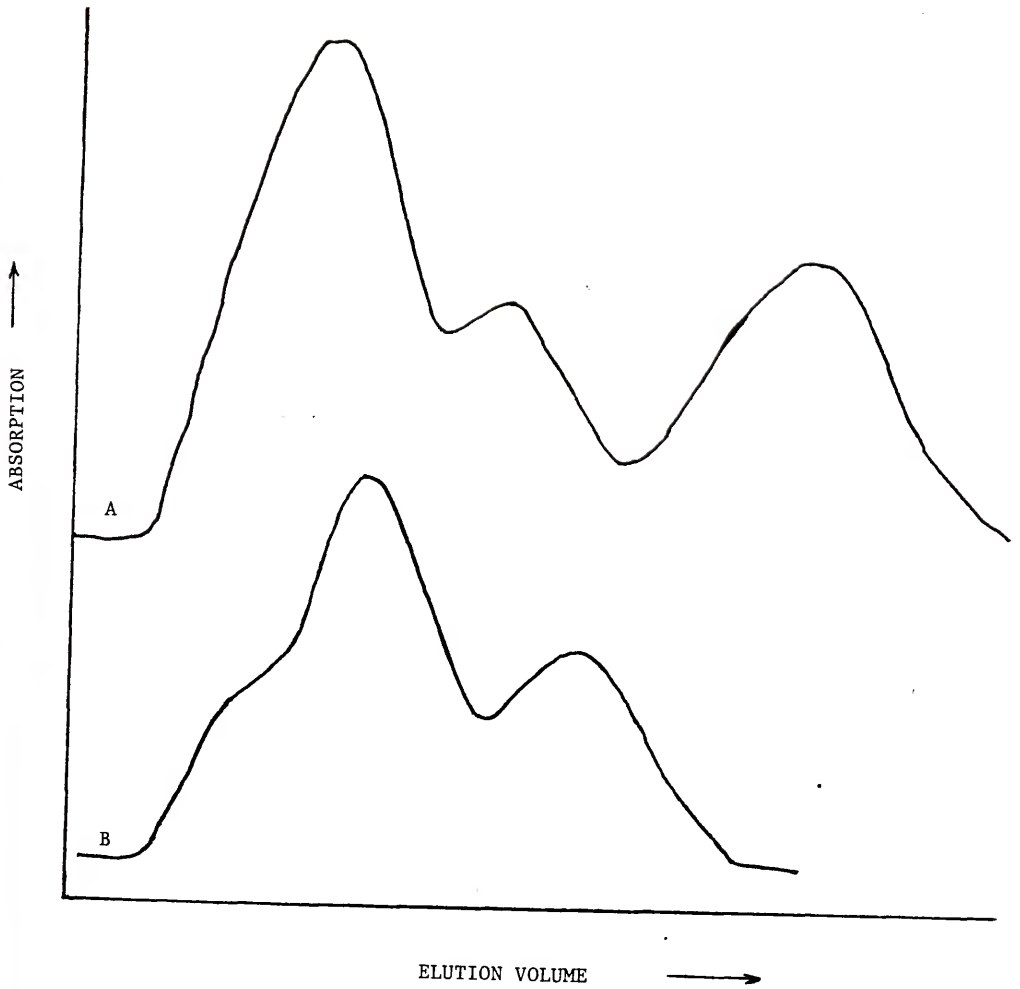

Figure I-1. Elution pattern of CM-cellulose positive proteins. The proteins were fractionated via Sephadex G-100 chromatography (see text). A: The column was equilibrated with 0.1 M NaAc at pH 7.5. The first band is pink, the second purple. B: The column was equilibrated with 0.1 M acetate pH 4.8. The first main band is of violet coloration. The two patterns are not on the same abscissa.

Lowry method

The Lowry reagents are prepared as follows:

A. 2% Na_2CO_3 in 0.10 N NaOH

B. 0.5% $CuSO_4 \cdot 5H_2O$ in 1% tartrate

C. 50 ml A plus 1 ml B (good one day only)

D. 1 N Folin - Ciocalteu reagent (from Sigma)

Procedure: To 0.2 ml of each protein sample (0.05 to 0.5 mg/ml) add 1 ml of reagent C and let stand 10 minutes. Then add 0.10 ml reagent D with rapid mixing and allow to develop for 60 minutes. Read absorbance at 750 nm. Bovine serum albumin was used to prepare the standard curve.

Biuret method

The biuret solutions are prepared as follows. Reagent A contains 1.5 g $CuSO_4 \cdot 5H_2O$ and 6.0 g solution potassium tartrate in a final volume of 0.50 l. Reagent B is 10% carbonate free sodium hydroxide. The biuret reagent was prepared prior to use by mixing equal volumes of A and B. The unknown protein solution (1 to 10 mg/ml) is added to the biuret solution in a volume ratio of 1:5. The absorbance at 540 nm is recorded after 15 minutes. Bovine serum albumin was used as the standard.

Iron Determination

The method below is that described for nonheme iron in serum using tripyridyl-S-triazine (TPTZ) as the chromogen.[9]

To 0.5 ml of protein add 0.5 ml 1 N HCl and allow 10 minutes for the iron to be split off. Add 0.5 ml of 10% TCA to precipitate the protein. Centrifuge at 2500 x g for 15 minutes, then remove 1.0 ml of protein-free

supernatant. Add 0.5 ml of a freshly prepared mixture of 50% ammonium acetate, 10% hydroxylammonium chloride and 0.004 M TPTZ in a volume ratio of 2:1:1. After 10 minutes record the absorbance at 593 nm. Ferrous ammonium sulfate was used as standard. All glassware was soaked in 1 N HCl overnite and rinsed in deionized or glass-distilled water and dried prior to use.

Spectroscopy

All UV visible absorption spectra and O.D. measurements were taken on a Beckman Acta C III double beam instrument with digital readout. The recorder scale was variable in increments of 0 to 0.1, 0 to 1, 0 to 2 and 0 to 3 O.D. units. Thunberg-type cuvettes were used for anaerobic studies.

Electron spin resonance spectra were obtained using Varian E3 and E9 spectrometers which operate at X-band. 100 kHz modulation was used in both cases. Spectra at 77^{o} K were obtained by means of a Scanlon dewar insert or with a Heli-Tran variable temperature accessory. In the latter case, the temperature was monitored using a chromel vs. gold (with 0.07 atom % iron) thermocouple. The microwave frequency was calibrated by insertion of a quartz capillary containing solid DPPH ($g = 2.0037$).[10]

Circular dichroism measurements were made with a Jasco CD/ORD 20. The instrument was calibrated with 10-camphorsulfonic acid prior to use.[11]

Measurement of Phosphatase Activity

Phosphatase activity was determined by two methods: either by measurement of inorganic phosphate or, when p-nitrophenyl phosphate (pNPP) was used as substrate, measurement of p-nitrophenol (pNP) as the nitrophenylate ion. Controls containing no enzyme were employed with every series of trials. The specific activity of an enzyme is expressed as micromoles of product formed per minute per mg protein added under the conditions of the assay. Eppendorf pipettes, used in the addition of microliter volumes, were calibrated with distilled water at 22^{o}.

Inorganic phosphate determination

This method[12] is a modification of the Fiske-SubbaRow assay.[13] Reagent A consists of 1% Elon (Kodak) and 3% sodium bisulfite. Reagent B is prepared by diluting 272 ml concentrated sulfuric acid to 700 ml with deionized water and the solution allowed to cool. 50 g of ammonium molybdate are added to 100 ml deionized water. These are then mixed and diluted to a final volume of 2000 ml.

After suitable incubation of substrate with enzyme, the reaction is stopped by addition of reagent B. Reagent A is then added and the absorbance at 660 nm recorded after 15 minutes. The volume ratio of reaction mixture:reagent A:reagent B is 8:1:1. It has been reported that adenosine phosphates and pyrophosphates interfere with the assay by the formation of a colorless complex with the molybdate.[14] A 4-fold excess of molybdate over substrate insures normal color development. K_2HPO_4 was used as the standard.

p-Nitrophenylate ion determination.

The enzyme will cleave pNPP into inorganic phosphate (Pi) and p-nitrophenol. The anion formed upon ionization of the phenolic proton absorbs around 410 nm, whereas neither pNPP nor pNP absorbs appreciably above 400 nm.[15] Thus the amount of product can be easily determined spectrophotometrically.

Continuous assay. The initial assays were carried out at room temperature in 0.1 M ammonium acetate, pH 6.0, 12 mM in pNPP. Enzyme is added to an optical cuvette containing the buffered substrate solution, the contents mixed and the absorbance at 405 nm is followed vs. time using the chart drive of the Acta. pNP in buffer was used as standard. The linear portion of the trace was used in calculating the initial reaction velocity.

Discontinuous assay. The reaction is carried out under the desired conditions and stopped by addition of 0.25 N KOH. pNP liberated is determined using a molar extinction coefficient of 16,200 at 410 nm.[15]

In the early assays, the data were accumulated as the average of six trials since there was a considerable fluctuation in successive determinations. Better consistency was obtained with 0.1 M sodium chloride present. The best results were achieved using silanized test tubes, with which replication of assays was within 5% of the average value. The test tubes were first washed thoroughly and dried. They are then immersed for about one minute in a solution of 1% dimethyl diclorosilane in benzene at 55°. The hydrophobic layer formed on the surface of the test tube apparently prevents the basic protein from absorbing onto the glass.

Sulfhydryl Titration

Sulfhydryl groups will react with a number of metals to form mercaptides. Divalent mercury has two sites open to coordination, thus only monomercaptides are formed when the mercury is covalently bound to an organic residue. One such organometallic is p-mercuribenzoate (pMB) which gives rise to an ultraviolet spectral shift upon mercaptide formation. The change is greatest around 250 nm where there is an increase of absorption. The nature of this reaction has been discussed by Boyer.[16]

The method used was that of Riordan and Vallee.[17] About 0.08 mM pMB is prepared by dissolving in a slight excess of alkali, diluting to approximate concentration with desired buffer and centrifuging to remove precipitate. One ml of this solution is added to one of a pair of matched optical cuvettes; the other cuvette contains 1.00 ml buffer only. Ten microliters (2-3 nanomoles) of PP are added to both reference and sample cuvette. Therefore, any contribution of the protein to the UV absorbance is blanked out with the double beam spectrometer. The contents are mixed and the increase in absorbance due to mercaptide formation is followed at 250 nm. When the O.D. no longer changes, the absorbance is recorded and another aliquot of protein added. All the pMB has reacted when the absorbance no longer increases. A plot of A250 against nanomoles of PP added will show two straight lines, the intersection of which gives the stoichiometry of the reaction. The concentration of pMB can be standardized either by using a molar extinction coefficient of 16,200[16] at 233 nm, pH 7.0, or by titration with a solution of reduced glutathione, a small molecule containing a single thiol group. These methods agreed to within about 5%.

Gel Electrophoresis

Electrophoresis was carried out at pH 4.5 using β-alanine buffer as described by Reisfeld et al.[18] A current of 6 to 8 mA per tube was run for 30 minutes with the anode at the top. Gels were stained for protein using 0.125% (w/v) Coomassie blue in 10% (v/v) acetic acid and 40% (v/v) ethanol.

Results and Discussion

Chemical and Physical Properties

Iron content

Based on the iron determination of PP from different pigs at different stages, there is 1.0 ($\pm$ 0.1) mole of iron per 32,000 molecular weight.

Absorption spectra

PP can be obtained in various forms which absorb between 500 nm (the pink form) and 550 nm (the purple form). The optical spectrum of the purple species, shown in Figure I-2, also has a shoulder at 320 nm and peaks at 280 nm and 215 nm (not shown). The absorption at 280 nm is due to the aromatic amino acids tryptophan, tyrosine and phenylalanine which are present in a ratio of 8:6:13. This band at 280 nm strongly resembles that of tryptophan as this amino acid absorbs much more strongly than the other two.[19] The absorption in the far UV is due to transitions of the peptide bond.[20] The spectrum of the pink form is similar to that of the purple except for the shift of the visible absorption maxima to higher energy. Also the 320 nm shoulder is either absent or hidden under the 280 nm peak as it is no longer distinguishable. One can find a correlation between the color of the protein and intensity of the 320 nm shoulder; the more purple the color, the stronger the 320 nm absorption

Figure I-2. Optical absorption spectra of PP. The intensity of trace A has been increased 10-fold and that of trace B 2-fold compared to that of trace C. The concentration of PP is 45 μM in 0.1 M acetate at pH 4.9.

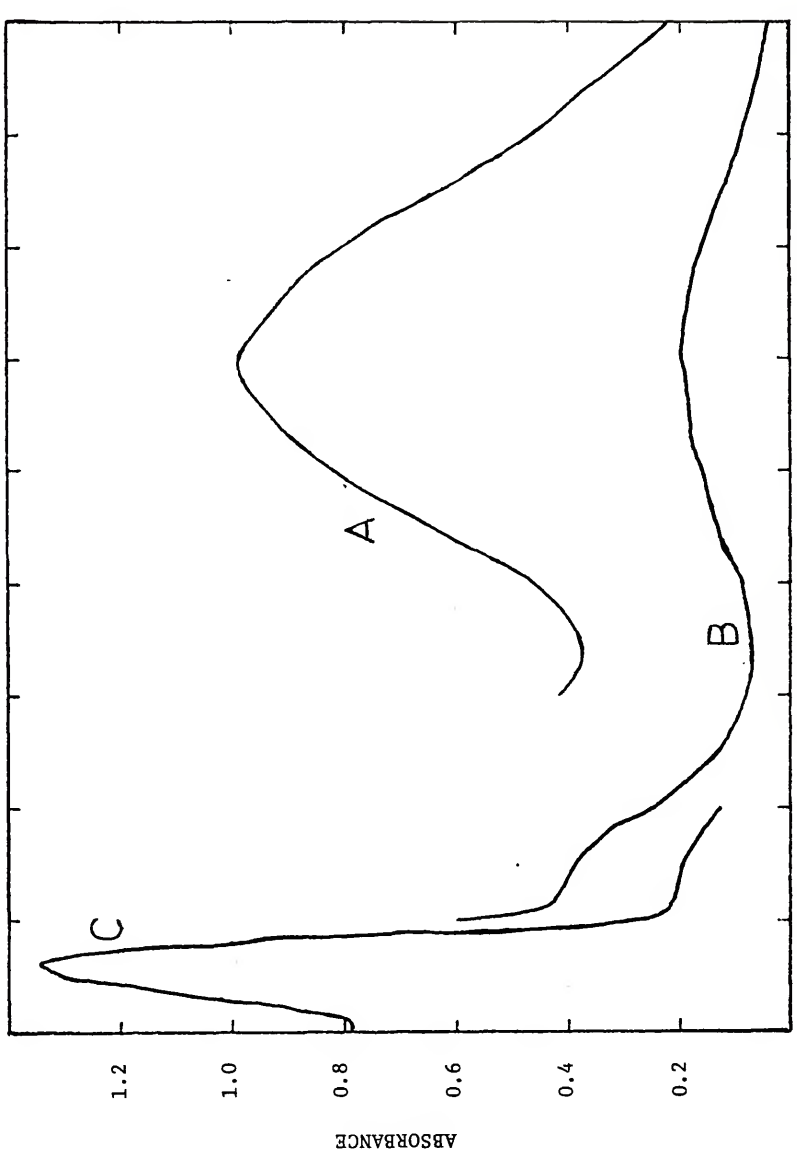
ABSORBANCE
1.2
1.0
0.8
0.6
0.4
0.2
300
400
500
600
700
λ (nm)
A
B
C

and vice versa. A mixture of the pink and purple species will have a visible absorption maximum between the two noted extremes.

The molar extinction coefficient at 550 nm for the purple form was calculated to be 2200 based on iron content. The absorbance of 1.0 O.D. at 280 nm is indicative of 1.0 mg protein per ml as determined both by the biuret method and by the Lowry method. This gives a theoretical ratio of A280/A550 of 14. Approximate purity of protein preparations could be readily determined from this ratio.

As the pink form was eluted from the Sephadex column with an apparent molecular weight greater than that of the purple, it was thought that perhaps the former was a dimer. A change in protein conformation upon going from monomer to dimer could influence the environment about the iron atom which would explain the shift in the visible region of the spectrum. Since this protein is rich in sulfhdryl groups, dimerization could be due to the formation of intermolecular disulfide bonds. These would be broken by sulfhydryls. 0.1 M 2-ME however, had no effect on the visible spectrum of the pink form. On the other hand, 2-ME caused the color of the purple form to change to pink within about ten minutes. Cysteine and ascorbic acid had the same effect, whether by direct addition or by dialysis and subsequent removal. The spectrum of the nascent pink was the same as the naturally occurring species. The addition of low concentrations of dithionite, a powerful reducing agent, also caused the same spectral shift but with gradual loss of visible absorption. At higher concentrations, dithionite caused immediate loss of color. Prolonged exposure to 2-ME or ascorbate also has this bleaching effect. Fractions of the pink form could be made purple by oxidizing agents, either within a few minutes by addition of 1 mM hydrogen peroxide (Figure I-3) or more slowly by dialysis against ferricyanide.

Figure I-3. Effect of H_2O_2 on the optical spectrum of the pink form of PP. Solid line: 1.0 ml of PP as isolated after dialysis against 0.1 M acetate at pH 4.8; dotted line: same sample scanned 2 minutes after the addition of 0.1 ml of 8.8 mM oxidant. As mentioned in the text, reducing agents shifted the spectrum of the purple form of PP to higher energy.

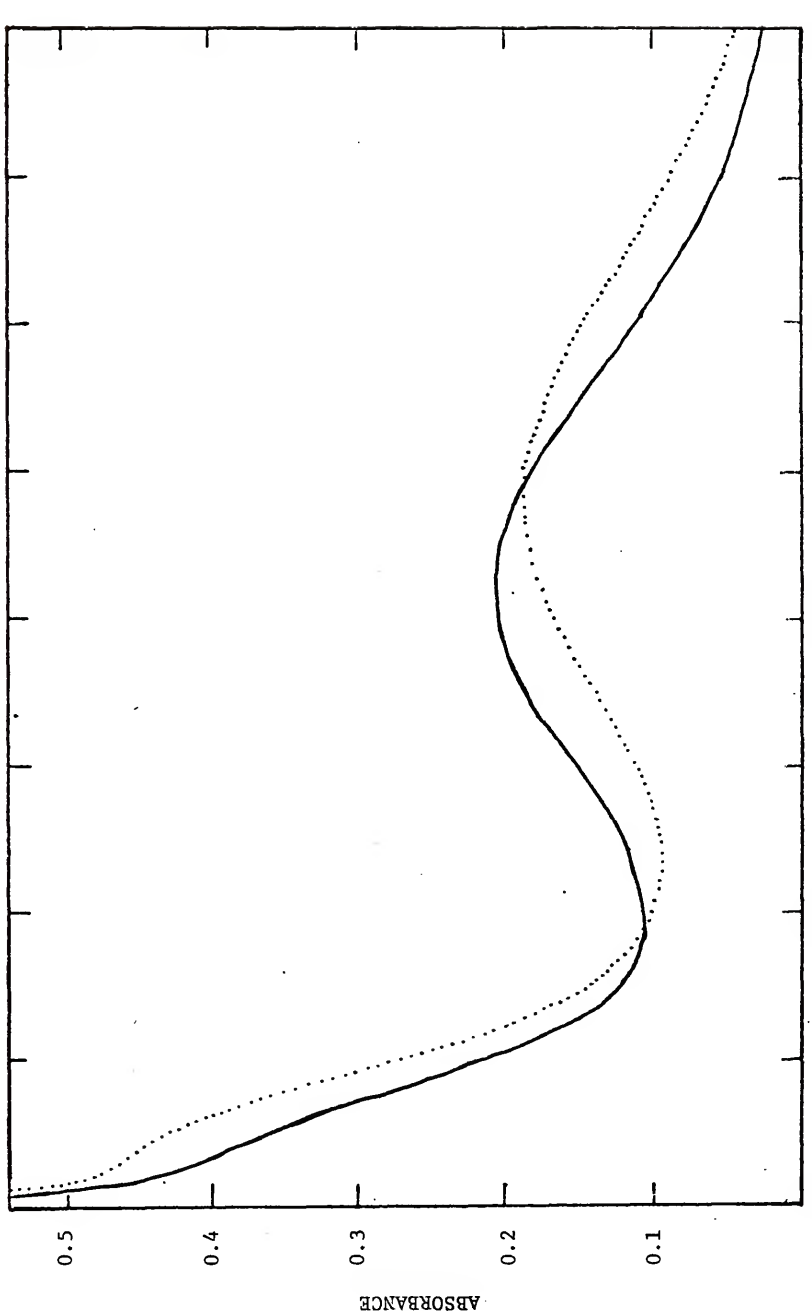
ABSORBANCE
0.5
0.4
0.3
0.2
0.1
300
400
500
600
700
λ (nm)

Optical activity

The rotation of the plane of polarized light and the unequal absorption of right- and left-circularly polarized components, that is, optical activity, is a property of a molecule that is not superimposable on its mirror image.[21] Such molecules are referred to as dissymmetric and can have no axis of improper symmetry. Commonly, dissymmetric molecules have no symmetry at all or belong to point groups having only proper rotation such as C_n or D_n. These molecules have the property of possessing different molar absorbancies and refractive indices for circularly right- and left-polarized light.

A beam of plane polarized light can be regarded as two beams of right- and left-circularly polarized light rotating in phase with equal amplitudes. A circularly polarized beam is one in which the electric vector rotates through 2π in a direction perpendicular to the direction of propagation. The resultant electric vector is the sum of the right and left rotating electric vectors and appears to be confined to a plane when viewed along the direction of propagation and traces out a sine wave when viewed perpendicular to the direction of propagation. When plane-polarized light passes through an optically active sample, the difference in the refractive index causes a retardation of one of the electric vectors and the difference in molar absorbancy causes a difference in vector amplitude. The vector sum will trace out an ellipse. Θ may be defined as the angle whose tangent is the ratio of the minor to major axis of the ellipse. Θ is directly proportional to the difference in molar extinction coefficients between right and left polarized light, i.e., $(E_l - E_r) = \Delta E$. The observed ellipticity can be converted to the molar ellipticity by

$$\Theta M = (100 \cdot \Theta obs)/(1 \cdot C)$$

where l is pathlength of light through the sample and C is the molar concentration of sample. The units of ΘM are $(deg \cdot cm^2)/dmol$. The unequal absorption and unequal velocity of transmission of right- and left-circularly polarized light is called the Cotton effect.

The circular dichroism spectrum of PP is shown in Figure I-4, where protein concentrations of 0.367 mM and 0.045 mM in 1 cm pathlength cells were used in the visible and ultraviolet regions respectively. The sample of enzyme used had an absorption maximum at 545 nm whereas the maximum molar ellipticity occurred at 520 nm and was calculated to be 5700 $(deg \cdot cm^2)/dmol$. The positive peak around 275 nm is due to the aromatic amino acids. The sharp negative peak at 294 nm and positive peak at 289 nm is probably due to tryptophan; studies with model tryptophanyl compounds have shown this to be the region where C.D. maxima occur.[22] In addition, there are bands of both positive and negative ellipticity in the near ultraviolet region. The ellipticity in this region is not due to the aromatic amino acids as tyrosine and phenylalanine do not contribute above 300 nm and tryptophan can generate ellipticity only up to 320 nm.[23] The ellipticity of the peaks are of the same magnitude as found for a number of disulfide bonds.[23] The position and intensity of the UV absorption depends upon the dihedral angle of the disulfide group. However, molecules containing disulfide bonds which absorb above 300 nm have extinction coefficient about ten times less than that which can be approximated for the 320 nm shoulder of PP.[24,25]

ESR spectra

The ESR spectrum of PP at pH 5, taken near 77^{o} K, is shown in Figure I-5. Seen are two prominant absorptions at about g = 4.3 and g = 2.0. The point of zero derivative in the low field peak corresponds

Figure I-4. Circular dichroism spectrum of PP. The protein was buffered in citrate-phosphate at pH 7. Visible region: 0.367 mM PP, right-hand ordinate; ultraviolet region: 0.045 mM PP, left-hand ordinate. A 1 cm pathlength cell was used in both cases; the baseline was taken using buffer only.

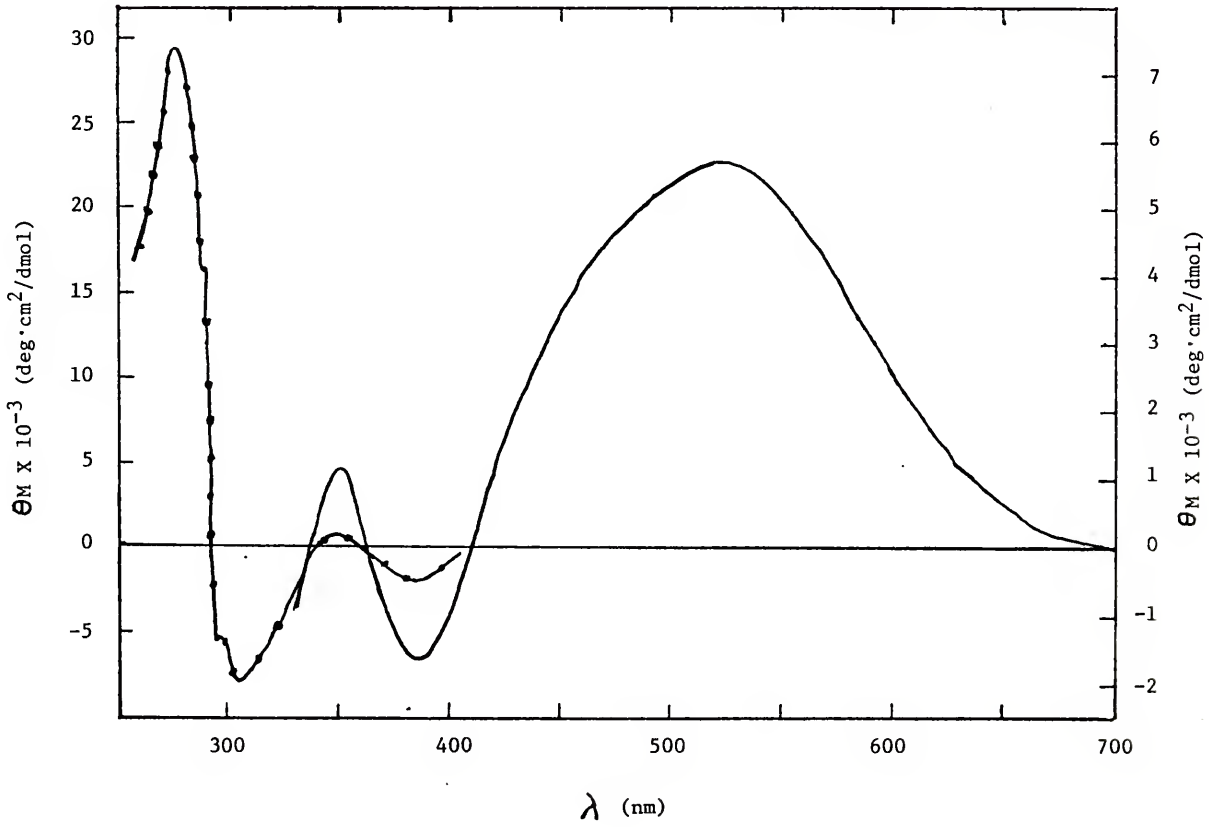
30
25
20
15
10
5
0
-5
θM X 10−3 (deg·cm2/dmol)
7
6
5
4
3
2
1
0
-1
-2
θM X 10−3 (deg·cm2/dmol)
300
400
500
600
700
λ (nm)

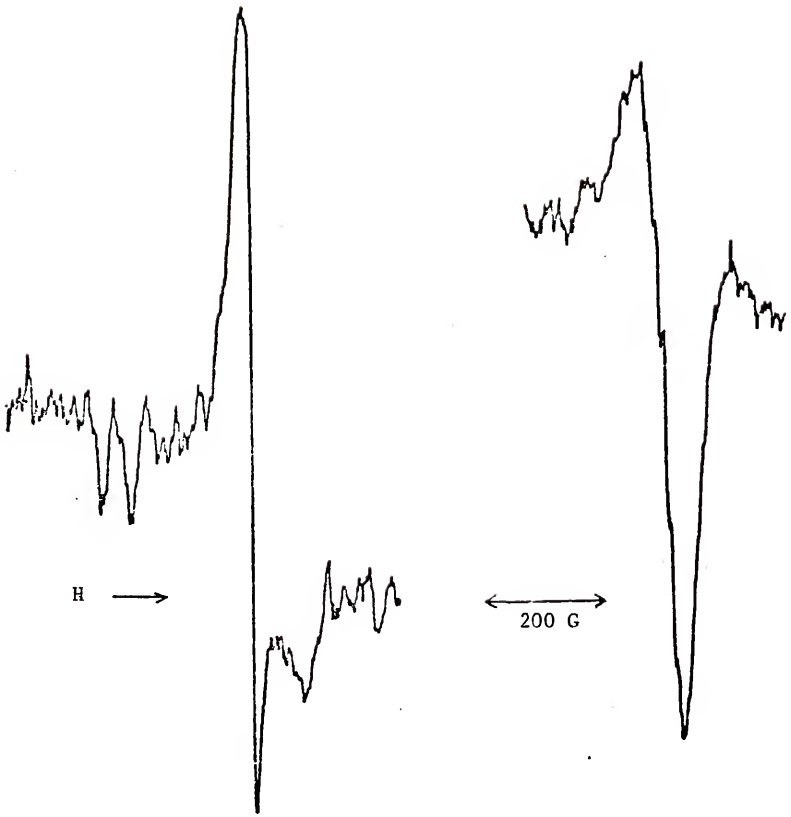

Figure I-5. Liquid nitrogen ESR spectrum of PP in acetate, buffered, pH 4.9. The low field peak is at g = 4.3; the high field peak is at g = 2.05. The microwave power was set at 25 mWatts and the modulation amplitude at 5 G.

to g = 4.29. There is a low field shoulder and a peak to higher field at g = 4.04. Thus there appear to be three transitions in this region. Figure I-6 shows this in expanded scan.

The signal at g = 2.05 is shown expanded in Figure I-7. Clearly resolved are at least 6 hyperfine lines with splitting of 15 gauss. The sample of PP used for this ESR experiment was then dialyzed for 11 hours at 4^{o} against 0.01 M bipyridine at pH 5 in acetate buffer, followed by dialysis for 26 hours and 3 changes which removed the chelating agent. ESR spectra were taken using the same quartz sample tube. The signal at g = 2 was found to be decreased in intensity by about 50% relative to the g = 4.3 peak. A standard sample of 0.1 mM $CuCl_2$ was prepared in 1.0 mM EDTA and 0.1 M acetate, pH 5.[26] The ESR signal intensity around g = 2 was at least ten times stronger than the g = 2 signal from the protein. The ratio of the g = 2 peak to the g = 4.3 peak was found to vary in different preparations of PP.

A third signal, having a peak-to-peak separation of about 120 gauss was found around g = 11. The intensity of this varied with respect to the g = 4.3 signal, depending upon the preparation of protein. This signal was not identified. The signals at g = 4.3 and g = 2.0 which were assigned to Fe^{+3} and Cu^{+2} respectively, will be discussed later in this chapter.

Sulfhydryl titration

The abundance of half-cystine residues in the protein indicates a strong possibility of PP being an iron-sulfur protein,[27,28] although the visible spectrum is not similar to the rubredoxins, wherein the sulfur atoms of four cysteine residues are coordinated about the iron in a distorted tetrahedron. Addition of mercurial to rubredoxin leads to a loss of visible spectrum.[27]

Figure I-6. ESR of PP at 77°K. The spectrum is indicative of high-spin ferric iron. Conditions are as in Figure I-5.

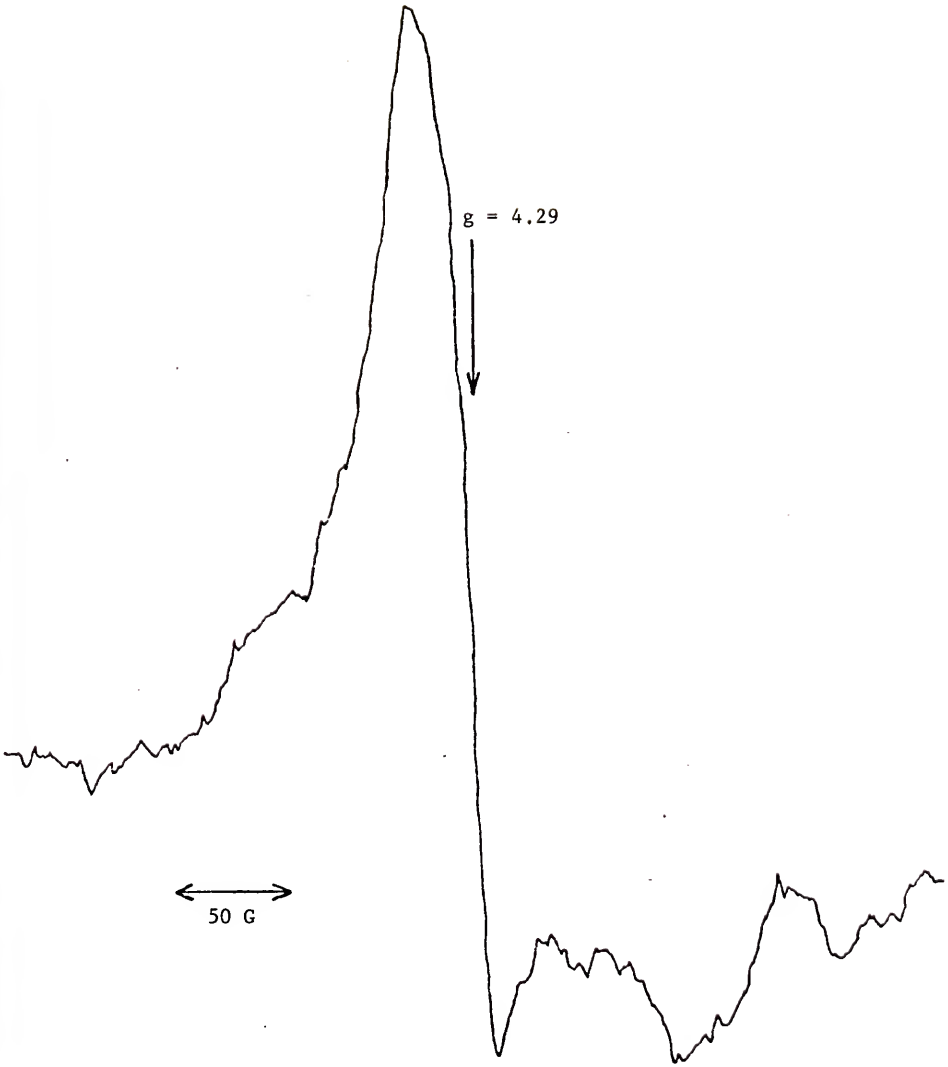
g = 4.29
50 G

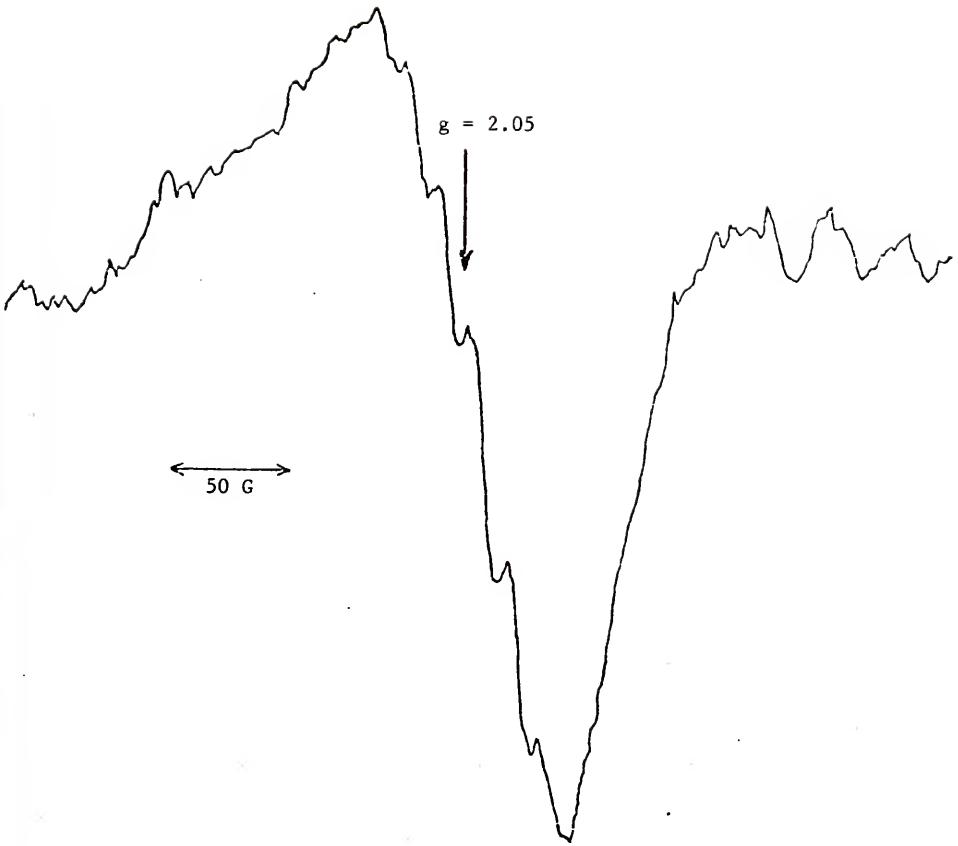

Figure I-7. ESR of PP at 77°K. This signal was assigned to the cupric ion. The 6 hyperfine lines are split by 15 G. Conditions are as in Figure I-5.

Titration of PP with a sulfhydryl reagent could possibly give information as to the ligands of the iron atom in PP. p-mercuribenzoate was selected as it is known to be a specific, reversible sulfhydryl reagent.[17] The reaction can be quantitated spectrally by the use of difference spectroscopy.

pMB at 0.08 mM was found to react very slowly with PP at pH 7, and the number of reacting groups could not be determined. However, when the protein was preincubated for 30 to 90 minutes in 1 M guanidine hydrochloride, a denaturing agent, the titration showed 9 ($\pm$ 1) reacting sulfhydryl groups of the 10 found by amino acid analysis (see Fig. I-8). The visible spectrum of guanidine treated PP was found not to greatly change; the spectrum remained unchanged when a stoichiometric amount of pMB was added. From this evidence it seems certain that the iron is not completely coordinated by sulfurs. From the difference in reactivity of pMB toward the untreated and guanidine treated PP, it appears as though most of the sulfhydryls are buried within the three-dimensional structure of the protein. Away from the surface of the molecule, these sulfhydryl groups would be somewhat protected from oxidation and the possible formation of inter-molecular disulfide bonds.

Enzymatic Properties

Because it has been reported that phosphatase activity increases in the early pregnant uterus,[29,30] crude uterine and allantoic fluids were tested for the ability to hydrolyze pNPP. No activity was found in tris-buffer at pH 8.2, but there was indeed phosphatase activity at pH 6.0 in ammonium acetate. Testing the basic proteins showed activity in the purple fractions but not in the eluent corresponding to Fraction V. Samples of PP

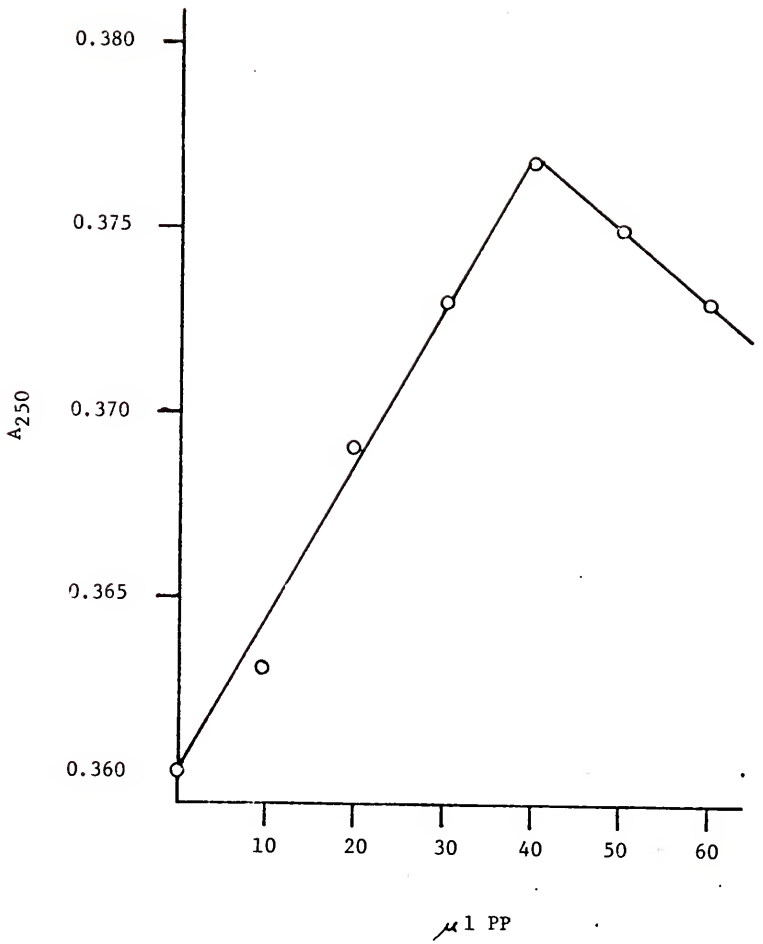

Figure I-8. Sulfhydryl titration. Aliquots of guanidine-treated PP (at 216 μM) were added to 1.00 ml of 78.0 μM pMB as described in the methods section. The absorbance at 250 nm at pH 7 was recorded against PP added. The curve indicates a stoichiometry of 9 (± 1) reacting sulfhydryl groups on the protein.

having the highest purity as determined by gel electrophoresis were found to have the greatest activity. The effect of the concentration of PP on the rate of hydrolysis at pH 6.0 is shown in Figure I-9, and indicates a linear relationship. This experiment was later repeated at 30^{o}, pH 4.9. The initial rate of reaction increased linearly over a 10-fold PP concentration range.

Effect of ionic strength

The effect of ionic strength on the rate of reaction at pH 6.0 was studied using sodium chloride and potassium chloride. The concentrations of these salts in the reaction mixture were varied from 0 M to 2 M. The results are shown in Figure I-10. Increasing salt concentration decreases enzyme activity whereas some phosphatases have been found to be unaffected or stimulated by salts. Also, certain phosphatases have been found to be specifically affected by either Na^{+} or K^{+}; this is not the case with PP.

pH profile

PP functions as an acid rather than an alkaline phosphatase. However, it was desirable to know more accurately the pH at which maximum activity occurs. 30^{o} was selected as the temperature at which to run the reaction with 12 mM pNPP. The following were used to prepare buffers of 0.1 M concentration: citrate, acetate, maleate and imidazole. The pH range examined was from 3 to 8. 5 minutes after enzyme was added to the reaction mixture at 30^{o}, KOH was added and the pNP liberated was determined. Figure I-11 shows the pH optimum to be at 4.9 in 0.1 M acetate buffer.

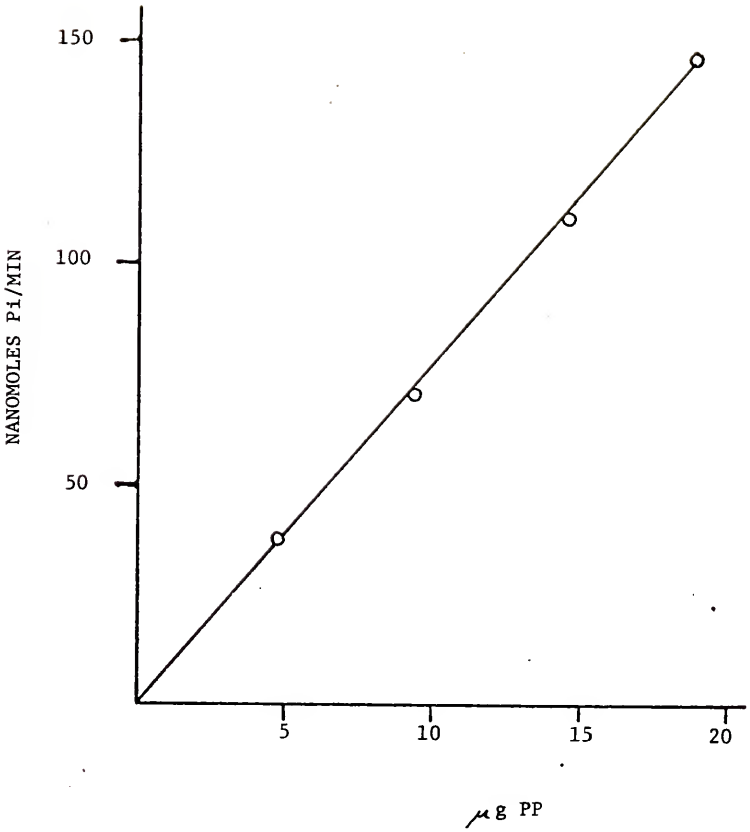

Figure I-9. Linearity of reaction with enzyme concentration. Protein was added to 12 mM pNPP in 0.1 M NH_4Ac, pH 6, at 22°. The absorbance at 405 nm was recorded versus time with a Beckman Acta cIII. The linear portion of the trace was used to determine initial reaction velocity.

Figure I-10. Effect of ionic strength. The reaction with pNPP was run at room temperature in 0.1 M NH_4Ac at pH 6.0. Activity was determined as pNP liberated. ○: NaCl; △: KCl.

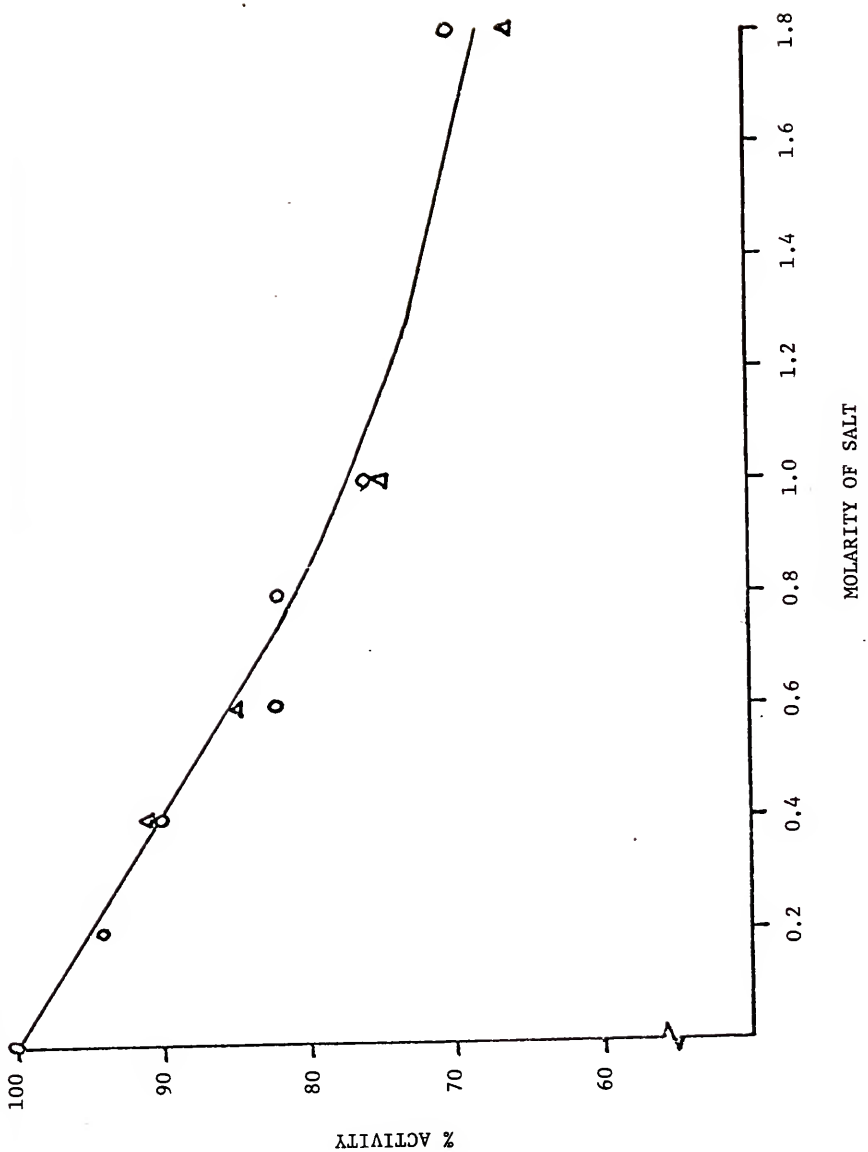
% ACTIVITY
100
90
80
70
60
0.2
0.4
0.6
0.8
1.0
1.2
1.4
1.6
1.8
MOLARITY OF SALT

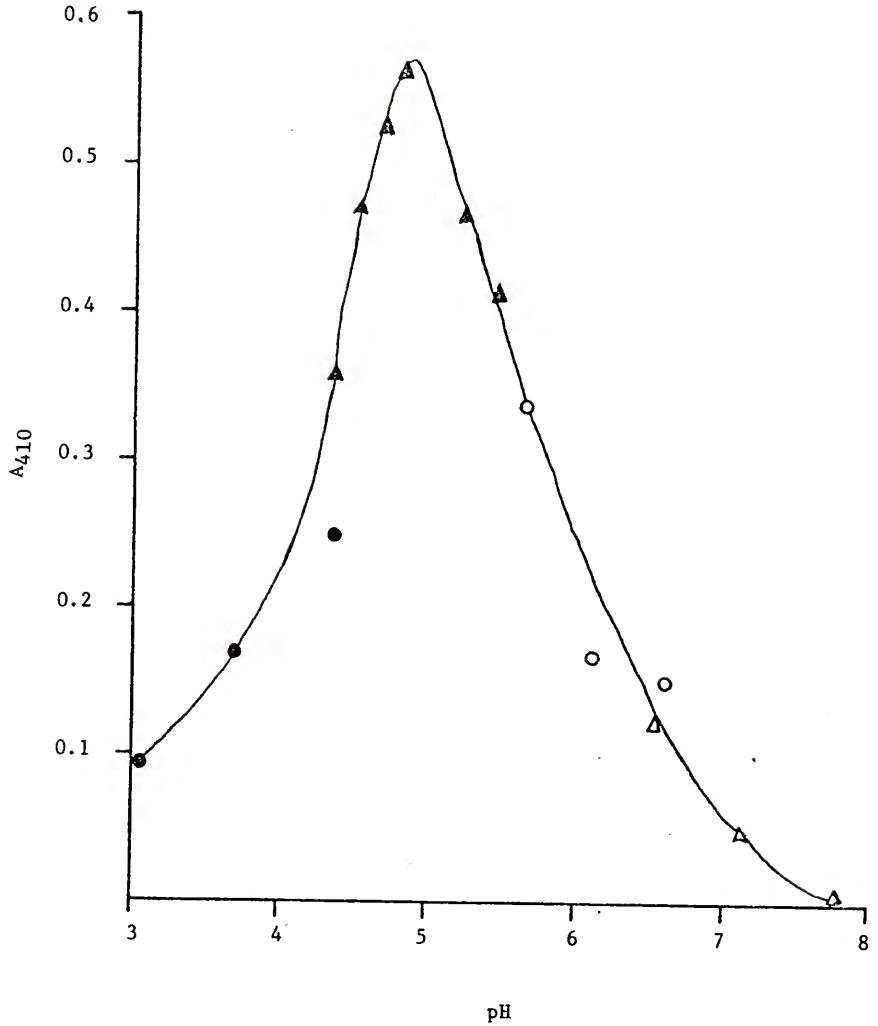

Figure I-11. pH profile. The reaction was run in 0.1 M buffer using pNPP as substrate. The reaction was stopped with KOH and the absorbance at 410 nm was recorded. Buffers were: ● citrate; ▲ acetate; ○ maleate; △ imidazole-HCL.

Product formation versus time

The linearity of product formation versus time was tested with enzyme solutions of varying specific activities. Generally, 5 ml of 12 mM pNPP in acetate at pH 4.9 was incubated in the presence of enzyme at 30°. 0.5 ml aliquots were withdrawn periodically and added to a known volume of KOH to stop the reaction and develop the color. The results of one trial is shown in Figure I-12 for both 12 mM and 1.2 mM pNPP. It was found that for solutions of 12 mM pNPP, the reaction would be linear up to about 10 minutes if the amount of enzyme added produced an optical density of less than 1.5 O.D. at 410 nm in a final volume of 6 ml (1 ml reaction mixture plus 5 ml of KOH). This corresponds to about 0.5 mM pNP produced in the original reaction mixture, i.e., hydrolysis of 4% of the substrate.

Km determination

A quantitative theory on enzyme kinetics was first developed by Henri. This theory now bears the names of Michaelis and Menten who extended Henri's work and devised graphical methods for evaluating the constants Km and Vmax. The theory assumed rapid formation of an intermediate complex which would break down in the rate-limiting step to form product.[31]

$$E + S \underset{k_2}{\overset{k_1}{\rightleftharpoons}} ES$$

$$ES \xrightarrow{k_3} E + P \qquad (1)$$

Here E, S, P and ES stand for enzyme, substrate, product and the enzyme-substrate complex. The equilibrium position of the first reaction was believed not to be significantly disturbed by breakdown of ES. However,

Figure I-12. Linearity of reaction with time. The reaction was run at 30° in 0.1 M acetate at pH 4.9 using pNPP as substrate. Aliquots were taken at various time intervals and analyzed for product (see text). ●: 1.2 mM pNPP, 1.22 μg PP/ml; o: 12 mM pNPP; 0.61 μg PP/ml.

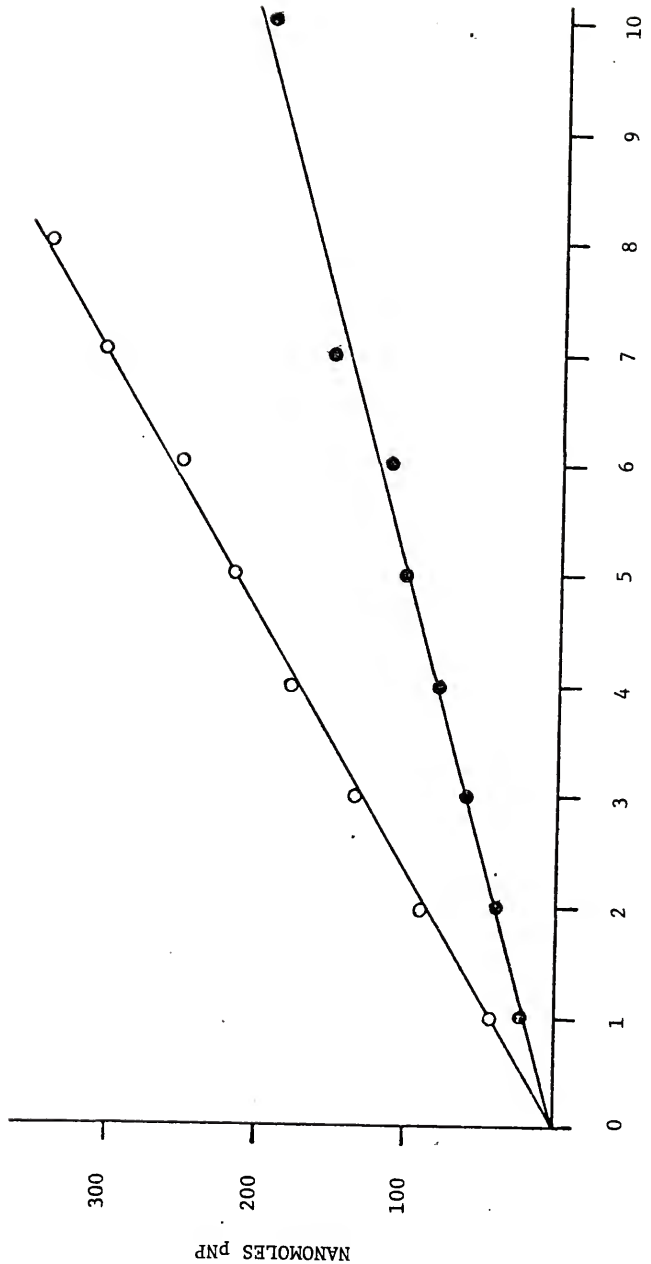
NANOMOLES pNP
300
200
100
0
1
2
3
4
5
6
7
8
9
10
REACTION TIME (MIN)

Briggs and Haldane showed that this assumption was unnecessary, that a steady state could be attained in which the change of [ES] with time is zero:

$$k_1[E][S] = k_2[ES]+k_3[ES]$$

or

$$k_1[E][S]-(k_2+ k_3)[ES] = 0. \qquad (2)$$

In studying enzyme reactions, the molar concentration of substrate is generally very much greater than the concentration of enzyme. As a result the amount of S bound by E at any given time is negligible compared to [S], the total concentration of substrate. The total concentration of enzyme, [Eo] is equal to that of the free enzyme, [E], plus the concentration of complex, [ES], i.e.,

$$[Eo] = [E] + [ES].$$

Solving this equation for [E], substituting into equation (2) and dropping the bracket notation for concentration gives

$$k_1(S)(Eo - ES) - (k_2 + k_3)(ES) = 0.$$

Solving for ES gives

$$ES = \frac{k_1(Eo)(S)}{k_2+k_3+k_1(S)}. \qquad (3)$$

The rate of reaction is then

$$v = k_3(ES) = \frac{k_1k_3(Eo)(S)}{k_2+k_3+k_1(S)}.$$

Since S is the initial concentration of substrate, v is the initial rate

$$v = \frac{k_3(Eo)(S)}{Km + (S)}. \qquad (4)$$

Note that

$$Km = \frac{k_2+k_3}{k_1}. \qquad (5)$$

Km is referred to as the Michaelis constant. When the substrate concentration is much smaller than Km, S may be neglected in the denominator of (3),

$$v = \frac{k_3}{Km} (Eo)(S).$$

The kinetics are first order in substrate concentration. When S is much greater than Km, equation (4) becomes

$$v = k_3 \, Eo = Vmax \tag{6}$$

and the kinetics are independent of substrate concentration. A plot of rate versus substrate concentration at constant Eo should be linear for low substrate concentrations and asymptotically approach Vmax at high substrate concentrations. Substituting the right side of equation (6) into equation (4) gives

$$v = \frac{Vmax \cdot S}{Km + S} \tag{7}$$

The condition for half-maximal velocity, i.e., $v = 1/2 \cdot Vmax$ is readily seen by solving equation (7) and is

$$S = Km.$$

Km is thus the concentration of substrate necessary to half-saturate the enzyme and is a useful property in the characterization of enzymes. Km has additional significance in two special cases. If $k_2 >> k_3$ in equation (4), then $Km = k_2/k_1$, the enzyme-substrate dissociation constant. If $k_2 << k_3$, then $Km = k_3/k_1$, a kinetic constant.

Km and Vmax are not fixed values. Both vary with substrate, pH and temperature. The type of plot mentioned above is not convenient to use in the determination of Km as it requires an extrapolation to Vmax. If one takes the reciprocal of equation (7), one obtains the Lineweaver-Burk equation

$$1/v = (Km/Vmax \cdot 1/S) + 1/Vmax. \tag{8}$$

Plotting 1/v versus 1/S results in a straight line with slope of Km/Vmax, x-intercept of -1/Km and y-intercept of 1/Vmax. Putting the experimental data in this form makes Km and Vmax readily accessible providing Michaelis-Menten kinetics are obeyed. In this work, Km was determined from a least squares analysis of the data.

The basic assumptions in the formulation of equation (4) are as follows.[32] (i) There is an intermediary complex of enzyme and substrate. Though this seems quite reasonable, not all workers studying enzyme catalysis in the early days accepted this postulate. (ii) One substrate is bound at one catalytic site. If this is not true the rate expression in equation (4) will involve powers of S and the reciprocal plot of 1/v versus 1/S will not be linear. Of course, one protein may have more than one active site. (iii) The free substrate concentration is equal to the total amount of substrate added since Eo<<S as discussed. This assumption allows a further observation. The derivative of equation (4) can be taken with respect to Eo. This gives $(dv/dEo)_S = k_3 \cdot S/(Km + S)$, a constant, which means v is proportional to enzyme concentration. This is important as it allows one to vary the initial enzyme concentration during measurement of initial rates. (iv) The overall reaction is irreversible. Enzymes are known to catalyze reactions in both the forward and reverse directions; there is no change in the value of the equilibrium constant. However, if the measurements of the rate are made early in the reaction while the concentrations of products are low, the assumption of irreversibility is justified.

Km was determined in 0.1 M acetate, pH 4.9, using concentrations between 1.2 mM and 12 mM pNPP. From five determinations Km was calculated

to be 2.2 mM (± 0.3 mM) at 30° and was little changed at 0°, namely, 2.8 mM for three determinations. Compared to other phosphatases, these values are somewhat high. Under optimum conditions and using the activating agents to be described later, the greatest specific activity obtained was 170 nanomoles/min/μg. This corresponds to a turnover number of 5400 molecules of substrate per minute per molecule of enzyme. The graphs of one experiment are shown in Figures I-13 and I-14.

The location of PP in vivo implies a possible function of the enzyme to be that involving general hydrolysis. PP could be supposed to be active in some phase of the catabolism of substances found in the allantoic fluid. With this in mind, a number of molecules were tested as substrates at pH 4.9. As can be seen from Table I-2, no esterase, sulfatase or phosphodiesterase activity was found. The phosphate groups of the protein phosvitin were hydrolyzed only poorly. PP was then assayed for the ability to hydrolyze a number of phosphate-containing molecules of biological importance. Of the phosphomonoesters and anhydrides tested, the only appreciable activity was found towards ATP and pyrophosphate. Thus PP is most active towards molecules containing high-energy phosphate bonds.

Heat stability

The specific activity changed very little when the enzyme was stored at 4° at concentrations of about 1 mg/ml. However, when the enzyme was diluted about 100 times for use in assays, the lability increased. The denaturation of diluted enzyme when stored at 4° in 0.1 M acetate at pH 4.9 is shown in Figure I-15. After 20 days there is still about 20% activity remaining. 2-ME, described later as an activating agent,

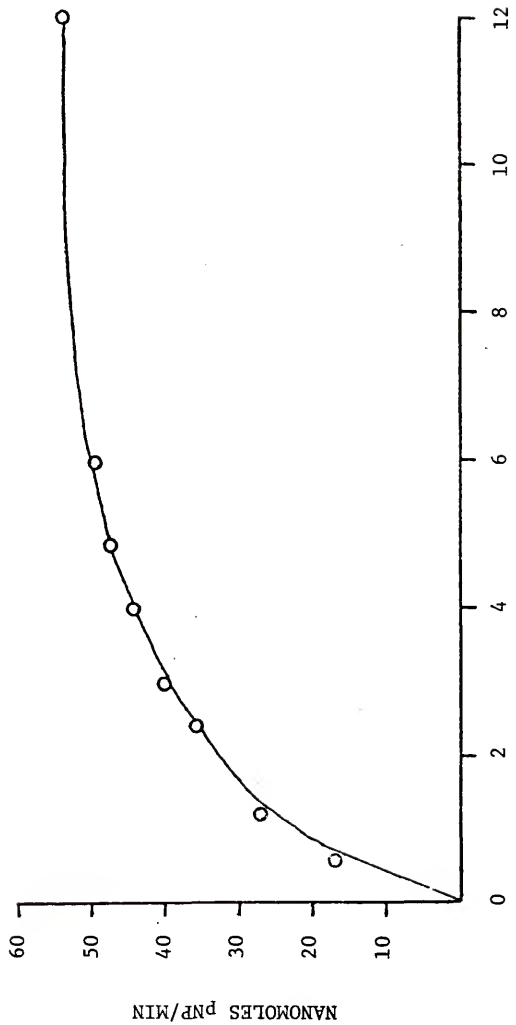

Figure I-13. Reaction velocity versus substrate concentration. The initial concentration of pNPP was varied and the concentration of enzyme was held constant (2.07 μg). The reaction was carried out at 30° in 0.1 M acetate, pH 4.9.

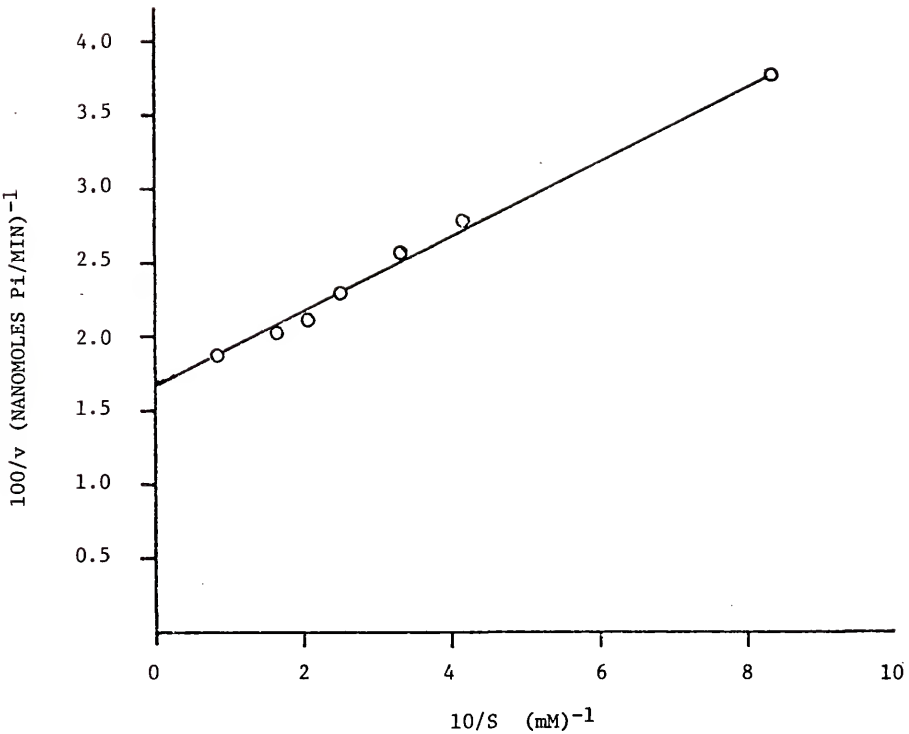

Figure I-14. Lineweaver-Burk plot of the data of Figure I-13. A least squares analysis gives a Km of 1.6 mM.

Table I-2. Hydroytic activity of PP towards various esters.[a]

Substrate	Activity (nmoles Pi/5min)
p-nitrophenylphosphate	414
ATP	149
Sodium pyrophosphate	58
β-glycerophosphate	10
pyridoxal phosphate	9
AMP	6
bis-p-nitrophenylphosphate	0
phosvitin	6
p-nitrophenylacetate	0
p-nitrophenyl sulfate	0

[a]Reactions carried out at 5 mM substrate concentration using 2 μg enzyme. Buffer was 0.1 M acetate, pH 4.9 containing 0.1 M NaCl. Phosvitin was approximately 5 mM with respect to phosphate groups.

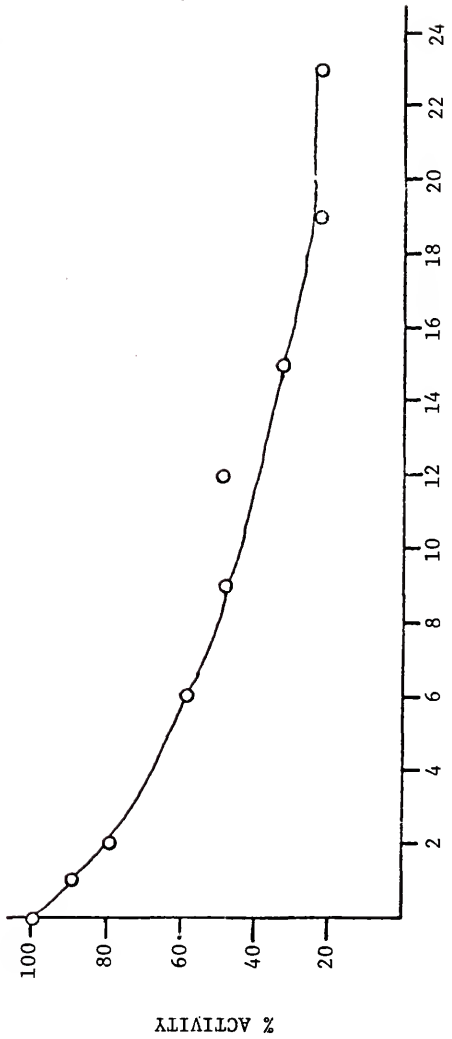

Figure I-15. Denaturation of diluted PP. The protein was diluted to 6.1 μg/ml and stored at 4°. Aliquots were withdrawn periodically and the specific activity towards pNPP was determined at pH 4.9, 30°.

could not increase the activity to that found at the start of the experiment. The rate at which the enzyme lost activity could be significantly increased by storing the enzyme in acetate buffer containing 0.5 M NaCl. To test the stability of PP at increased temperatures, the enzyme was preincubated in sealed test tubes in water baths at 30^{o}, 50^{o} and 70^{o}. At the higher temperatures, the enzyme solutions were cooled in an ice-water bath and then a few minutes were allowed for the temperature to stabilize at 30^{o}, at which temperature the reaction was run. Increasing the preincubation temperature and the length of exposure resulted in decreased activity, shown in Figure I-16. The diluted enzyme is relatively stable to heat; there is still 12% residual activity after 30 minutes at 70^{o}.

It is known that proteins in dilute solution become denatured at surfaces. Various surface active agents have been used to retard denaturation; these compete with the protein for the available surface area. One such surfactant used successfully in the protection of acid phosphatases is Triton X100.[33,34] A room temperature enzyme solution containing 0.005% Triton in acetate buffer was assayed at pH 4.9 and compared to an identical solution which lacked the Triton. The former was found to lose activity at twice the rate of the control. Possibly the detergent caused a loosening of the protein structure. No other surface active agents were examined.

Energy of activation of the catalytic reaction

The temperature variation of a chemical reaction follows the equation of Arrhenius

$$\partial \ln k/\partial (1/T) = -Ea/R$$

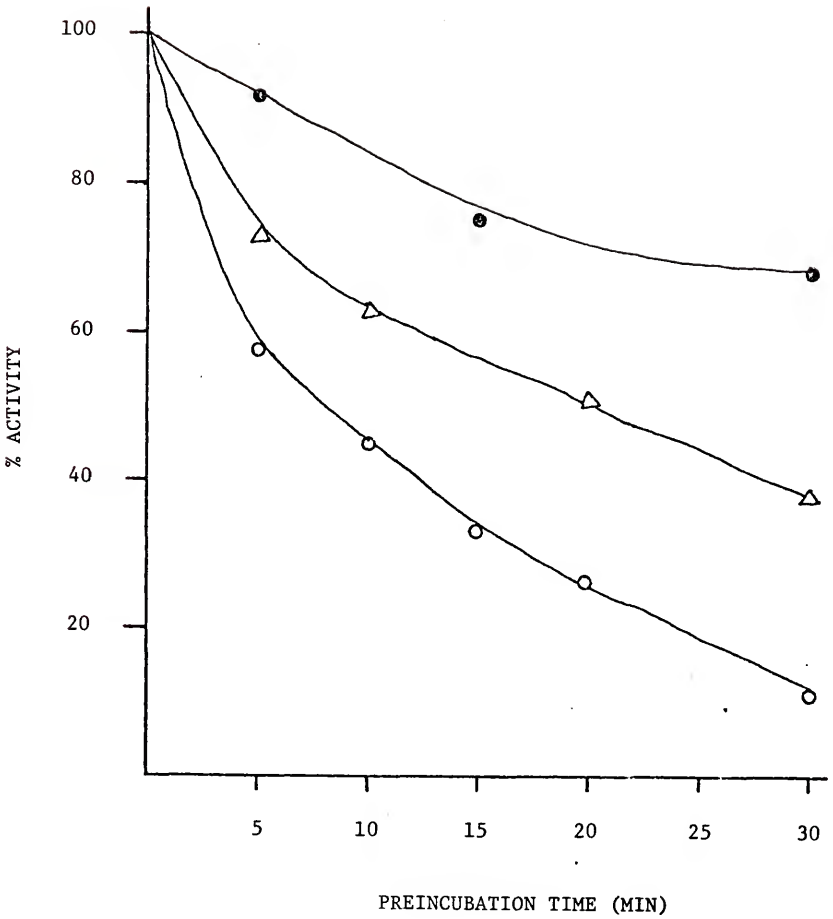

Figure I-16. Heat stability. The enzyme was preincubated at elevated temperatures prior to assay with pNPP at pH 4.9, 30°. ●: 30°; Δ: 50°; o: 70°.

where Ea is a constant, the energy of activation. Ea will depend upon the activation energies of the elementary reactions which are given in equation (1). In the case of equation (1) a plot of ln k_3 against 1/T would give a straight line, the slope of which is -Ea/R. If ES is kept constant as the temperature is varied, then v is proportional to k_3 and Ea could be determined from a plot of ln v versus 1/T. If the concentration of substrate is kept constant but very large, then ES will approximate Eo, the total concentration of enzyme, and thus ES can be taken to be constant. If S is not large, then ES will equal (Eo)(S)/(Km + S) as seen in equation (3). Experimentally it is easier to work at constant substrate rather than constant ES. The error involved has been determined by Gibson[35] and found to be

$$\overset{*}{Ea} - Ea = Km/(S+Km) \cdot R\, \partial \ln Km/\partial (1/T) . \qquad (9)$$

$\overset{*}{Ea}$ is the apparent activation energy and the term containing the partial derivative is equal to (1/R) · ΔHm, the change in heat content accompanying the formation of ES, provided Michaelis-Menten kinetics apply. In the theory of Briggs and Haldane, the formation of a pre-equilibrium is not required. Therefore Km is not an equilibrium constant unless $k_2 >> k_3$.

In any case one can find the value of the partial derivative by using the experimental values of Km at 0^o and 30^o given before. The right-hand side of equation (9) becomes +1.3 kcal·Km/(S + Km). The concentration of substrate used in the activation energy determination was 40 mM. Thus the value of Km/(S + Km) will be about 0.05. Equation (9) reduces to

$$\overset{*}{Ea} - Ea = (0.05)\cdot(1.3\text{kcal}) = 0.065 \text{ kcal} .$$

The difference between the apparent and true activation energies is found to be less than experimental error under the conditions of the assay.

The apparent activation energy was determined at pH 4.9 in 0.1 M acetate buffer, 0.1 M NaCl. pNP liberated was measured after the reaction had proceeded for 5 minutes at the desired temperature. The natural log of the absorbance at 410 nm in the undiluted reaction volume was plotted against $10^3/T$, where the temperature is on the Kelvin scale. The plot was linear as seen in Figure I-17 and the apparent activation energy was found from a least squares analysis to be 11.1 kcal/mole. This value can be compared to the energies obtained for alkaline phosphatase from bone,[36] 9.2 kcal, and from P. laevis,[37] 4.9 kcal and for acid phosphatase from T. confusum,[38] 13.0 kcal, and from P. laevis,[39] 8.2 kcal. However, it seems likely that some of these experimental values may contain the errors mentioned above.

Rate effectors

A number of metal ions and polyanions were tested as inhibitors of the hydrolysis of pNPP at pH 4.9. The results are shown in Table I-3. Molybdate was found to be extremely inhibitory and, to a lesser degree, arsenate and phosphate. The type of kinetic inhibition was not studied. pNP was also tested and found to show no effect when at 1 mM. Of the metal ions tested, mercury(II) showed the greatest effect. pMB and zinc were also inhibitory.

Several experiments were carried out using cysteine or 2-ME to reactivate the Hg^{+2} - inhibited PP. The concentration of mercury used was 1μM. Enzyme with and without mercury was preincubated at room temperature for 10 minutes in acetate at pH 4.9. To one series of test tubes, 2-ME in buffer was added to give a concentration of 10 μM; the control series was buffer without the sulfhydryl. After an additional 10 minutes of

Figure I-17. Energy of activation. The apparent energy of activation (Ea*) was determined as described in the text with 40 mM pNPP in 0.1 M acetate 0.1 M NaCl at pH 4.9. The reaction was stopped by the addition of 5 ml of 0.25 N KOH and the absorbance at 410 nm recorded. The slope of the curve gives Ea* = +11.1 kcal/mole.

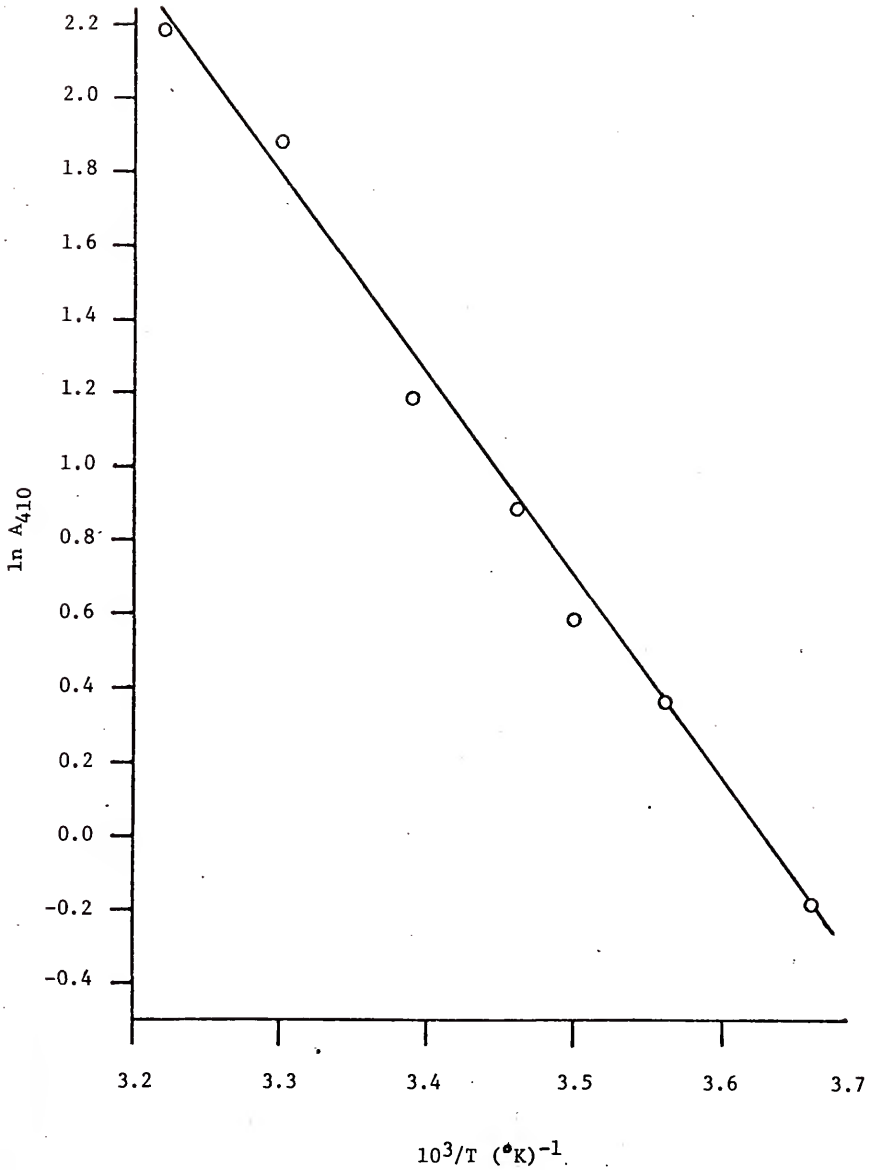
2.2
2.0
1.8
1.6
1.4
1.2
1.0
0.8
0.6
0.4
0.2
0.0
-0.2
-0.4
ln A_{410}
3.2
3.3
3.4
3.5
3.6
3.7
$10^3/T$ $(^{\circ}K)^{-1}$

Table I-3. Rate effectors of pNPPase activity.[a]

Added Compound	Concentration (mM)	Activity (% Control)
Na molybdate	1	1
Na molybdate	0.1	18
Na phosphate	1	58
Na arsenate	1	28
Na arsenate	0.1	48
$AgNO_3$	0.1	97
$HgAc_2$	0.01	5
$HgAc_2$	0.0001	73
$HgAc_2$	0.0003	22
$PbCl_2$	0.1	98
pMB	0.05	85
$ZnSO_4$	1	77
EDTA	1	116
Bipyridine	1	104
Pyridoxal phosphate	1	96
ATP	1	87
Na pyrophosphate	1	90
NaF	1	22
NaF	0.1	67
NaCl	20	100
NaBr	20	104
NaI	20	98

[a] Reactions were carried out using 12 mM p-nitrophenylphosphate in 0.1 M acetate buffer, pH 4.9, for 5 minutes. Each compound was incubated with the enzyme for 10 minutes at room temperature before addition of substrate. Phosphatase activity was measured as p-nitrophenol released.

preincubation, pNPP was added. Repeating this experiment several times gave the same results: that the low concentration of 2-ME used did not affect the specific activity compared to that of the control containing no 2-ME; that while Hg^{+2} was a powerful inhibitor, a 10-fold molar excess of 2-ME over metal completely restored activity with respect to the control. The same results were obtained with 10 μM cysteine and 10 μM ascorbic acid.

Enzymes which require the presence of an SH group in or near the active site, the so called sulfhydryl enzymes, are often found to be inhibited by the mercuric ion through mercaptide formation. Also, reactivation can occur by adding excess sulfhydryl which competes for the bound mercury. Presumably ascorbate can also interact in the same manner. Since the effect of Hg^{+2} is not specific for sulfhydryl groups, it can not be assumed from the data that the protein requires a thiol group for catalysis. Webb[40] has cautioned that different sulfhydryl reagents will have varying degrees of inhibition on sulfhydryl enzymes. One particular reagent may completely inhibit one enzyme at a given concentration and yet have little effect on another. The slightly stimulating effects, seen in the table, of EDTA and bipyridine on PP activity may be due to chelation of potentially inhibitory metals present in the reaction solution.

A third point which is illustrated by Table I-3 is the lack of significant inhibition by ATP, PPi and pyridoxal phosphate on the hydrolysis of pNPP as measured by the determination of pNP. The concentration of each was 1 mM compared to 12 mM pNPP. Apparently these compete only poorly with pNPP for the active site of the enzyme. Km determinations were not carried out for these substrates.

The final information in Table I-3 concerns the effect of the halide ions. It was found that neither sodium nor potassium ions had a specific effect on phosphatase activity; therefore, the sodium salts were prepared in buffered solutions. Chloride, bromide and iodide are seen to have little effect, yet fluoride is a strong inhibitor. A concentration of 0.1 mM fluoride results in 67% activity remaining.

Effect of oxidants and reductants

Because oxidizing and reducing agents were found to have a decided effect on the absorption spectrum of PP, these were tested as to their influence on the rate of hydrolysis of pNPP. Various concentrations of oxidant or reductant were preincubated with the enzyme for 10 minutes; the reaction was then run at 30°, pH 4.9 as usual. The results of one such series using enzyme which had maximum visible absorption at 545 nm are shown in Table I-4. Reducing agents such as 2-ME and ascorbate were found to give a pronounced increase in enzymatic activity. Dithionite, a powerful reducing agent, also increased activity at low concentrations but when present at, or greater than 10 mM, completely inhibited hydrolysis. This would correspond to the concentrations of dithionite needed to bleach the purple color of the protein. 1 mM hydrogen peroxide had an inhibitory effect on the reaction. Figure I-18 is a plot of activity versus concentration of 2-ME following a 10 minute preincubation. Increasing the concentration of 2-ME increases activity, but the slope of the curve is found to be greatest at low concentrations. Two Km determinations with pNP gave an average value of 2.2 mM in the presence of 0.1 M 2-ME. Thus, 2-ME affects the rate but not the binding of substrate. It was found later that an excess of 2-ME, ascorbate and dithionite causes loss of

Table I-4. Effect of reductants and oxidants on the pNPPase activity of the purple form of PP.[a]

Added Species	Concentration (mM)	Activity (% Control)
Na dithionite	0.1	117
Na dithionite	1	127
Na dithionite	10	0
Na dithionite	100	0
2-ME	1	132
2-ME	20	171
2-ME	120	222
Ascorbate	100	245
H_2O_2	1	28

[a] Reaction conditions specified in Table I-3.

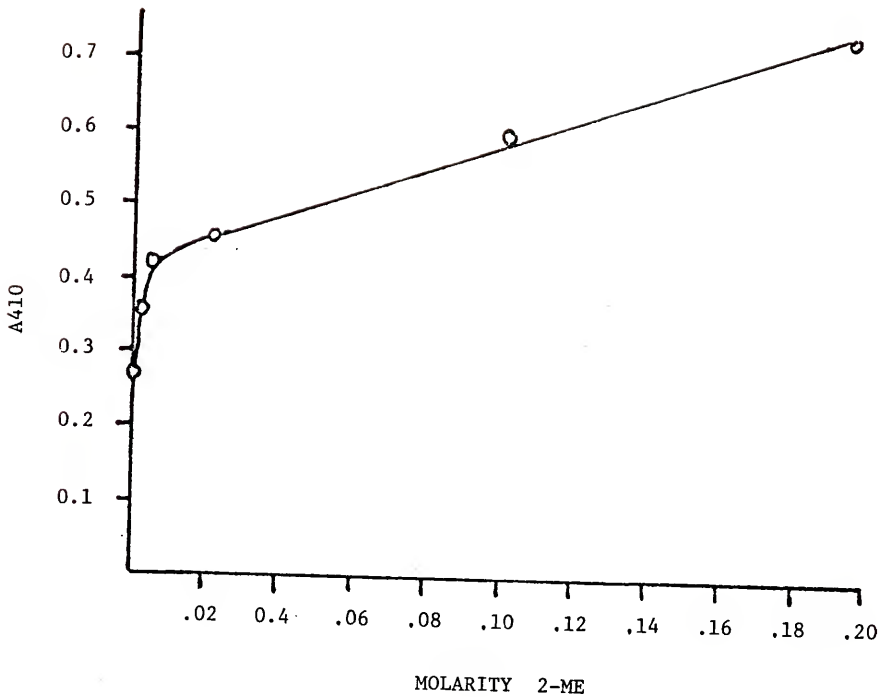

Figure I-18. Effect of 2-ME on the reaction velocity. The enzyme was preincubated with 2-ME for 10 minutes at room temperature. The assay was carried out with pNPP at 30°, pH 4.9.

iron from the protein with concomitant loss of activity. This will be discussed in more detail later. Mild reducing agents had either no effect or a slightly deactivating influence on the pink form (512 nm) of PP. As with the purple form, pink PP was completely inhibited by 10 mM dithionite. 1 mM hydrogen peroxide left only 2% residual activity.

The effect of 2-ME and ascorbate was found to be variable and dependent not only on the color of the enzyme but on the age as well. As mentioned before, preparations of diluted enzyme which were allowed to denature could not be completely reactivated by 2-ME.

Preparation of ApoPP

In the spectral studies of PP, dithionite in sufficient concentration causes rapid bleaching of the purple color. Also found was a definite effect of dithionite upon enzymatic activity; as the concentration of dithionite was increased, the activity first increased, as with all reducing agents tried, and then decreased to zero. Based on these observations, the following experiment was attempted in order to determine if these conditions cause loss of iron, or at least decreased affinity of the protein for the iron. Dithionite was added to a solution of PP which was 1 mM in bipyridine and the solution quickly became pink, the color of the ferrous-bipyridine complex. The loss of iron, as determined by the pink color, took on the order of 10 seconds, about the same time required for dithionite to bleach the color of PP in solution alone.

Removal of iron

A 3.5 ml solution of 55 μM PP with A280/A545 = 13.4 was transferred into a dialysis bag. The bag was sealed and then inverted several times to mix protein solution with any residual water left in the bag. The

bag was cut in half, with about equal volumes of solution in each half, and resealed. This careful procedure was used to insure that each bag would contain solutions of equal protein concentration. One bag was placed in 100 ml of 0.1 M acetate, pH 5.0, the other in 100 ml of buffer and 50 mM dithionite. Both contained 1 mM bipyridine. Solutions were made from glass-distilled water and all dialysis was done in the cold. Within 5 minutes the contents of the dithionite treated bag began to turn pink. After 3.5 hours with one change of the respective solutions, the dialysate was changed to buffer plus bipyridine in both cases. After 2 hours the dialysate was changed to buffer only. After 5.5 hours and one additional change of buffer, the optical spectrum of each solution was taken. The control had A280/A545 = 13.4 as before; there was no iron lost. The treated protein had no distinct absorption in the visible region and no 320 nm peak. The specific activities of the two solutions were measured as usual at pH 5 using pNPP as substrate, and found to be 0.3 and 36 for treated and control. The assay was repeated after 10 minutes preincubation in the presence of 0.1 M 2-ME for 10 minutes. The specific activities were found to be 0.5 and 108. The iron content of each was determined by the TPTZ method. The control was found to contain 1.08 mole Fe per mole protein while the dithionite treated sample had 0.05 mole Fe per mole protein.

The remainder of each solution was dialyzed against 1 mM ferric chloride in acetate for 4 hours and then against buffer only to remove excess iron. Assays gave the specific activities to be 21 and 7 for treated and control respectively, and 20 and 66 for samples preincubated for 10 minutes in 0.1 M 2-ME. The decrease in activity of the control is most probably due to oxidation by ferric iron. The 9-fold increase

in activity upon treatment with 2-ME (the greatest increase yet observed) shows that oxidation is reversible if the protein is not allowed to age. That is, the oxidation of a critical group or groups may be followed by a slow irreversible denaturation. However, 2-ME had little effect on the treated sample. There was not enough of either sample to obtain visible spectra or to do an iron analysis.

An experiment was undertaken as above but 50 mM ascorbic acid in acetate, pH 5, was used in place of dithionite. Again the contents of the ascorbate treated bag turned pink. After 4 hours the dialysate was changed to acetate buffer and dialysis continued to remove all ascorbate. The optical spectrum of each sample was recorded. The treated was found to have only half of the visible absorption as the control and decreased 320 nm shoulder. The specific activities towards pNPP at pH 5 were found to be each 33. However, when both were preincubated in 0.1 M 2-ME for 10 minutes the activity of the control had increased about three times while the ascorbate treated sample was unchanged. Thus it appears in this case that the ascorbate treated protein is already fully "reduced", insofar as the required groups are concerned, as it would appear to contain only half the iron of the control, seen from the visible absorbance, but still has the same specific activity. An iron determination was not carried out however.

Reconstitution of apoPP

Enzymatic reconstitution. Three experiments were carried out to remove the iron from PP and determine reconstitutability enzymatically. Two involved using gel filtration and one used dialysis as means of

separating the liberated iron and excess dithionite from the protein. In the first method, either 50 mM dithionite, in one case, or 50 mM dithionite plus 1 mM bipyridine in the other, was added to solutions of PP. After allowing 15 minutes at 0°, the treated solutions of PP were passed through Sephadex G-10 column (1.5 x 15 cm) equilibrated in acetate buffer at room temperature. Fractions were collected and scanned in the UV region. There was good separation of the smaller molecules from the protein. Fractions of apoPP were pooled and aliquots were added to pH 5 buffered solutions which were 8 μM in one of the following metals: Mg^{+2}, Mn^{+2}, Cr^{+3}, Fe^{+3}, Co^{+2} or Cu^{+2}. The protein concentration at this point was 1.2 μM. The solutions were allowed to stand at 4° for 20 minutes after the addition of protein;then the mixtures were assayed with pNPP at pH 5. The results are shown in Table I-5. The control used was 1.2 μM apoPP in metal-free buffer. The table shows that the ferric and cupric ions give significantly greater activity over the control, while the other ions show little effect. The order of the entries in the table is the chronological order in which the assays were done. As additional time is allowed for the ferric or cupric ions to bind to the apoprotein, more activity is found. The second column experiment investigated the change in specific activity versus time for apoPP plus either iron or copper. The results were similar to the third experiment which is described next.

A solution of PP was dialyzed in the cold against 50 mM dithionite and 1 mM bipyridine in acetate, pH 5. Changes of buffer during 23 hours insured removal of the iron-bipyridine complex and excess dithionite. Aliquots of apoPP were added to solutions of either 9-fold molar excess

Table I-5. Reconstitution of pNPPase activity by addition of metals to apoPP.

Metal Present[a]	Specific Activity
none	3, 6[b], 10[c]
Fe^{+3} (chloride)	17, 35[b], 43[c]
Cr^{+3} (K-sulfate)	3
Co^{+2} (acetate)	4
Cu^{+2} (sulfate)	29, 41[b], 41[c]
Mn^{+2} (chloride)	4
Mg^{+2} (sulfate)	5

[a] apoPP was added to 4^{o} solutions of 80 μM in metal (a 7-fold molar excess) buffered in 0.1 M acetate at pH 4.9. Twenty minutes after mixing these solutions were assayed for activity towards pNPP. The order of the table is the order in which the assays were done.

[b] As above but the assay was repeated 90 minutes after mixing.

[c] As above but the assay was repeated 4 hours after mixing.

Cu^{+2}, 8-fold excess Fe^{+3} or to metal-free buffer which was used as the control. The mixtures were at room temperature and aliquots were withdrawn periodically and assayed with pNPP at pH 5. A plot of specific activity (based on total protein present) versus time after addition of enzyme is shown in Figure I-19. As stated above, these results are essentially the same as for the second G10 column experiment. The activity of the copper enzyme reaches a maximum after about one hour past mixing. The activity of reconstituted Fe^{+3}-PP reaches a maximum after about two hours and in two of the three experiments had a specific activity of about twice that of Cu^{+2}-PP. The control shows slow restoration of activity; this is no doubt due to low levels of contaminating iron found in the reagents used to prepare the buffer. The protein is present at approximately 1 μM. Thus 1 nanomole Fe/ml of solution would provide the stoichiometric amount of metal required for reconstitution. If the copper- or iron-restored protein is stored at 4^{o}, the loss of activity is only 15% and 10% respectively over 16 hours. This is about the same rate of decay as found for native protein which had been diluted as discussed previously. The effect of a 10 minute preincubation with 0.1 M 2-ME was studied on the reconstituted iron and copper enzymes. No increase in activity was found.

Spectroscopic reconstitution. ApoPP was prepared by treatment of about 1.4 mg protein with dithionite and bipyridine, followed by dialysis as before. The apo-enzyme was scanned and found to have no definite visible absorption bands. A 10-fold molar excess of ferric chloride was added to both the sample cuvette containing apoPP and the reference cuvette containing the dialysis buffer; this would compensate for iron absorption in the

Figure I-19. Restoration of enzymatic activity by addition of copper and iron to apoPP. apoPP was prepared as described in the text and then added to room temperature solutions of 0.1 M acetate at pH 5 containing no metal (0), 9-fold molar excess Fe^{+3} (▲) or 8-fold molar excess Cu^{+2} (●). Aliquots of each solution were withdrawn at the indicated time intervals and assayed with pNPP in acetate at 30°. The specific activity calculated was based on total protein present.

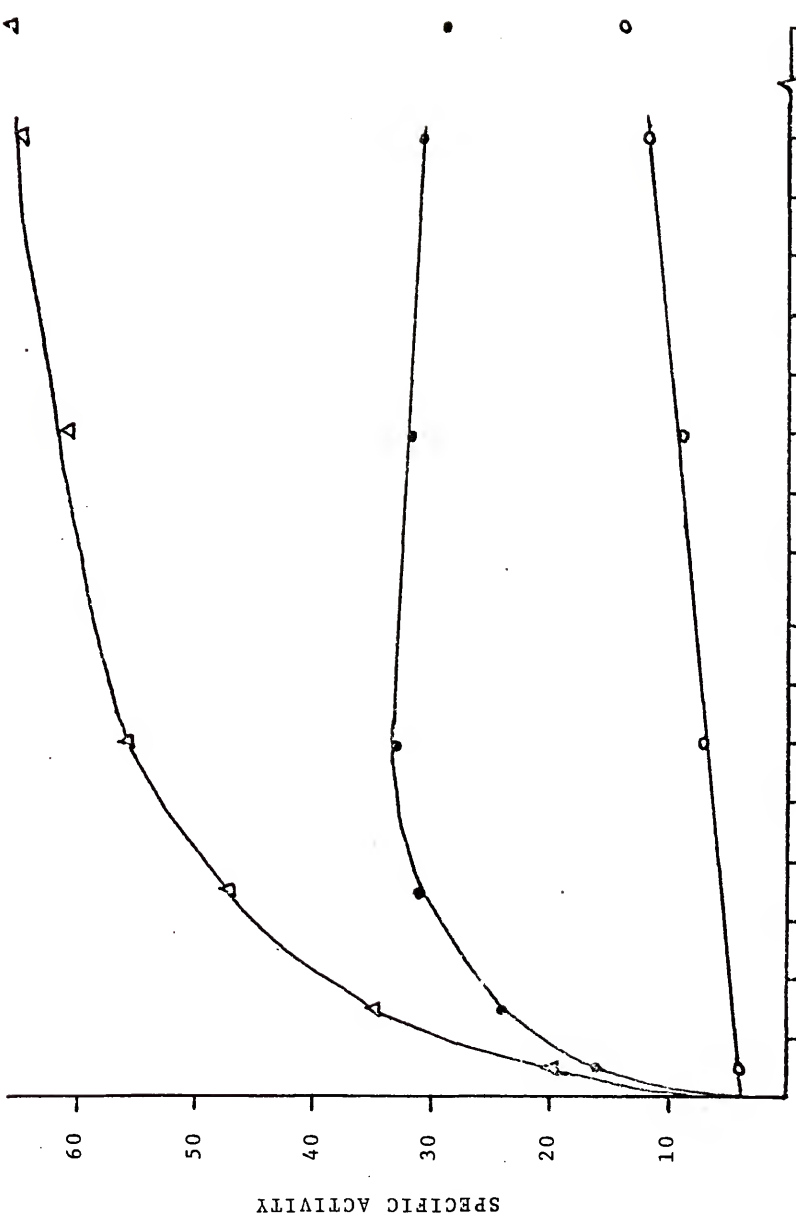
SPECIFIC ACTIVITY
10
20
30
40
50
60
20
40
60
80
100
120
140
160
220
TIME (MIN)

blue and UV portion of the spectrum. The mixture was scanned periodically. After 8 minutes, the absorption at 540 nm was about 2/3 that of the maximum obtained after 40 minutes. The spectrum was identical to that of naturally occurring PP. The mixture was dialyzed overnight to remove excess iron and the spectrum then recorded. The spectrum was found to be virtually unchanged.

Cu^{+2}-PP

ApoPP was prepared as described in the above paragraph and the spectrum recorded. Aliquots from a stock solution of copper sulfate were added to reference and sample cuvette to give a 4-fold molar excess of Cu^{+2}. After 12 minutes the spectrum was taken. No increase had occurred in the visible region but there was an increase in the 280 nm peak of 4%. Then Fe^{+3} was added to a 6-fold excess and slow increase in absorbance at 550 nm was followed versus time. After 90 minutes the spectrum was recorded. The visible region contains the same features as native PP.

This experiment was repeated using a 4-fold excess of Cu^{+2} or Fe^{+3}. ApoPP plus Fe^{+3} again gave the results as obtained in the previously described reconstitution experiments. The increase in absorbance at 550 nm was 0.024 O.D., 19 minutes after addition of Fe^{+3}. The addition of Cu^{+2} to apoPP again gave only an increase in the UV region but the change occurred within about 2 minutes. 4-fold excess Fe^{+3} was then added to the Cu^{+2} plus apoPP solution. After 22 minutes the spectrum was taken. The increase in A550 was found to be 0.017 O.D. From these results it would seem that the presence of copper inhibits the binding of iron. Whether this is because the copper binds in or near the iron binding site or acts to distort this site cannot be determined from this preliminary

study. The increase in the 280 nm absorption which occurs after addition of copper could be caused either by amino acid - copper interaction, or by a change in the environment in one or more of the aromatic amino acid residues, resulting from an alternation in peptide conformation.

General Discussion

PP has been found to be an acid phosphatase possessing a rather narrow range of hydrolytic ability. It is produced in the uterus and later found in the allantoic fluid of the young embryo. It is inducible by progesterone and can be obtained in relatively large amounts. Further, the protein is at its highest level during a critical phase in pregnancy when embryonic mortality is high. Due to these facts, and because PP is most active towards the biologically unimportant molecule p-nitrophenyl-phosphate, it seems likely that the true physiological function has not yet been discovered. Perhaps PP is important in maintaining a suitable environment for embryonic development. It is possible that the chelation of free iron is its function; however, all PP found contained, within experimental error, 1 mole of iron per 32,000 molecular weight. It would seem that if binding iron is the role of PP, then an appreciable amount of apoPP should be found.

Enzyme Activation

Reducing agents were found to have an activating influence on the enzyme when present in proper concentrations. 0.1 M 2-ME was found to increase the rate of hydrolysis of pNPP by 2 to 4 times but the value of Km at 30°, pH 4.9, was unchanged. Treatment of PP with reducing agents of sufficient concentration or prolonged exposure resulted in loss of

activity and loss of iron. It was also found that very low concentrations of Hg^{+2} had a potent inhibitory effect upon the reaction. Coupling these data, it seems quite possible that a free thiol group is required for catalysis. Oxidation either by air or hydrogen peroxide would generate the formation of a disulfide bond if a second sulfhydryl group were in close proximity. This would impose a slight constraint on the conformation of the protein and perhaps affect the environment of the iron enough to cause a spectral shift to around 550 nm and the appearance of the 320 nm peak (certainly due to the iron) seen in the spectrum as a shoulder. Addition of such as 2-ME would reduce the disulfide to two free thiols, thus the shift of visible absorption maximum to the blue as the ligands of the iron rearrange to the native conformation. It should be recalled that reconstituted PP prepared from lengthy exposure to reductants did not show increased activity toward pNPP after preincubation with 2-ME. From this, one might have expected the enzyme to be restored, by addition of iron, to the pink form. At the low concentration of apoPP used for spectral restoration it was difficult to identify the peak maximum precisely. However, the maximum was near 540 nm, which is close to the purple extreme found around 550 nm. Perhaps the lability of apoPP is greater than PP and although iron can be added to give color, a high percentage of protein is no longer capable of enzymatic activity. Two types of iron-containing protein may be formed: the pink species which is a minority component and another species which absorbs around 540 nm, but has become irreversibly denatured. Clearly more work needs to be done on this intriguing problem.

From experiments involving the reactions of acid and alkaline phosphatases in $H_2{}^{18}O$, it has been found that the hydrolysis is via cleavage of the O-P bond in C-O-P.[41] One could postulate a mechanism of hydrolysis involving the formation of an intermediate sulfur-phosphorous bond as molecules of the type $ROP(S)(SH)_2$ are known.[42] The observed stimulatory effect of reducing agents under this theory would be due to the liberation of the essential sulfhydryl group via reduction of the disulfide bond. Thus 2-ME is seen to increase the number of catalytically active proteins in solution rather than increasing the efficiency of the reaction. The variable effect found, even with a constant concentration of 2-ME and constant preincubation time, is due to different protein solutions having different concentrations of "oxidized" enzyme.

Prolonged exposure to 0.1 M 2-ME or ascorbate or 10 mM dithionite results in reduction of the iron. One cannot be certain which event occurs first: conversion to the ferrous ion, or release of iron from the protein, due to some other effect, then subsequent reduction. The metal, required for catalysis, could simply be a site of attraction for one or two of the oxygen atoms of the phosphate group. This could serve to orient the substrate into the proper configuration for catalysis to occur. Assuredly, more information needs to be gathered on the effects of sulfhydryl reagents on PP.

Nature of Glycoproteins

Though this work has not dealt with the carbohydrate groups of the glycoprotein, a few points can be considered here. Two recent reviews on glycoproteins were found to be helpful.[43,44] Both have demonstrated

that while the function of a molecule as a whole is understood, the role of the carbohydrate portion is often not known at all. For example, RNAse B, a glycoprotein, has the same enzymatic activity as RNAse A, but the latter contains no sugar groups. There are some general concepts pertaining to the carbohydrate moieties which will be briefly mentioned, in that one or more of these may be important in regard to PP. The carbohydrate group may increase the resistance of the protein to hydrolysis by proteolytic enzymes, increasing its life *in vivo*. These groups also increase protein solubility due to their strong hydration.

Carbohydrates are important in two facets of recognition. It has been found that if one type of terminal sugar unit has been selectively removed from a glycoprotein which is then injected into test animals, these altered proteins will be removed from the serum, whereas the untreated control will not be removed.[44] Secondly, carbohydrates may be involved in recognition and the transport of the protein into the cell. It is known that sugars are abundant on the surface of cell membranes. It has been proposed that these are instrumental in intercellular communication, so called contact inhibition, and in recognition of large molecules. A final interesting finding is that a particular glycoprotein, C'9, has been found to chelate iron; the bonds formed are believed to be from carbohydrate groups.[45]

ESR

ESR studies of iron in glass gave a signal at g = 4.27 which was analyzed by Castner *et al.*[46] and found to be due to the high spin ferric ion. Since the ground state of this atom is ^6S, one would expect a line

at g = 2 with perhaps some broadening due to crystal fields within the glass. These workers examined the spin Hamiltonian in regard to D, the coefficient of the axial part of the Hamiltonian, and E, the coefficient of the rhombic part. By considering D = 0, they were able to predict a splitting corresponding to g = 30/7 for each of the three principal axes for the middle Kramers doublet. The g values of the upper and lower doublets were found to be strongly anisotropic. In a detailed study, Blumberg[47] showed that for $|E/D| = 0$, i.e., axial symmetry, then an increase in this ratio represents an increase in rhombicity. Further, $|E/D| = 1/3$ represents a completely rhombic field and the energy separation between the three Kramers doublets is equal and is $4\sqrt{7}\ D/3$. Also shown in this work[47] were plots of the ratio of microwave frequency/magnetic field in units of the Bohr magneton/ Planck's constant versus magnetic field. D was held constant at 0.75 wavenumbers and E was varied. The results showed that the effective g values departed from 30/7 as the strength of the magnetic field increased and as the rhombicity decreased. Dowsing and Gibson[48] have also investigated high-spin d^5 systems. They have constructed six graphs of $D/h\nu$ versus $H/h\nu$ and D versus H for E/D ranging from 0 to 1/3. They conclude that for E/D near 1/3 and D greater than 0.23 wavenumbers, absorption would be around 1500 gauss (ν = 9.3 GHz). More precise information on the values of D and E could be obtained from the experimental g values if a complete set of these graphs were available. The only conclusions that can be drawn in regard to the iron in PP is that the symmetry of the paramagnetic site is highly rhombic and one has a lower limit on the value of D from the aforementioned graphs.

ESR spectra of a number of nonheme iron proteins have shown the g = 4.3 absorption. A detailed analysis of the ESR spectrum of rubredoxin from P. oleovorans was undertaken by Peisach et al.[49] at temperatures below 12° K; signals arising from the lower Kramers doublet could be observed; as predicated from theory, they were markedly anisotropic. The signal intensity of the observed transitions was measured over a range of temperature from 1.4 to 40° K. The data were fit to a Boltzmann distribution over the three Kramers doublets. From this and knowledge of the effective g values, the values of D and E which gave the best fit of the data on solving the spin Hamiltonian gave D = 1.76 wavenumbers, E = 0.495 wavenumbers and E/D = 0.28; this corresponds to 84% rhombicity. With the instruments available, this type of evaluation could not be undertaken for PP.

In light of the arc emission data, it seems likely that the signal at g = 2.05 is due to copper(II). In simple theory, the cupric ion can be thought to be in the center of an octahedron of ligands. The d^9 system can be considered as an unpaired hole in one of the e_g orbitals. The Jahn-Teller theorem states however, that the two orbitals in the e_g set are not degenerate, though the difference in energy may be small. The hole is restricted to either the dz^2 or dx^2-y^2 orbitals and the orbital contribution to the magnetism is quenched. Thus, g values for Cu^{+2} are expected to be close to free spin. In the first approximation, the deviation of the g values from free spin will be related to the ratio of the spin-orbit coupling constant to the crystal field splitting. Since copper complexes typically absorb light around 600 nm, one can use 16,000 wavenumbers as a value of Δ. Hence one can calculate $g_{11} = 2.4$ and $g_{\perp} = 2.1$ from the equations given by

Vänngård.[50] More refined treatments require consideration of covalency between metal and ligands. Characteristic of copper ESR spectra are the hyperfine splittings due to the isotopes ^{63}Cu and ^{65}Cu, each with spin of 3/2. Since the magnetic movements of the two nuclei are of similar magnitude, the hyperfine lines from the two isotopes are usually not separated.

Inspection of the g = 2.05 signal of PP shows this to be the perpendicular-type transition. The intensity of the parallel lines would be expected to be such that they would be lost in the noise present in the spectrum. The 6 hyperfine lines can be tentatively explained in two ways. First, the splitting could be due to one nitrogen (I = 1) nucleus. If the symmetry about the copper atom deviates slightly from axial, two closely overlapping transitions would occur near g = 2.05. Thus one would see two triplets lying fortuitously close to each other. Such a slightly non-axial spectrum was found at 35 GHz for ^{63}copper-transferrin-bicarbonate, pH 7.6.[31] In the low field parallel line for ^{65}Cu-transferrin,[51] three line hfs was found at X-band. Computer simulation matched this experimental line assuming the presence of a single nitrogen nucleus, splitting 9.5 gauss. The alternative explanation is that the splitting is from 2 or more nitrogen nuclei. Six line hyperfine near g = 2.0, similar to that of the PP spectrum, has been observed in Cu-transferrin, bicarbonate-free at pH 9.2,[51] and Cu-transferrin,[52] conditions unspecified. In the former case, ^{65}Cu-transferrin was studied and computer simulation of the low field parallel peak, which contained at least seven hyperfine lines, agreed well with the observed spectrum assuming four equivalent nitrogen nuclei with splitting of 12 gauss. The spectrum of Cu-conalbumin was also similar to that of PP in the perpendicular region.[53]

To review a few facts briefly: iron is required for the catalytic action of the protein; iron can be removed without protein precipitation and added to form an active enzyme having the same spectral absorption as the native; copper is the only other metal, out of several tried, which can be added to apoPP with at least partial restoration of activity. This evidence gives credence to the proposal that copper is binding at a site the same as, or similar to, the iron binding site. It is not certain whether the copper ESR signal observed is due to copper occupying an iron site or copper bound to another portion of the polypeptide. It is not known if copper is able to successfully compete with iron for the protein. If it can, then copper may be used as a spin probe in an attempt to discover some of the ligands of the iron, especially in regard to nitrogen hyperfine. The data currently available are not amenable to the type of analysis performed on Cu-transferrin. However, as increasing amounts of enzyme are purified, ESR experiments with ^{65}Cu-PP and Mössbauer of ^{57}Fe-PP will become a possibility.

Iron-Containing Acid-Phosphatases

PP, a number of whose properties have been described in this work, appears to be a member of an expanding family of iron-containing phosphatases. These proteins have in common a purple color and phosphatase activity. However, they all differ in molecular weight, amino acid composition, pI, pH maximum and substrate specificity, insofar as these properties are known. They have been found in plants, animals and fungus.

The first was discovered in beef spleen[54-58] nearly 20 years ago and was described as a "phosphoprotein phosphatase" because of its ability to hydrolyze phosphate groups on the milk protein, casein. The published spectrum of the basic glycoprotein is virtually identical to that of the purple form of PP. One paper[57] reported that no metals were found to be present from either arc emission analysis or ESR spectroscopy. Almost no further work was carried out on this enzyme during the past ten years save for a paper in 1973 by Campbell and Zerner,[59] who found the presence of 1 mole of iron per mole of protein, making this the first example of a metallo-acid-phosphatase. Previously however, solutions containing a repressible acid phosphatase from N. crassa had been reported to have a purple color, although no metal analysis was attempted.[60] This basic protein is about 9.5% carbohydrate and believed to exist as a dimer. An iron-containing phosphatase active toward ATP was discussed at the Biochemistry/Biophysics 1974 meeting.[61] Also a glycoprotein, it has broad visible absorption at 565 nm, very similar to PP, and an ESR signal at g = 4.3 at 77^{o} K. The source of enzyme is the red kidney bean.

Thus PP is another example of an iron-containing purple-colored phosphatase. The fact that the sources of these proteins are highly diversified should not be overlooked. None of the mentioned enzymes have a clearly understood reason for existence. Though certainly important, their physiological significance remains to be discovered.

References

1. Murray, F. A., Jr., Bazer, F. W., Wallace, H. D., and Warnick, A. C., Reprod. 7, 314 (1972).

2. Chen, T. T., Bazer, F. W., Cetorelli, J. J., Pollard, W. E., and Roberts, R. M., J. Biol. Chem. 248, 8560 (1973).

3. Vallee, B. L., and Roberts, R. M., unpublished results.

4. Chen, T. T., and Bazer, F. W., J. Animal Sci. 37, 304 (1973).

5. Perry, J. S., and Rowlands, I. W., J. Reprod. Fert. 4, 175 (1972).

6. O'Malley, B. W., and McGuire, W. L., Endocrinology 84, 63 (1969).

7. Krishnan, R. W., and Daniel, J. C., Jr., Science 158, 490 (1967).

8. Lowry, O. H., Rosebrough, N. J., Farr, A. L., and Randall, R. J., J. Biol. Chem. 193, 265 (1951).

9. Fischer, D. S., and Price, D. C., Clin. Chem. 10, 21 (1964).

10. Weil, J. A., and Anderson, J. K., J. Chem. Soc., 5567 (1965).

11. Cassim, J. Y., Yang, J. T., Biochem. 8, 1947 (1967).

12. Allen, C. A., private communication.

13. Fiske, C. H., and SubbaRow, Y., J. Biol. Chem. 66, 375 (1925).

14. Seddon, B., and Fynn, G. H., Anal. Biochem. 56, 566 (1973).

15. Bessey, O. A., Lowry, O. H., Brock, M. J., J. Biol. Chem. 164, 321 (1946).

16. Boyer, P. D., J. Amer. Chem. Soc. 76, 4331 (1954).

17. Riordan, J. F., Vallee, B. L., Methods in Enzymology (Hirs, C. H. W., ed.), Vol. XI, p. 541. Academic Press, New York, 1957.

18. Reisfeld, R. D., Lewis, U. J., and Williams, O. E., Nature 195, 281 (1962).

19. White, A., Handler, P., Smith, E. L., Principles of Biochemistry, 5th ed., p. 92. McGraw-Hill, New York, 1973.

20. Gratzer, W. B., Poly-α-Amino Acids (Fasman, G. D., ed.), p. 177. Marcel Dekker, New York, 1967.

21. Cotton, F. A., and Wilkinson, G., Advanced Inorganic Chemistry, 3rd edition, pp. 581-585. Interscience, New York, 1972.

22. Strickland, E. H., Horwitz, J., and Billups, C., Biochem. 8, 3205 (1969).

23. Beychock, S., Poly-α-Amino Acids (Fasman, G. D., ed.), p. 293. Marcel Dekker, New York, 1967.

24. Boyd, D. B., J. Amer. Chem. Soc. 94, 8799 (1972).

25. Boyd, D. B., J. Phys. Chem. 78, 1554 (1974).

26. Broman, L., Mälmstrom, B., Aasa, R., and Vänngård, T., J. Mol. Biol. 5, 301 (1962).

27. Tsibris, J. C. M., and Woody, R. W., Coord. Chem. Rev. 5, 417 (1970).

28. Orme-Johnson, W. H., Ann. Rev. Biochem. (Snell, E. E., ed.) Vol. 42, p. 159.

29. Bredeck, H. W., and Mayer, D. T., Mo. Agr. Exp. Sta. Res. Bul. 491, 1 (1955).

30. Goode, L., Warnick, A. C., and Wallace, H. D., J. Animal Sci. 24, 4 (1965).

31. Webb, E. C., Comprehensive Biochemistry (Flochin, M., and Stotzy, E. H., eds.) Vol. 12, p. 1 Elsevier, Amsterdam, 1964 (and references therein).

32. Webb, J. L., Enzyme and Metabolic Inhibitors, Vol. I, chapter 2. Academic Press, New York, 1963.

33. Tsuboi, K. K., and Hudson, P. B., Arch. Biochem. Biophys. 55, 191 (1955).

34. Tsuboi, K. K., and Hudson, P. B., Arch. Biochem. Biophys. 55, 206 (1955).

35. Gibson, K. D., Biochim. Biophys. Acta 10, 221 (1953).

36. Bodansky, O., J. Biol. Chem. 129, 197 (1939).

37. Saleem, M., and Alikhan, M. A., Comp. Biochem. Physiol. 49B, 129 (1974).

38. Chaudhary, K. O., Moorijani, S., and Lemonde, A., Can. J. Biochem. 42, 1769 (1964).

39. Saleem, M., and Alikhan, M. A., Comp. Biochem. Physiol. 49B, 129 (1974).

40. Webb, J. L., Enzyme and Metabolic Inhibitors, Vol. III, chapter 7. Academic Press, New York, 1966.

41. Dixon, M., and Webb, E. C., Enzymes, 2nd edition, pp. 279-282 Academic Press, New York, 1964.

42. Cotton, F. A., and Wilkinson, G., Advanced Inorganic Chemistry, 3rd edition, p. 385. Interscience, New York, 1972.

43. Heide, K., and Schwich, H-G., Angew. Chem. Internat. Edit. 12, 721 (1973).

44. Sharon, N., Sci. Amer. 230, 78 (1974).

45. Hadding, U., and Müller-Eberhard, H. J., Immunology 16, 719 (1969).

46. Castner, T., Jr., Newell, G. S., Holton, W. C., and Slichter, C. P., J. Chem. Phys. 32, 668 (1960).

47. Blumberg, W. E., Magnetic Resonance in Biological Systems (Ehrenberg, A., Malmström, B. G., and Vänngård, T., eds.), p. 119. Pergamon Press, Oxford, 1967.

48. Dowsing, R. P., and Gibson, J. F., J. Chem. Phys. 50, 294 (1969).

49. Peisach, J., Blumberg, W. E., Lode, E. T., and Coon, M. J., J. Biol. Chem. 246, 5877 (1971).

50. Vänngård, T., Biological Applications of Electron Spin Resonance (Schwartz, H. M., Bolton, J. R., and Borg, D. C., eds.), p. 411. Wiley-Interscience, New York, 1972.

51. Aasa, R., and Aisen, P., J. Biol. Chem. 243, 2399 (1968).

52. Windle, J. J., Wiersema, A. K., Clark, J. R., and Feeney, R. E., Biochem. 2, 1341 (1963).

53. Aasa, R., Malmström, B. G., Saltman, P., and Vänngård, T., Biochim. Biophys. Acta 75, 203 (1963).

54. Sundararajan, T. A., and Sarma, P. S., Biochemical J. 56, 125 (1954).

55. Singer, M. F., and Fruton, J. S., J. Biol. Chem. 229, 111 (1957).

56. Glomset, J. A., Biochim. Biophys. Acta 32, 349 (1959).

57. Glomset, J., and Porath, J., Biochim. Biophys. Acta 39, 1 (1960).

58. Sabel, K-G., Glomset, J., and Porath, J., Biochim. Biophys. Acta 50, 135 (1961).

59. Campbell, H. D., and Zerner, B., Biochem. Biophy. Res. Comm. 54, 1498 (1973).

60. Jacobs, M. M., Nye, J. G., and Brown, D. M., J. Biol. Chem. 246, 1419 (1971).

61. Nochumson, S., O'Rangers, J. J., and Dimitrov, V., Fed. Proc. 33, abstract 876, 1378 (1974).

II. INTERACTION OF NITRIC OXIDE WITH CYTOCHROME P450 AND P420 FROM *Pseudomonas putida*

Introduction

Cytochrome P450 is a hemoprotein whose name is derived from its unusual visible spectrum when reduction of the iron of the heme group is followed by addition of carbon monoxide. Whereas most ferrous hemoprotein-CO complexes absorb maximally at 420 nm, P450-CO absorbs around 450 nm. In 1958 Klingenberg[1] and Garfinkel[2] discovered this cytochrome in the microsomal fraction of rat livers. Subsequent studies on P450 from mammals have shown this to be an enzyme functioning in a mono-oxygenase system. Mono-oxygenases, whose role is the insertion of a hydroxyl group into the substrate, are important in fatty acid oxidation, steroid metabolism and drug detoxification. P450 present in mammals is membrane bound and can be solubilized only with difficulty. Detergents have been used for this purpose. Early attempts at purification resulted in an appreciable amount of an inactive form of P450 which absorbed at 420 nm upon reduction plus CO; this was named P420.

A soluble P450 can be induced in the bacterium *Pseudomonas putida* when grown on camphor as the sole carbon source.[3,4] (From this point P450 will be used to denote the oxidized enzyme from the bacterium and $P450_{cam}$ the camphor complexed species unless otherwise noted.) The soluble nature of this cytochrome makes it very attractive for study

as a model of other mono-oxydases. The hydroxylase system consists of a flavoprotein (Ea), and iron-sulfur protein (Eb) and cytochrome P450 (Ec). While other flavoproteins can substitute for Ea,[5] the iron-sulfur protein, putidaredoxin, is quite specific. The first step in the enzymatic degradation of camphor is hydroxylation at the 5-exo position.

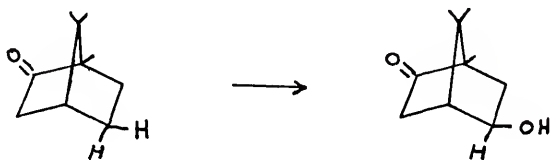

The stoichiometry of the reaction, which is inhibited by carbon monoxide, is

$$NADH + H^+ + O_2 + cam \longrightarrow NAD^+ + H_2O + cam\text{-}OH$$

and the order of electron flow from the reducing agent, nicotinamide adenine dinucleotide to molecular oxygen is:

$$NADH \longrightarrow Ea \longrightarrow Eb \longrightarrow Ec \longrightarrow O_2.$$

However, camphor must be present before Eb reduction of P450 can occur.[5] A ternary complex of reduced P450, O_2 and camphor can be observed spectroscopically,[5,6] but product formation will not occur unless putidaredoxin is present. This complex could be formed independent of the methods, either chemical or enzymatic, used to reduce the iron. Attempts at forming oxy-P450 in the absence of camphor were unsuccessful.

The molecular weight of P450 is 45,000.[7] Each molecule contains one ferriprotoporphyrin IX group,[7] shown in Figure II-1, and a covalently linked carbohydrate group was also found.[5] Isoelectric

Figure II-1. The heme group. Exclusive of the side chains, the ring has 4-fold symmetry. The iron has two sites of coordination remaining (along the axial direction).

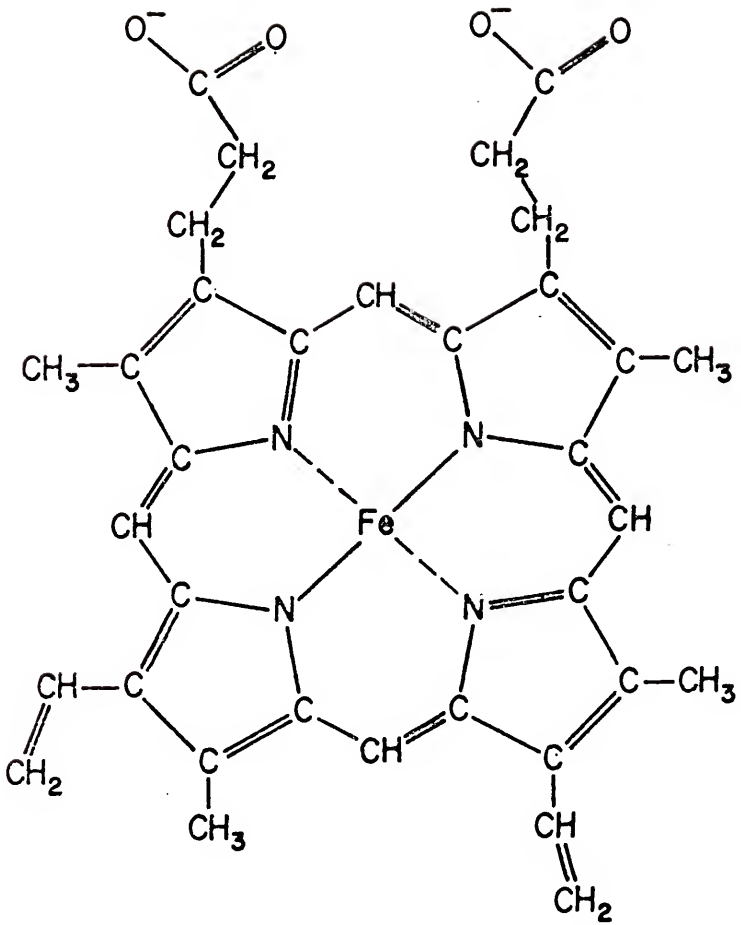
O⁻
O
C
CH2
CH2
C
CH
C
C
CH3
C
C
C
N
N
C
CH
Fe
CH
C
N
N
C
CH
C
C
C
CH3
C
CH
C
CH3
CH2
CH
CH2

points of pH 4.55 for P450 and 4.67 for $P450_{cam}$ have been reported.[8] The UV and visible absorption spectra have been published.[5,8] The spectrum of oxidized P450, in which form the enzyme is isolated, is typical of low spin hemoproteins. Addition of camphor causes a blue shift of the Soret peak (417 mm to 391 mm); this has been assigned as a shift of the iron from low spin to high spin. ESR[9] and Mössbauer[10] studies between liquid nitrogen and liquid helium temperatures have also shown ferric P450 to be low spin and camphor complexed P450 to exist in a high spin/low spin mixture. The binding of carbon monoxide to reduced P450 was found to occur at a slower rate in the presence of camphor by stopped-flow studies.[11] Thus the substrate camphor has a pronounced effect upon the active site of the enzyme, believed to be in a hydrophobic pocket.

As in the case of mammalian systems, denatured P450, i.e., P420, can also be formed. The enzyme has been found to be quite labile at room temperature, although presence of the substrate camphor or certain sulfhydryls, such as cysteine, act as protecting agents. Treatment with acid, acetone or guanidine result in conversion to P420. Activity can be restored by sulfhydryls in certain cases, depending upon time of exposure.[12]

A number of studies have been undertaken to discover the identity of the axial ligands of the iron. ESR[9,13] results and sulfhydryl titration[14] suggest that one ligand may be a sulfur atom from a cysteine residue. It has been postulated that the unusual absorption of reduced P450-CO is from coordination of sulfur and CO in the axial positions.[15] NMR measurements of the relaxation rate of water protons in the bulk solution, which is affected by the iron atom, have shown rapidly

exchanging protons within the coordination sphere of the paramagnetic ion.[14] The presence of an imidazole ring from a histidine residue, as proposed from isoelectric focusing experiments,[8] would be supported by the NMR data. Protons could be exchanged at the 3-nitrogen position while coordination to the iron would be through the 1-nitrogen. CO complexes of the highly studied hemoproteins such as hemoglobin, myoglobin and cytochrome c are known to have an imidazole nitrogen from a histidine residue in the second axial site.

Nitric Oxide as a Spin Probe.

In recent years nitric oxide has been successfully used as a spin probe of the heme environment of a number of hemoproteins. As nitric oxide has an unpaired electron ($^2\Pi$), its complexes with ferrous hemoproteins can be studied by ESR whereas the corresponding complexes of carbon monoxide and oxygen cannot. Examination of the ESR of nitric oxide complexes of cytochrome c,[16] hemoglobin[17] and myoglobin[18] has shown hyperfine splitting which was assigned to both the nitrogen nucleus of the NO molecule and the nitrogen of the second axial ligand, known to be that of an imidazole group.

This work was undertaken to study the interaction of nitric oxide with cytochrome P450 and P420 in an attempt to obtain information as to the identity of the axial ligands of the iron in the porphyrin group.

Materials and Methods

Protein Concentration

Concentrations of P450 and putidaredoxin were determined spectrophotometrically using published extinction coefficients.[5] These

purified enzymes were generously provided by Dr. I. C. Gunsalus of the University of Illinois.

Spectroscopy

Optical absorption, circular dichroism and ESR spectroscopies were described in the previous section. Fourier transform infrared spectra (Digilab) were taken by Dr. P. Callahan (University of Florida). Matched 0.025 mm pathlength Irtran 2 cells were used. Via computer interfacing, a typical difference spectrum was obtained as follows. Sixty scans of the sample were taken and summed. Sixty scans of the reference were also summed and then subtracted from the sample. The conventional spectrum of % transmittance vs wavenumbers was plotted.

Heme Removal

The heme group of any hemoprotein can be removed by the acid ketone method, providing it is not covalently bound. The method call for treatment with acid followed by heme extraction with methylethylketone (MEK).

HCl (0.1 N) is added to a solution of salt-free, ice-cold hemoprotein to pH 2, followed by an equal volume of cold MEK. The solution is swirled for several minutes then allowed to stand in the cold. The mixture will separate into an upper organic layer containing the heme and a lower aqueous phase of protein. The procedure may be repeated at this point to insure complete removal. The aqueous layer is then dialyzed against water to remove dissolved ketone.

Hemin was added to apomyoglobin to insure that the reconstituted protein had the same absorption characteristics as the native. Also

apomyoglobin could be spectrally titrated with hemin by observing the increase at 408 nm to verify that one heme group per molecule was bound.

Preparation of the Hemoprotein-Nitric Oxide Complexes

Nitric oxide gas was purchased from Matheson and was purified immediately before use by passage through a column (0.6 x 20 cm) containing silica gel and potassium hydroxide. Sodium nitrite was from MCB. 99.8% enriched ^{15}N-sodium nitrite was obtained from Prochem. The enzyme solutions were purged under an atmosphere of oxygen-free argon or nitrogen prior to gentle bubbling with NO. Samples for optical studies were sealed in Thunberg cuvettes. Samples for ESR studies were placed in quartz tubes, sealed with parafilm and then frozen in liquid nitrogen.

Results and Discussion

Optical Spectra

Figure II-2 shows the optical spectra of P450-NO complexes. Identical spectra of reduced P450-NO could be obtained either by adding nitric oxide to reduced P450 or by generating NO in solution from sodium nitrite in the presence of excess dithionite. Note that there is a difference in the spectra depending upon whether camphor is present or absent. Absorption maxima and extinction coefficients are given in Table II-1.

It has been shown that nitric oxide can act as a reducing agent toward certain hemoproteins. Ferric hemoglobin[19] plus NO will give

Figure II-2. Optical absorption spectra of complexes of cytochrome P450 and nitric oxide. Solutions are 5.42 μM in heme and are buffered in 50 mM phosphate, pH7.

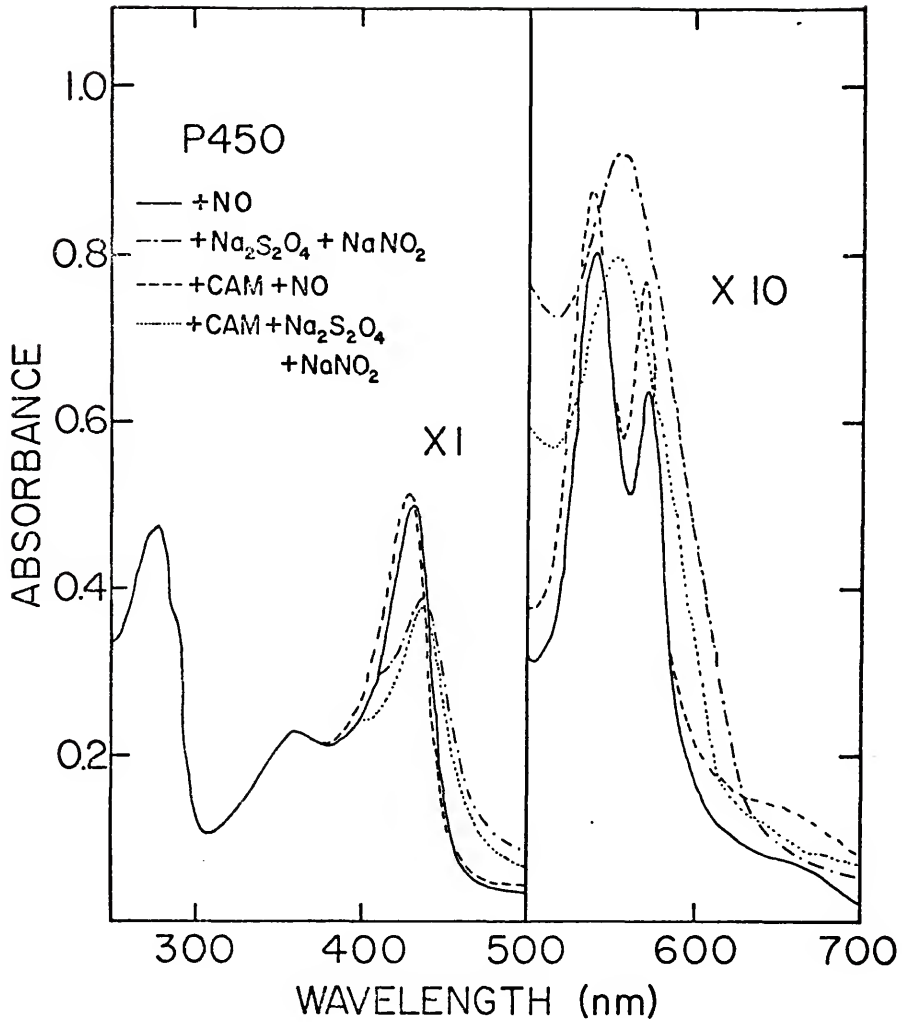
P450
+NO
+Na2S2O4 + NaNO2
+CAM +NO
+CAM +Na2S2O4 +NaNO2
X1
X 10
ABSORBANCE
1.0
0.8
0.6
0.4
0.2
300
400
500
600
700
WAVELENGTH (nm)

Table II-1. Optical data of cytochrome P450 in presence of nitric oxide.

Complex	Absorption Maxima (nm)	Extinction coefficient (mM)
ferric P450-NO	432	92
	538	15
	567	12
ferric $P450_{cam}$-NO	430	95
	537	16
	570	14
ferrous P450-NO	437	72
	558	17
ferrous $P450_{cam}$-NO	436	70
	554	14

ferrous hemoglobin and NO^+; with excess NO present, the net result is reduced Hb-NO. A similar reaction occurs with cytochrome c and NO giving reduced cyt c-NO^+. However, unlike the above example, NO^+ is not liberated and the complex is stable.[20] The visible spectrum of $P450_{cam}$-NO was found to remain unchanged after three hours at room temperature, i.e., no reduction occurred.

When NO solutions were not kept anaerobic, an absorption band at 360 nm would grow in. An optical density of 1 could be obtained in 5 to 20 minutes depending upon the time of exposure to air. As this peak grew in, it gradually resolved itself into a vibrational progression of five easily distinguished bands at 386, 371, 358, 346 and 336 nm. The formation of this new species caused a loss of Soret intensity and occasionally turbidity or protein precipitation. Further experiments showed that this could be formed by bubbling NO through distilled water in air. Keilin[21] has previously reported this species and ruled out the possibility that this could be NO_2. No further attempt at identification was made. A paper on the CD and UV and visible spectra of a number of hemoprotein-NO complexes shows an absorption spectrum containing the progression at 360 nm.[22] No mention was made of this by the authors who presumably thought that it was part of the cytochrome c-NO spectrum.

ESR Spectra at 77° K

The ESR spectrum of P450 contains absorptions with g values of 2.45, 2.26 and 1.91[9] and as mentioned before, the iron is low spin. Addition of camphor gives rise to signals attributed to high spin iron at g = 8, 4 and 1.8 only seen below 20° K, with concomitant decrease, but not complete abolition, of the low spin signals. Hence the assignment of the low spin/high spin mixture. Reduced P450 has no ESR absorption.

When nitric oxide is added to either camphor-free or camphor-bound P450, no ESR signals are seen. The spectra of reduced P450-NO complexes are shown in Figure II-3. The spectra are indicative of a paramagnetic site of rhombic symmetry with g values of 2.08, 2.00 and 1.97. Identical spectra were obtained by adding either nitric oxide (^{14}N, I = 1) or sodium nitrite to dithionite reduced P450. The three lines centered at g = 2 are separated by 20 gauss. ^{15}NO (^{15}N, I = 1/2) was generated from 99.8% enriched $Na^{15}NO_2$. The resulting spectrum contained a central doublet split by 28 gauss. Further splitting can be seen in the high and low field peaks. ESR spectra taken at room temperature were broad and without fine structure. Also present was a sharp signal at g = 2.00, probably from SO_2^-, a decomposition product of dithionite.[23]

Pseudomonas was grown in an ^{57}Fe (I = 1/2) - enriched environment to obtain between 80% and 90% $^{57}P450$ (gift from Dr. I. C. Gunsalus). The spectrum of reduced $^{57}P450_{cam}$-^{15}NO is compared to reduced $^{nat}P450_{cam}$-^{15}NO in Figure II-4. Here the central lines are broadened by about 50%, seen more easily in the inset. The high and low field peaks are also affected, though to a lesser extent.

P420

P420 can be obtained by treating cytochrome P450 with guanidine, acid or exposure to air at room temperature for extended periods. In the latter case the loss of P450 is found to occur over the course of many hours. The conversion to P420 takes days when stored near 0^o. When a solution of P450 is acidified with HCL to around pH 3, a species having broad maximal absorption around 360 nm and no distinct band in the

Figure II-3. Effects of nitrogen isotopic substitution on the ESR spectra of nitric oxide complexes of reduced P450. All spectra were of solutions buffered in 50 mM PO_4, pH7 at 77°K. Typical instrumental settings employed a modulation amplitude of 2.5 gauss and microwave power of 10 mWatts.

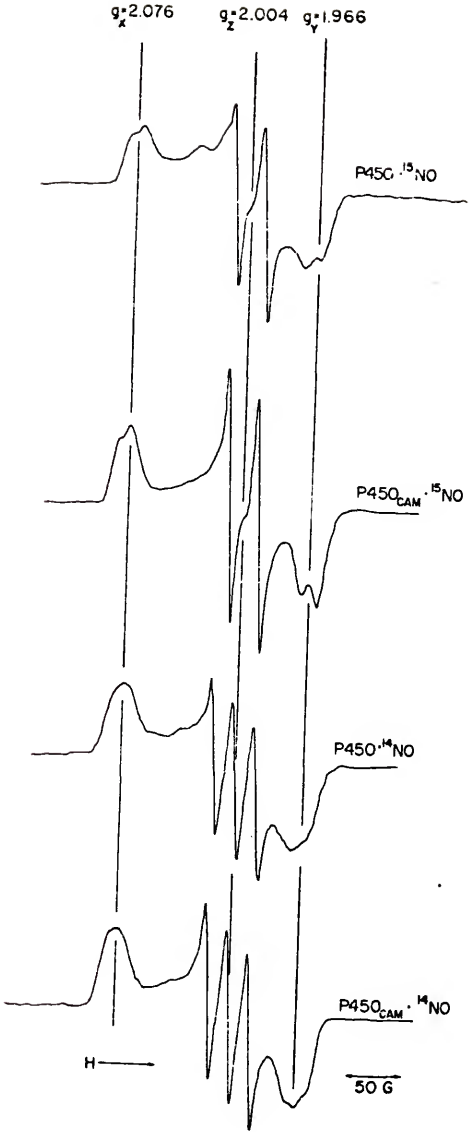
g_x=2.076
g_z=2.004
g_y=1.966
P450·^{15}NO
P450$_{CAM}$·^{15}NO
P450·^{14}NO
P450$_{CAM}$·^{14}NO
H
50 G

Figure II-4. ESR of natural abundance (0.10 mM) and 57-Fe enriched (0.14 mM) reduced cytochrome P450 plus ^{15}NO at 77°K. The upper right-hand corner shows an expanded scan of the central doublet. Experimental conditions are described in the legend to Figure II-3.

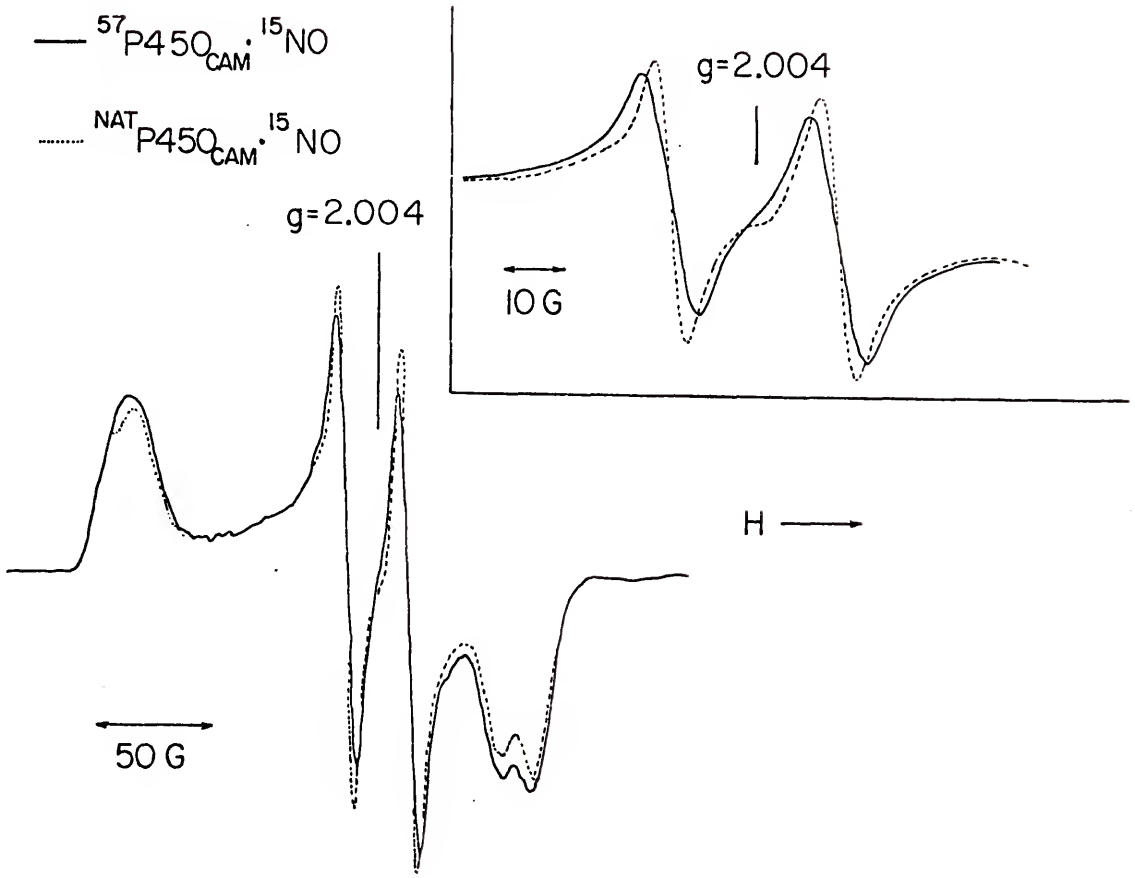
$^{57}P450_{CAM}$ · ^{15}NO
$^{NAT}P450_{CAM}$ · ^{15}NO
g=2.004
50 G
H
g=2.004
10 G

visible region was found and the usual spectrum of P450 was absent. The spectrum in general was similar to that of $P450_{cam}$, i.e., a high-spin species in which the Soret peak has been blue shifted. Such a preparation was neutralized with base and scanned periodically. The 417 nm Soret absorption increased in intensity at the expense of the 360 nm peak. Aliquots of the neutralized solution were withdrawn periodically and the Soret region scanned after addition of dithionite and carbon monoxide. Initially one could find predominately the 420 nm species. The decrease in the 360 nm peak could be correlated with a decrease in 420 nm absorption and an increase in 450 nm absorption upon reduction and addition of CO. If 5 mg/ml of cysteine is added after neutralization, both the yield and the rate of recovery, usually complete in about 15 minutes, of P450 are increased.

ESR of P420-^{15}NO

Figure II-5 is the ESR spectra of reduced P420-^{15}NO. Trace A shows, in addition to the typical spectrum of P450-^{15}NO, a new doublet at g = 2.01, split by 23 gauss. P420 content was estimated to be about 40% from the reduced plus CO visible spectrum. Trace C contains about 80% and trace B nearly 100% P420. The latter spectrum shows axial symmetry with g values of 2.08 and 2.01. As these data indicate a marked change in the iron environment upon denaturation of the enzyme, two further experiments were undertaken.

Heme transfer

It has been reported that heme transfer from P450 to apomyoglobin and hemopexin readily occurs.[24] Apomyoglobin is convenient to use as

Figure II-5. ESR spectra of reduced P420 plus ^{15}NO at $77^{o}K$. A) About 40% P420, B) nearly 100% P420, C) About 80% P420. Note that the abscissa of C is of a different scale than A and B.

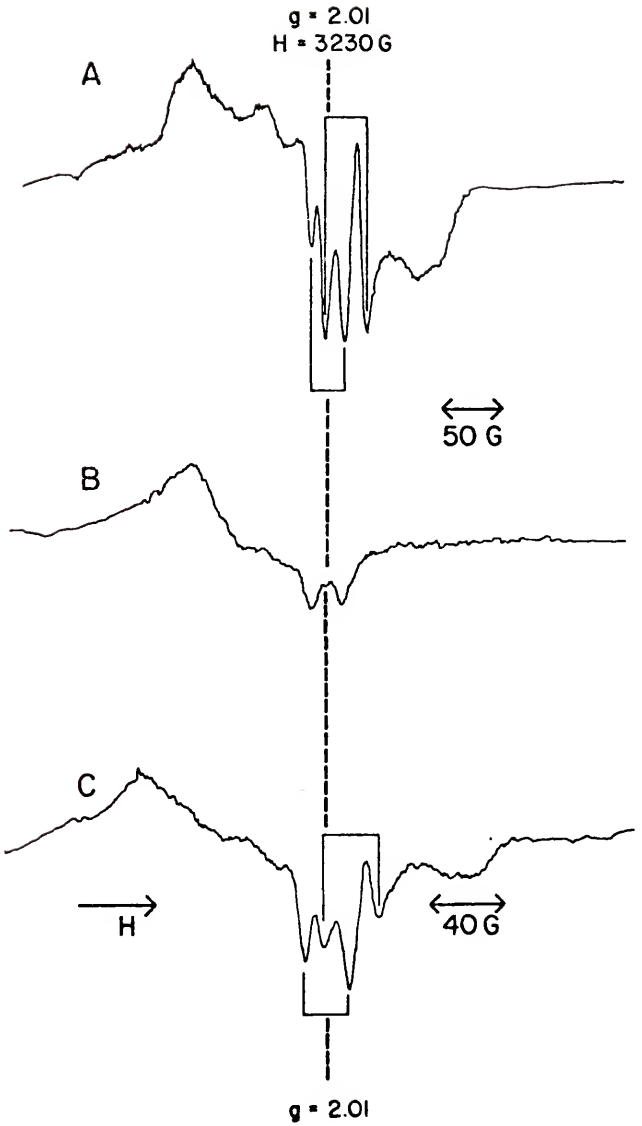
g = 2.01
H = 3230 G
A
50 G
B
C
H
40 G
g = 2.01

it does not absorb in the visible region. When P450 and apoMb are mixed, the transfer of heme can be followed by observing the increase in absorption at 408 nm, the wavelength at which holomyoglobin absorbs maximally (the molar extinction coefficient being 160,000).[25] At room temperature, heme transfer from P450 to apoMb was reported to reach equilibrium after about 20 minutes. Although, no estimation was made of P420 content, the published spectrum[24] of the cytochrome had an absorption at 360 nm nearly as intense as the Soret peak. Thus it appears as though the P450 used contained an appreciable amount of P420. The authors noted almost complete disappearance of the 360 nm peak upon incubation with apoMb.

In this work, transfer of heme from P450 to apoMb at room temperature was determined in either of two ways. In one, apomyoglobin was added to solutions containing the cytochrome and the mixture scanned periodically. Formation of holomyoglobin was indicated either as a new peak absorbing around 408 nm or as a blue shift in the P450 Soret peak (417 nm), which results from the superposition of the 408 nm and 417 nm Soret maxima. Controls, solutions containing no apoMb, were used to determine P420 formed as the reduced plus CO species. In the second method, the P450/apoMb mixture was passed through a column (1.2 x 65 cm) of Sephadex G-50 after a suitable incubation at room temperature. The absorption at 280 nm and in the Soret region of the eluted fractions was compared to the ratio of 280 nm to Soret absorption prior to mixing. An increase of A280/Asor indicated a loss of the heme chromophore and vice versa. The results are summarized as follows: (i) Mixtures initially high in P420 content showed a greater amount of heme transfer than mixtures having little P420. (ii) In solutions

of nearly 100% P450, transfer occurred very slowly (days at 0^{o} C) and followed P420 formation as determined by controls. (iii) Solutions containing either camphor or cysteine, which protect against P450 denaturation, showed decreased heme transfer compared to solutions lacking these.

Circular dichroism

Circular dichroism spectra of the enzyme have been reported.[26] In this work the CD spectra of P450/P420 mixtures were recorded in the Soret region and the strength of the negative CD band at 417 nm was measured against the amount of P420 present. As the ratio of P450 to P420 decreased, the intensity of the CD absorption decreased. These results were extrapolated to a complete lack of CD absorption upon 100% conversion to P420.

Difference IR

The usefulness of infrared spectroscopy as applied to aqueous solutions of carbonyhemoglobins has been demonstrated by Alben and Caughey.[27] In subsequent studies on the effect of isotopic substitution on the observed frequencies of the C-O stretch in carboxyhemoglobin, it was deduced that the ligation of CO to the iron was through the oxygen atom.[28] In the case of oxyhemoglobin[29] and oxymyoglobin,[30] the data indicated an axial, non-linear Fe-O-O bond, rather than the oxygen lying perpendicular to the heme plane. The method is restricted to infrared bands which lie within a "window" from about 1750 to 2800 wavenumbers for aqueous protein solutions.[31] Required are a pair of matched IR cells, preferably calcium fluoride or Irtran 2, which are

not easily dissolved by water and can also be used in taking visible absorption spectra. The optical pathlength is generally 0.025 mm. Cells with longer pathlengths are difficult to use in that too little light gets through the cell, intensity being lost to water absorption. Typical protein concentrations vary from 0.005 M to 0.02 M. The sample cell contains the hemoprotein and ligand to be studied; the reference cell contains only hemoprotein. Thus the net absorption will be due to the ligand only. The use of Fourier transform infrared was appealing as no provision for jacketing the cells to provide cooling was necessary since the cells do not become heated as in conventional IR. A spectrum of the region of interest could be taken at a resolution of 2 wavenumbers in about 10 minutes. As an initial test one Irtran cell was filled with 0.004 M reduced hemoglobin and another with reduced hemoglobin plus CO. The difference spectrum showed the C-O stretch to be at 1952 wavenumbers in agreement with the value of 1951 wavenumbers previously published.[32]

The success obtained with carbonylhemoproteins prompted this preliminary study of nitrosylhemoproteins. The N-O stretch of nitric oxide gas is at 1878 wavenumbers.[33] Upon complexing with iron, back-bonding from the metal would increase the electron density in the lowest lying orbital of the ligand which is an antibonding π. Thus the stretching frequency of metal-NO complexes would be expected to be less than that of free nitric oxide. The stronger the metal-ligand bond, the weaker the N-O bond becomes. A reduction in bond order of about 0.5 has been reported for oxygen and carbon monoxide bound to hemoproteins.[28]

Nitrosylcytochrome c was chosen to be the first NO-hemoprotein to be studied because it is more stable than the hemoglobin or myoglobin analogs. 250 mg of cytochrome c from horse heart (Grade IV, Sigma) was dissolved in a final volume of about 0.8 ml (0.02 M) of 50 mM phosphate buffer, pH 7. Nitric oxide was added in the usual manner. The IR difference spectrum from 2500 to 1700 wavenumbers contained no absorption. The experiment was repeated but D_2O replaced water, and DCl and K_2HPO_4 were used to prepare the buffer. D_2O has less absorption than water at lower energy. However, the region examined was still without absorption. Thus the N-O stretch probably lies below 1700 wavenumbers. Though no details were given, Barlow et al. reported a value of 1670 wavenumbers for pyridine-protoheme-NO and 1615 wavenumbers for NO-HbA.[27] The large amount of protein necessary to do this experiment coupled with the possibility of getting no absorption prevented the IR examination of the P450-NO complex.

Conclusions

The reaction of oxidized P450 with nitric oxide will result in either an S = 2 state (four unpaired electrons) or a diamagnetic molecule in the case of strong crystal fields. The former case will be unlikely to give rise to paramagnetic resonance at X-band. Kramers' theorem, that an electrostatic field cannot reduce degeneracy below two, does not apply to even-spin systems. That is, even in the absence of a magnetic field, the degeneracy of spin states may be completely removed. A shifting of the relative energies of the

nondegenerate levels would occur in the presence of a magnetic field. One would not observe an ESR spectrum if the resulting separation of these states is greater than that of the microwave quantum. In other cases, some of the allowed transitions could occur and the ESR spectrum should be seen to be very anisotropic.[34] The optical absorption of oxidized P450 plus NO indicates low spin iron as the spectrum is typical of that of low spin hemoprotein complexes which have a red-shifted Soret band and no absorption peaks around 650 nm.[35]

The ESR spectra of ferrous hemoprotein-NO complexes have been analyzed by Kon and Kataoka,[36] who studied model complexes of NO, protoheme and nitrogenous bases such as pyridine, quinolines and imidazole. If liquid, the base itself was used as solvent. Otherwise the base was dissolved to near saturation in a solvent such as dimethyl sulfoxide or chloroform, depending upon polarity requirements. Addition of hemin was followed by NO and the ESR spectra were taken at 77° K. Although more than one type of species is present in such a mixture, the complex observed would be that of base-heme (Fe^{+2})-NO. In some cases the NO nitrogen hyperfine lines around g = 2.0 were well resolved, but in other cases they were not. The shape of the spectrum obtained when γ-picoline was used as the base was similar to that of Hb-NO. Splitting not only from the nitrogen of nitric oxide was apparent but also the nitrogen of picoline. Several of the spectra contained sharp NO-nitrogen hyperfine lines, but no further splitting. No simple relationship could be found between the basicity of the nitrogenous compound and the type of spectrum obtained.

The anisotropic contribution of the pyrrole nitrogens of the porphyrin ring is expected to be minimal when the external magnetic

field is parallel to the heme normal and likewise the absorption should be narrow. Thus the well-resolved nitrogen hyperfine lines centered at g = 2.004 in P450-NO can be assigned to g_z, where the z-axis is taken to be perpendicular to the heme plane. The low and high field peaks have then been assigned as g_x and g_y. That the splitting observed is due to the nitrogen nucleus of nitric oxide is certain from the isotopic substitution: ^{14}NO gives a triplet, ^{15}NO a doublet. The ratio of the total splitting in gauss, $^{14}N/^{15}N$ = 2 x 20/28 = 1.4, agrees well with the absolute value of the ratio of the magnetic moments of the two nuclei.[37] The spectra of P450-NO with camphor present also show hfs in the high field peak with splitting ratio $^{14}N/^{15}N$ = 2 x 10/14 = 1.4. Generally, the hfs in the high and low field peaks were not well resolved.

One can observe a shift of g_y towards free spin in the camphor-free as compared to the camphor-bound form; the effect was reproducible and thus not an artifact. A difference in the absorption spectra was also noted in P450-NO complexes and in reduced P450-CO complexes[26] between camphor-free and camphor-bound forms. As g values will deviate from free spin with increasing spin-orbit coupling, one can say that the presence of substrate camphor in solutions containing P450-NO affects the energy separation of the molecular orbital of the unpaired electron and the orbitals coupled to it.

Mössbauer evidence has shown that the iron of reduced P450 is high spin and may be pentacoordinate.[38] Results of high resolution nmr[39] also suggested the presence of only one axial ligand, as is known to be the case for the reversible oxygen binding hemoproteins

myoglobin[40] and hemoglobin.[41] An experiment was carried out with a sample of P450 to which 1) addition of NO was followed by dithionite and 2) the iron was first reduced with dithionite and then NO was added. No difference in the ESR spectra was apparent. Nitric oxide must bind at the same site irrespective of whether coordination is to ferrous or ferric iron.

As to the identity of the second axial ligand in the NO complexed P450, the data are not definitive. The lack of superhyperfine splitting does not preclude its presence. Further hyperfine may not be observable due to low spin density or fast relaxation. As noted in the work with model complexes of nitrogenous bases, super hfs was not always found. If sulfur is the remaining ligand contributed by the protein, one might expect an entirely different spectrum, as sulfur can form δ bonds. However, the spectra shown in Figure II-3 are very similar to those of other hemoprotein-NO complexes. The spectrum of reduced horseradish peroxidase plus ^{15}NO is shown in Figure II-6. If it is the interaction of the π orbitals of the second axial ligand with the iron d orbitals which breaks down the symmetry in the x- and y-directions, as postulated by Kon and Kataoka,[36] it is tempting to say that the ligand present in HRP-^{15}NO, thought to be the imidazole group from a histidyl residue,[18] is the same ligand as in P450-NO. NO itself is not the cause of the rhombicity as seen in the axial P420-NO spectra. Perhaps ESR measurements near liquid helium temperatures would sharpen the spectrum sufficiently to allow additional lines to be resolved. ESR spectra of microsomal P450 plus NO are somewhat different from that found above.[42,43]

Figure II-6. The ESR spectrum of reduced horseradish peroxidase plus ^{15}NO at 77°K.

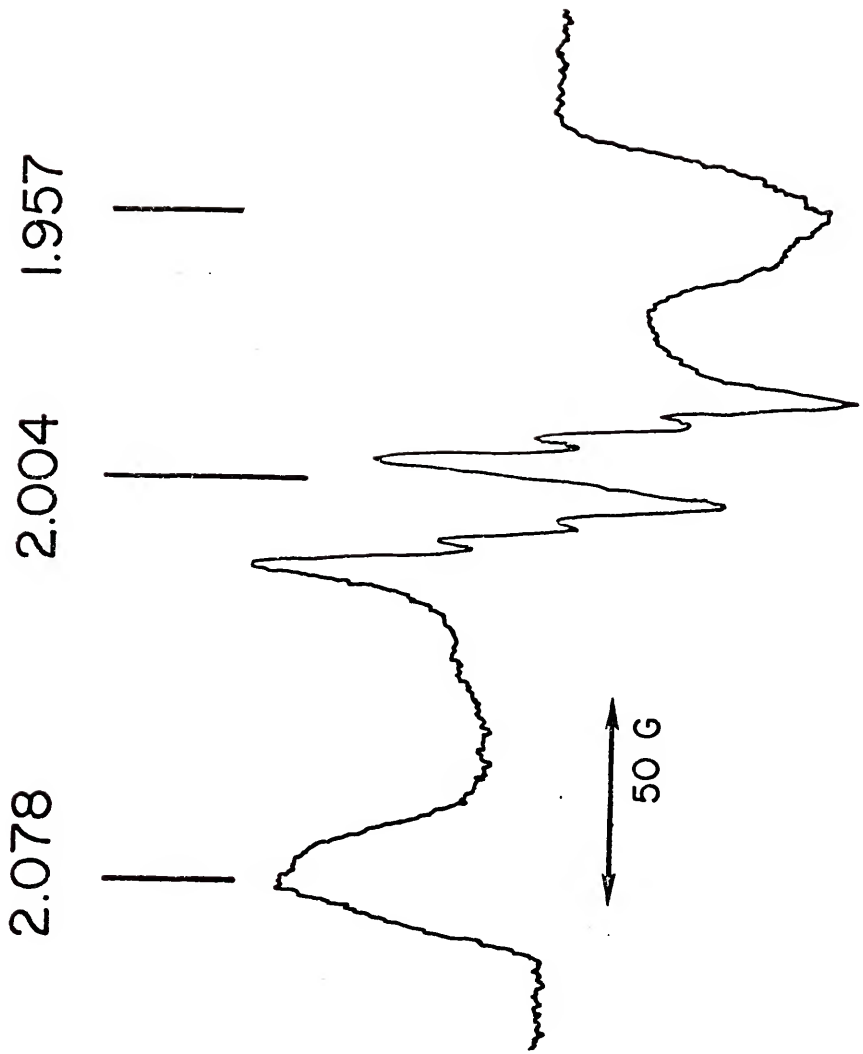
2.078
2.004
1.957
50 G

P420

The ESR of reduced P420-^{15}NO is seen to be of axial symmetry. The spectrum is similar to that of SDS treated Hb plus NO,[17] where the protein structure is "relaxed", and also to that of imidazole, protoheme and NO in DMSO.[34] In the latter, the porphyrin group is in a polar environment. The heme transfer experiments also demonstrate that conversion of P450 to P420 is accompanied by a decreased affinity of the protein for the heme. Studies on the heme transfer from microsomal P450 to albumin suggests, that while heme is released from P420, it is not transferable from P450.[44] The CD data may be approached as follows. Because of its symmetry, porphyrin alone is not optically active. However, Cotton effects are induced upon binding to the protein from heme-protein interactions. The magnitude and sign of these effects have been found by theoretical calculations to be affected by coupling to aromatic groups from the protein side chains.[45] Thus the decrease in Soret CD absorption intensity with increasing P420 content indicates a decrease in the interaction of the heme group with the protein. P420 certainly consists of more than one species since varying amounts of activity can be restored depending upon age of the P420 preparation. However, this study indicated the conversion of P450 to some forms of P420 is accompanied by decreased affinity of the protein for the heme group and a decrease in the hydrophobicity of the heme binding site.

References

1. Klingenberg, M., Arch. Biochem. Biophys. 75, 376 (1958).

2. Garfinkel, D., Arch. Biochem. Biophys. 77, 493 (1958).

3. Katagiri, M., Ganguli, B. N., and Gunsalus, I. C., Fed. Proc. 27, 525 (1968).

4. Katagiri, M., Ganguli, B. N., and Gunsalus, I. C., J. Biol. Chem. 243, 3543 (1968).

5. Tyson, C. A., Lipscomb, J. D., and Gunsalus, I. C., J. Biol. Chem. 247, 5777 (1972).

6. Peterson, J. A., Ishimura, Y., and Griffin, B. W., Arch. Biochem. Biophys. 149, 197 (1972).

7. Yu, C-A., and Gunsalus, I. C., J. Biol. Chem. 249, 94 (1974).

8. Dus, K., Katagiri, M., Yu, C-A., Erbes, D. L., and Gunsalus, I., C., Biochem. Biophys. Res. Comm. 40, 1423 (1970).

9. Tsai, R., Yu, C-A., Gunsalus, I. C., Peisach, J., Blumberg, W., Orme-Johnson, W. H., and Beinert, H., Proc. Nat. Acad. Sci. 66, 1157 (1970).

10. Sharrock, M., Münck, E., Debrunner, P. G., Marshall, V., Lipscomb, J. D., and Gunsalus, I. C., Biochem. 12, 258 (1973).

11. Peterson, J. A., and Griffin, B. W., Arch. Biochem. Biophys. 151, 427 (1972).

12. Yu, C-A., and Gunsalus, I. C., J. Biol. Chem. 249, 102 (1974).

13. Bayer, E., Hill, H. A. D., Röder, A., and Williams, R. J. P., Chem. Comm., 109 (1968).

14. Peterson, J. A., and Griffin, B. W., Drug Metab. Disp. 1, 14 (1973).

15. Peisach, J., Stern, J. O., and Blumberg, W. E., Drug. Metab. Disp. 1, 45 (1973).

16. Kon, H., Biochem. Biophys. Res. Comm. 35, 423 (1969).

17. Kon, H., J. Biol. Chem. 243, 4350 (1968).

18. Yonetani, T. Yamamoto, H., Erman, J. E., Leigh, J. S., Jr., and Reed, G. H., J. Biol. Chem. 247, 2447 (1972).

19. Chien, J. C. W., J. Amer. Chem. Soc. 91, 2166 (1969).

20. Ehrenberg, A., Szczepkowski, T. W., Acta. Chem. Scand. 14, 1684 (1960).

21. Keilen, J., Biochem. J. 59, 571 (1955).

22. Bolard, J., Garnier, A., C. R. Acad. Sci. Paris C. 272, 732 (1971).

23. Atkins, P. W., Horsfield, A., and Symmons, M. C. R., J. Chem. Soc., 5220 (1964).

24. Muller-Eberhard, U., Liem, H. H., Yu, C-A., and Gunsalus, I. C., Biochem. Biophys. Res. Comm. 35, 229 (1969).

25. Breslow, E., J. Biol. Chem. 239, 486 (1964).

26. Peterson, J. A., Arch. Biochem. Biophys. 144, 678 (1971).

27. Alben, J. O., and Caughey, W. S., Hemes and Hemoproteins (Chance, B., Estabrook, R. W., and Yonetani, T., eds.), p. 319. Academic, New York, 1966.

28. Alben, J. O., and Caughey, W. S., Biochem. 7, 175 (1968).

29. Barlow, C. H., Maxwell, J. C., Wallace, W. J., and Caughey, W. S., Biochem. Biophys. Res. Comm. 58, 91 (1973).

30. Maxwell, J. C., Volpe, J. A., Barlow, C. H., and Caughey, W. S., Biochem. Biophys. Res. Comm. 58, 166 (1974).

31. McCoy, S., and Caughey, W. S., Biochem. 9, 2387 (1970).

32. Caughey, W. S., Biochem. 8, 59 (1969).

33. Nakamoto, K., Infrared Spectra of Inorganic and Coordination Compounds, p. 78. John Wiley and Sons, New York, 1963.

34. Wertz, J. E., and Bolton, J. R., Electron Spin Resonance: Elementary Theory and Practical Applications, chapter 10. McGraw-Hill, New York, 1972.

35. Hill, H. A. O., Röder, A., and Williams, R. J. P., Structure and Bonding 8, 123 (1970).

36. Kon, H., and Kataoka, N., Biochem. 8, 4757 (1969).

37. Weast, R. C., ed., Handbook of Chemistry and Physics, 51st. edition, p. E-75. CRC, Cleveland, 1970.

38. Sharrock, M. P., Ph.D. thesis (1973).

39. Keller, R. M., Wuthrich, K., and Debrunner, P. G., Proc. Nat. Sci. 69, 2073 (1972).

40. Nobbs, C. L., Watson, H. C., and Kendrew, J. C., Nature 209, 339 (1966).

41. Perutz, M. F., Nature 228, 226 (1970).

42. Miyake, Y., Gaylor, J. L., and Mason, H. S., J. Biol. Chem., 243, 5788 (1968).

43. Miyake, Y., Mori, K., and Yamano, T., Arch. Biochem. Biophys. 133, 318 (1969).

44. Maines, M. D., and Anders, M. W., Drug. Metab. Disp. 1, 293 (1973).

45. Hsu, M-C., and Woody, R. W., J. Amer. Chem. Soc. 93, 3515 (1971).

III. ELECTRONIC QUENCHING OF Al AND Ga ATOMS ISOLATED IN RARE GAS MATRICES

Introduction

Various atoms trapped and isolated in rare gas matrices have been investigated in the last decade,[1] starting with the optical work of McCarty and Robinson[2] and the ESR (electron spin resonance) work of Jen, Foner, Cochran and Bowers.[3] By using these techniques, it had been hoped that the states of the free atoms would be modified by the matrix cage only to a minor extent; in general, severe matrix perturbations were observed, however.[1] While the correlation of the observed optical bands with gas phase data in most cases allowed an identification of the trapped atom in question, detailed information about the nature of the trapping site and the interaction with the surrounding rare gas cage was usually not accessible. In all cases complexities such as multiple trapping sites, low symmetry of trapping sites, large linewidths of individual transitions, and presence of impurities or dimerization products made a straightforward analysis of the experimental results impossible. With the exception of a recent paper by Brewer and Chang[4] on matrix isolated Pb atoms, the reported optical data deal almost exclusively with the np $\leftarrow$ ns resonance transition of metals which have an outermost singly or doubly occupied ns shell in their electronic ground state (alkali metals, alkaline earths, Group IIb metals, transition metals).

ESR has been shown to be a powerful tool for elucidating details of the electronic structure of molecules and ions in crystals and in solutions, especially in systems with one unpaired electron exhibiting partial p, d or f character. Because ESR transitions depend only on properties of the electronic ground state, exhibit very narrow lines in diluted samples, and are very sensitive to small changes in the environment of the paramagnetic species, this method should be ideally suited for clarifying the nature of the trapping sites of matrix isolated atoms. Unfortunately, available ESR data of atoms or ions in rare gas matrices[5-9] exclusively relate to isotropic Zeeman parameters (g values) of orbitally nondegenerate (S-state) species. No ESR signals from atoms with nonzero orbital angular momentum in rare gas matrices have ever been reported, although they have been thoroughly searched for in several cases.[3] The failure to observe ESR transitions of atoms with orbitally degenerate ground states in matrices has been explained in terms of anisotropic matrix fields which broaden the resonance beyond recognition.[3]

Due to the difficulties involved in the interpretation of the very small g shifts (Δg) in the case of the previously studied atoms with single unpaired s electrons or half-filled shells, the ESR method has contributed very little beyond an unambiguous identification of the trapped species (by its characteristic hyperfine pattern) and a clear distinction between different sites. It appears that little information about the actual site symmetry of the investigated ^2S atoms can be obtained from the ESR data reported so far. This main effect of noncubic components in the rare gas potential would consist of small

p, d or f admixtures to the singly occupied s orbital. Typical coefficients should be of the order 0.1 to 0.01, corresponding to less than 1% p, d or f character. If these anisotropic contributions to the hyperfine tensor are estimated from $\langle r^{-3} \rangle_{nl}$ parameters calculated from atomic Hartree-Fock wavefunctions,[10,11] it turns out that they would hardly exceed the experimental line width (typically of the order of 1 G) and therefore would remain undetectable. For this reason apparently isotropic ^2S state atomic ESR spectra do not necessarily imply an octahedrally symmetric site.

Data from matrix isolation of Group III metal atoms (B, Al, Ga, In, and Tl) sharing the common property of an s^2p^1 electron ground configuration would be of interest. Due to their single unpaired p electron outside closed shells, these atoms are extremely reactive and form strong chemical bonds with all atoms of the periodic system except the rare gases.

This work contains optical and ESR data for the Group III metal atoms Al and Ga isolated in rare gas matrices. This constitutes the first successful ESR analysis of matrix-isolated atoms in orbitally degenerate ground states, and it will be shown that the ESR method is a more efficient tool for deriving useful information about the nature of the occupied site of these $^2P_{1/2}$ atoms than in the case of S-state atoms. Here all the interesting splitting effects, which in the case of the S-state atoms take place in the excited state only, occur in the ground state and strongly influence the ESR spectra. It will also be shown that ESR signals observed in this laboratory by Knight, Easley, and Weltner,[12,13] first ascribed to AlO and later tentatively to a weakly bonded molecular complex "Al-X", in fact originated from matrix-isolated aluminum atoms.

Materials and Methods

Successful ESR experiments at 4.2° K were performed for Al in Ar and Ga in Ar, Kr and Xe. For Ga in Ar and Kr, ESR spectra were also recorded at higher temperatures. After the identification of the aluminum ESR spectra in argon as the Al-X spectra reported by Knight and Weltner,[13] no further ESR experiments on Al atoms were attempted. ESR experiments for In in Ar and Xe, and for Ga in Ne were unsuccessful; no signals attributable to matrix-isolated metal atoms could be obtained in these cases.

Optical spectra in the range 2000-8000 Å were taken for Al and Ga in all four rare gas matrices at several temperatures. The doped matrices were prepared in the usual manner on a CaF_2 window for the optical studies and on a flat sapphire rod for the ESR work. The furnace, the Dewar, the X-band ESR apparatus and the optical spectrometer have been described previously.[14-16] For the visible region (8000-3600 Å) a tungsten lamp source was used; the UV region (3700-2000 Å) was investigated by using a deuterium lamp source and an RCA 7200 photomultiplier. Interchangeable gratings with blaze appropriate for each spectral region were calibrated with mercury emission lines.

Aluminum rods (99.999% pure from Spex. Co., Inc.) were vaporized from resistance-heated tantalum cells (1 inch long, 0.03 inch wall thickness) through an effusion hole 1/16 inch in diameter. For both gallium samples (slugs, 99.99% pure from Fisher Scientific Company) and indium samples (wire, 99.99% pure from Indium Corp. of America), graphite cells of the same dimensions were used. All cell temperatures were measured with a calibrated optical pyrometer using approximate corrections for emissivity. No attempts have been made to calculate the

metal to rare gas ratios accurately. Instead the cell temperatures were varied over a wide range (~400°) until optimum conditions for optical and ESR experiments were achieved.

Convenient evaporation cell temperatures for optimum ESR conditions were typically some 150° higher than the corresponding temperatures for optimum optical conditions. For aluminum, 1200° was finally used for ESR experiments and 1050° for optical experiments; for gallium, the corresponding temperatures were 1175° and 1020°. A crude estimate of the metal concentrations gives a few tenths of a percent for the best ESR spectra and about 10 times less for the best optical spectra. No ESR spectra were observed at the dilute optical conditions. This and other reasons led Knight and Weltner[13] to the conclusion that their ESR spectra could not be satisfactorily ascribed to matrix-isolated Al atoms. In contrast, from the present investigation it is concluded that both the optical and the ESR signals should be ascribed to the same species, i.e., to matrix-isolated Al and Ga atoms. The fact that unusually high metal concentrations are necessary for obtaining reasonable ESR spectra can be explained by the large spread of the spectra and by the large linewidths (see last column of Tables III-5 and III-6). The following experimental observations support this assignment: (i) Optimum ESR matrices were still transparent, i.e., colorless to light green. When the concentration was increased further, the matrices assumed a deep green color; new ESR signals appeared in the g = 2 region while the intensity of the original spectra apparently showed no further significant increase. (ii) No changes in the ESR line positions were observed when the metal concentration was decreased until the spectra were too weak for observation. (iii) When higher than optimum concentrations for

the optical studies were used, the strongest bands gained further in intensity, while other peaks which were very weak or nondetectable in dilute runs reached considerable strength. This indicates that under both optimum ESR and optimum optical conditions the same species was predominant.

Results

Optical Spectra

The ultraviolet spectra of aluminum and gallium atoms isolated in all four rare gas matrices are shown in Figures III-1 and III-2; the corresponding band maxima are given in Tables III-1 and III-2.

Figure III-3 illustrates the strongly allowed electronic transitions from the ground state of free Group III atoms (approximately to scale for gallium) together with the expected modifications in cubic or axially distorted cubic matrix fields. In the Hartree-Fock approximation these "resonance lines" correspond to one-electron jumps from the singly occupied np shell into the empty nd and (n+1) s shells (n = 3 for Al; n = 4 for Ga). As can be seen from the bottom of Tables III-1 and III-2, the $^2D \leftarrow {}^2P$ transition is located approximately at 3000 Å, and the $^2S \leftarrow {}^2P$ transition approximately at 4000 Å for both aluminum and gallium atoms. From the close similarity of the Hartree-Fock valence orbital radii (Table III-3) of aluminum and gallium, the resemblance of the spectra of the matrix isolated atoms (Figures III-1 and III-2) is not surprising.

From a comparison of the observed bands with the free atom transition energies and an examination of their matrix dependence, the long wavelength part of the spectra has to be assigned to the $^2S \leftarrow {}^2P$

Figure III-1. Electronic absorption spectra of matrix-isolated aluminum atoms at 4.2°K; (a) neon matrix, (b) argon matrix, (c) krypton matrix, (d) xenon matrix. Absorption intensities increase from bottom to top. The bands assigned to the $^2S \leftarrow ^2P$ resonance transition are indicated with an arrow.

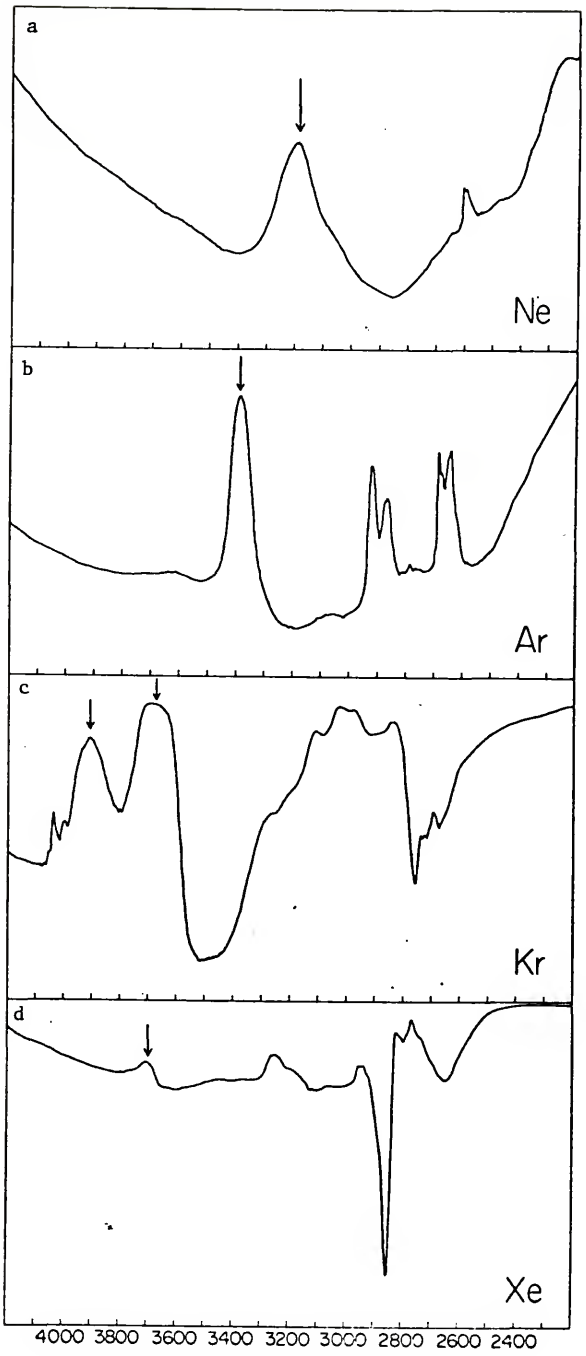
a
Ne
b
Ar
c
Kr
d
Xe
4000 3800 3600 3400 3200 3000 2800 2600 2400

Figure III-2. Electronic absorption spectra of matrix-isolated gallium atoms at 4.2°K. Explanations are given in Figure III-1.

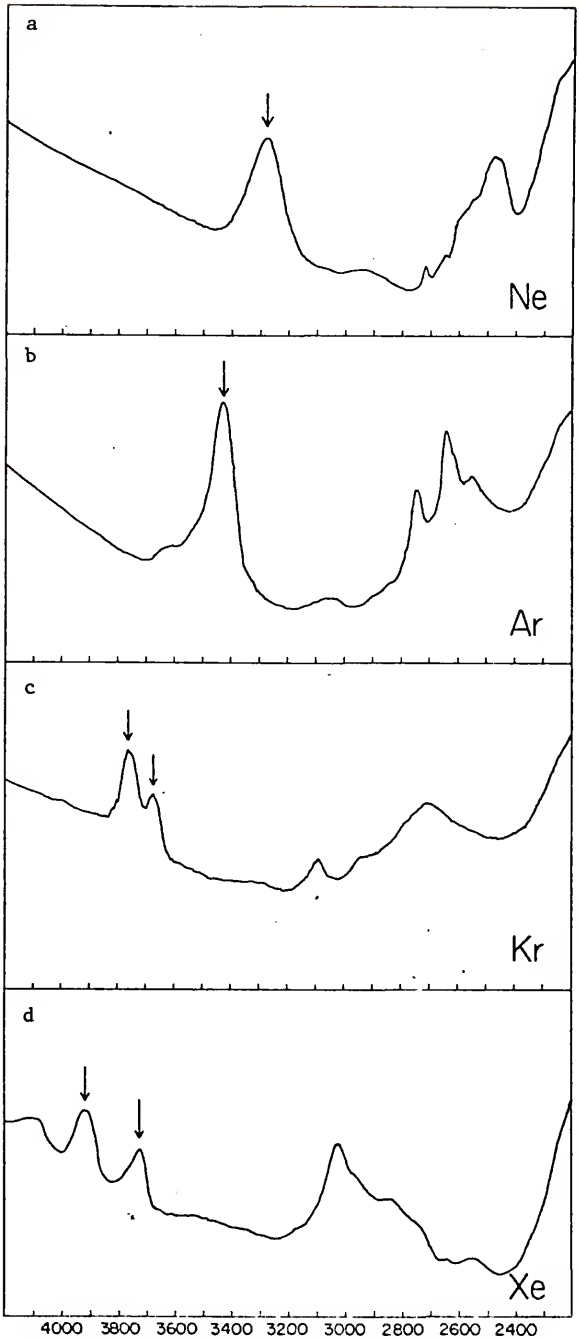
a
Ne
b
Ar
c
Kr
d
Xe
4000 3800 3600 3400 3200 3000 2800 2600 2400

Table III-1. Optical absorption spectra of Al atom in rare gas matrices.

System	$4s(^2S) \leftarrow 3p(^2P_{1/2})$		$3d(^2D) \leftarrow 3p(^2P_{1/2})$	
	λ(Å)	$\tilde{\nu}$(cm^{-1})	λ(Å)	$\tilde{\nu}$ (cm^{-1})
Ne Matrix	3200	31,250	2605	38,390
4.2°K			2595	38,540
	3390	29,500	2922	34,220
Ar Matrix			2867	34,880
4.2°K			2685	37,240
			2641	37,860
	3910	25,580	3270	30,580
	3680	27,170	3110	32,150
			3030	33,000
Kr Matrix			2970	33,670
4.2°K			2840	35,210
			2740	36,500
			2725	36,700
			2695	37.100
	3705	26,990	3254	30,730
			3180	31,440
Xe Matrix			(3055)	(32,730)
4.2°K			(2940)	(34,010)
			2821	35,440
			2809	35,600
free atom[a] (gas phase)	3944.03	25,348	3082.16	32.435

[a] From Refs. 17 and 18.

Table III-2. Optical absorption spectra of Ga atoms in rare gas matrices.

System	$5s(^2S) \leftarrow 4p(^2P_{1/2})$		$4d(^2D) \leftarrow 4p(^2P_{1/2})$	
	λ(Å)	$\tilde{\nu}$(cm^{-1})	λ(Å)	ν(cm^{-1})
Ne Matrix	3275	30,530	2920?	34,240?
4.2°K			2690	37,170
			2480	40,320
Ar Matrix	3430	29,150	2747	36,400
4.2°K			2644	37,820
			2553	39,170
Kr Matrix	(3980)	(25,120)	3085	32,410
4.2°K	3752	26,650	2920	34,240
	3667	27,270	2700	37,030
Xe Matrix	(4100)	24,390	3025	33,050
4.2°K	3950	25,310	2835	35,270
	3720	26,880	(2740)	(36,490)
free atom[a]	4032.98	24,788	2874.24	34,781.7
(gas phase)				34,788.0

[a] From Refs. 17 and 18.

Figure III-3. Simplified energy level diagram and resonance transitions of Group III metal atoms in octahedral and tetragonally distorted octahedral matrix fields. Strongly allowed electric dipole transitions from the ground level are indicated by the solid arrows. The diagram is approximately to scale for gallium in an argon matrix.

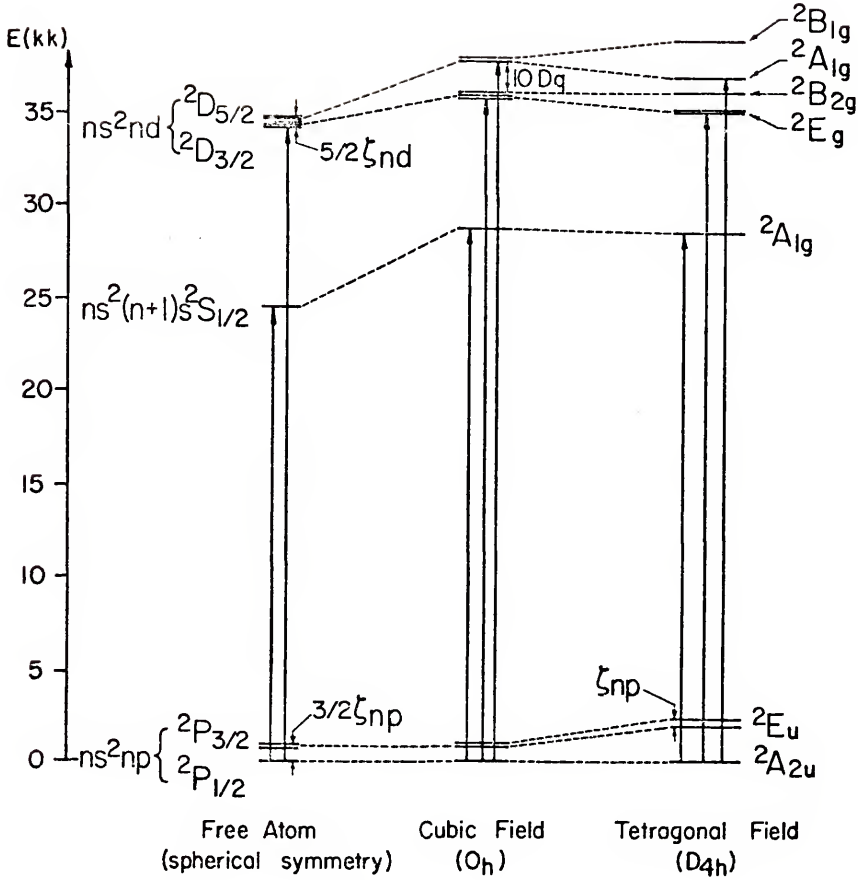
E(kk)
35
30
25
20
15
10
5
0
$ns^2nd\{^2D_{5/2}$
$^2D_{3/2}$
$5/2\zeta_{nd}$
$ns^2(n+1)s\,^2S_{1/2}$
$ns^2np\{^2P_{3/2}$
$^2P_{1/2}$
$3/2\zeta_{np}$
10 Dq
ζ_{np}
$^2B_{1g}$
$^2A_{1g}$
$^2B_{2g}$
^2E_g
$^2A_{1g}$
^2E_u
$^2A_{2u}$
Free Atom
(spherical symmetry)
Cubic Field
(O_h)
Tetragonal Field
(D_{4h})

Table III-3. Average radii of the valence orbitals of some atoms with an outermost p shell.[a]

Atom	n^b	$\langle r \rangle_{ns}$	$\langle r \rangle_{np}$	$\langle r \rangle_{(n-1)d}$
B	2	1.977	2.204	-
Al	3	2.599	3.434	-
Ga	4	2.489	3.424	0.7879
In	5	2.844	3.778	1.1569
Tl	6	2.967	3.926	1.3412
N	2	1.332	1.409	-
P	3	1.932	2.322	-
As	4	2.030	2.512	0.6674
Sb	5	2.390	2.901	1.0164
Bi	6	2.544	3.085	1.2059
Pb	6	2.726	3.419	1.2684
F	2	1.001	1.085	-
Cl	3	1.555	1.824	-
Br	4	1.739	2.112	0.5841
I	5	2.094	2.502	0.9130

[a] From Ref. 11.

[b] Principal quantum number.

transition, while the short wavelength part originates from the $^2D \leftarrow {}^2P$ transition. If this assignment is correct, the $^2S \leftarrow {}^2P$ transition (consisting of a single well-shaped band for both metals in argon and neon but exhibiting superpositions of bands in the heavier matrices) shows a matrix- and temperature behavior very similar to the closely related $^3P_1 \leftarrow {}^3P_0$ (7s ← 6p) transition of matrix-isolated Pb atoms, studied by Brewer and Chang.[4] After selecting arbitrarily the strongest observed band in the case of krypton and xenon, the matrix shifts were calculated for both Al and Ga in all matrices and compared with the shifts for Pb obtained by Brewer and Chang[4] (Table III-4). The matrix shifts are towards the blue and increase strongly from the heavy to the light rare gas matrices. Also in agreement with the observations by Brewer and Chang, the $^2S \leftarrow {}^2P$ bands for Al and Ga shifted reversibly to the red on warming in all matrices; for example, temperature increases of ~20° K resulted in shifts of -110 ±20 cm^{-1} for Ga in argon and -90 ±20 cm^{-1} in krypton. No significant shifts in the short wavelength part of the spectra were noted. If the temperature was increased above ~1/3 of the melting point of the rare gas matrices, irreversible loss of the UV spectra resulted, while new absorption bands appeared over the whole visible range, attributable to dimer and cluster formation.

The results in Table III-4 show that the matrix shifts for Al and Ga at 4.2° K are very similar and are significantly smaller than the corresponding shifts for Pb at 20° K. The close similarity of the p shell diameters (Table III-3) suggests that these three atoms occupy similar sites, and the observed matrix shifts reflect the expected strongly repulsive matrix-interaction of the excited states having the common characteristic feature of a single electron in an outer s orbit which substantially

Table III-4. Matrix-shifts for (n + 1)s ← np transitions.

Transition	Al[a] $4s(^2S) \leftarrow 3p(^2P_{1/2})$ (cm^{-1})	Ga[a] $5s(^2S) \leftarrow 4p(^2P_{1/2})$ (cm^{-1})	Pb[b] $6p7s(^3P_1) \leftarrow 6p^2(^3P_0)$ (cm^{-1})
in Xe	+ 1640	(+ 520, + 2090)	+ 2480
in Kr	+ 1820	+ 1860	+ 2970
in Ar	+ 4150	+ 4360	+ 5550
in Ne	+ 5900	+ 5740	

[a] This work, calculated from strongest band observed, at 4.2° K.

[b] Ref. 4, T = 20° K.

penetrates the valence shells of the rare gas cage. Furthermore the observed trends (largest repulsion in the lightest rare gases and red shift upon lattice expansion by warming) are in agreement with what would be expected from atoms occupying substitutional sites. In any case, the matrix and temperature dependence of these bands is quite different from the reported behavior of the np ← ns resonance transitions of atoms with an outermost s shell[1] mentioned in the introduction.

While the assignment of the $^2S \leftarrow {}^2P$ transition could be made with some confidence even in the more complicated cases, the high frequency part of the spectra exhibits considerable complexity. In principle, the ^2D state splitting pattern contains much more detailed information about the nature of the trapping site than the levels of ^2P or ^2S states of matrix-isolated atoms; in contrast to s and p orbitals, d orbitals are already split by the cubic component of the matrix field (Figure III-3) and behave differently under axial distortions of an octahedral site along the tetragonal or trigonal axes. However, because it is far from certain that all the observed peaks on the high energy side of the spectrum actually do belong to the $^2D \leftarrow {}^2P$-transitions, no attempt was made to analyze these bands in detail.

ESR Spectra

Aluminum atoms

A summary of the ESR results of Knight and Weltner[13] for matrix-isolated Al atoms, at that time ascribed to a molecular Al-X complex, is given in Table III-5. Figure III-4 shows the angular dependence of the ESR spectrum of Al in argon. The spectra and a discussion of their complex orientation and temperature behavior can be found in reference 13. In Table

Table III-5. ESR data for matrix-isolated Al atoms.[a]

Matrix	Site No.	g Tensor	A Tensor[b]	Linewidth (gauss)
Neon 4.2°K	1	$g_{\parallel}$ = 2.000(1)	$A_{\parallel}$ = +46.3(0.4)	∥: 6.5
		$g_{\perp}$ = 1.925(1)	$A_{\perp}$ = -35.3(0.4)	⊥: 6.5
		$\Delta g_{\parallel} = -0.002_3(1_0)$	$A_{\parallel}-A_{\perp}$ = 81.6(0.8)	
		$\Delta g_{\perp} = -0.077_3(1_0)$	A_{iso} = -8.1(0.1)	
	2	$g_{\parallel}$ = 2.000(1)	$A_{\parallel}$ = +46.3(0.4)	∥: 6.5
		$g_{\perp}$ = 1.927(1)	$A_{\perp}$ = -35.3(0.4)	⊥: 6.5
		$\Delta g_{\parallel} = 0.002_3(1_0)$	$A_{\parallel}-A_{\perp}$ = 81.6(0.8)	
		$\Delta g_{\perp} = -0.075_3(1_0)$	A_{iso} = -8.1(0.1)	
Argon 4.2°K	1	$g_{\parallel}$ = 2.000(1)	$A_{\parallel}$ = +47.7(0.4)	∥: 3.5
		$g_{\perp} = 1.951_5(1_0)$	$A_{\perp}$ = -34.0(0.4)	⊥: 3.5
		$\Delta g_{\parallel} = -0.002_3(1_0)$	$A_{\parallel}-A_{\perp}$ = 81.7(0.8)	
		$\Delta g_{\perp} = -0.050_8(1_0)$	$A_{iso} = -6.7_5(0.1_5)$	
	2	$g_{\parallel}$ = 2.000(1)	$A_{\parallel}$ = +47.7(0.4)	∥: 3.5
		$g_{\perp} = 1.956_5(1_0)$	$A_{\perp}$ = -33.7(0.4)	⊥: 3.5
		$\Delta g_{\parallel} = -0.002_3(1_0)$	$A_{\parallel}-A_{\perp}$ = 81.4(0.8)	
		$\Delta g_{\perp} = -0.045_8(1_0)$	$A_{iso} = -6.5_7(0.1_5)$	
Krypton 4.2°K	1	$g_{\parallel}$ = 2.001(1)	$A_{\parallel}$ = +45.3(0.7)	∥: 3.0
		$g_{\perp}$ = 1.989(1)	$A_{\perp}$ = -30.0(0.7)	⊥: 3.5
		$\Delta g_{\parallel} = -0.001_3(1_0)$	$A_{\parallel}-A_{\perp}$ = 75.3(1.4)	
		$\Delta g_{\perp} = -0.013_3(1_0)$	A_{iso} = -4.90(0.23)	
	2	$g_{\parallel}$ = 2.001(1)	$A_{\parallel}$ = +45.3(0.7)	∥: 3.0
		$g_{\perp}$ = ?	$A_{\perp}$ = ?	⊥: not observed
		$\Delta g_{\parallel} = -0.001_3(1_0)$	$A_{\parallel}-A_{\perp}$ = ?	
		$\Delta g_{\perp}$ = ?	A_{iso} = ?	
	3	$g_{\parallel}$ = 1.997(1)	$A_{\parallel}$ = +58.0(0.7)	∥: 2.0
		$g_{\perp}$ = 1.962(1)	$A_{\perp}$ = -25.3(0.7)	(krypton hfs of
		$\Delta g_{\parallel} = -0.005_3(1_0)$	$A_{\parallel}-A_{\perp}$ = 83.3(1.4)	~3.4 gauss obs.)
		$\Delta g_{\perp} = -0.040_3(1_0)$	A_{iso} = +2.47(0.23)	⊥: 7.0
Xenon 4.2°K	1	$g_{\parallel}$ = 2.001(2)	$A_{\parallel}$ = +46.7(1.0)	∥: 15.0
		$g_{\perp}$ = 2.02[c]	$\lvert A_{\perp}\rvert < 25$[c]	⊥ ~ 20[c]
		$\Delta g_{\parallel}$ = -0.001(2)	$A_{\parallel}-A_{\perp} < 72$[c]	
		$\Delta g_{\perp}$ = +0.02[c]	$A_{iso} \approx 0$[c]	

[a] From the data of Ref. 13 and private communication.

[b] ^{27}Al hfs tensor in units of 10^{-4} cm^{-1}; choice of signs, see text.

[c] Assignment uncertain, see Ref. 13.

Figure III-4. ESR spectra of aluminum atoms in an argon matrix at 4.2°K with the rod surface at an angle of 90° or 0° to the magnetic field direction (taken from reference 13).

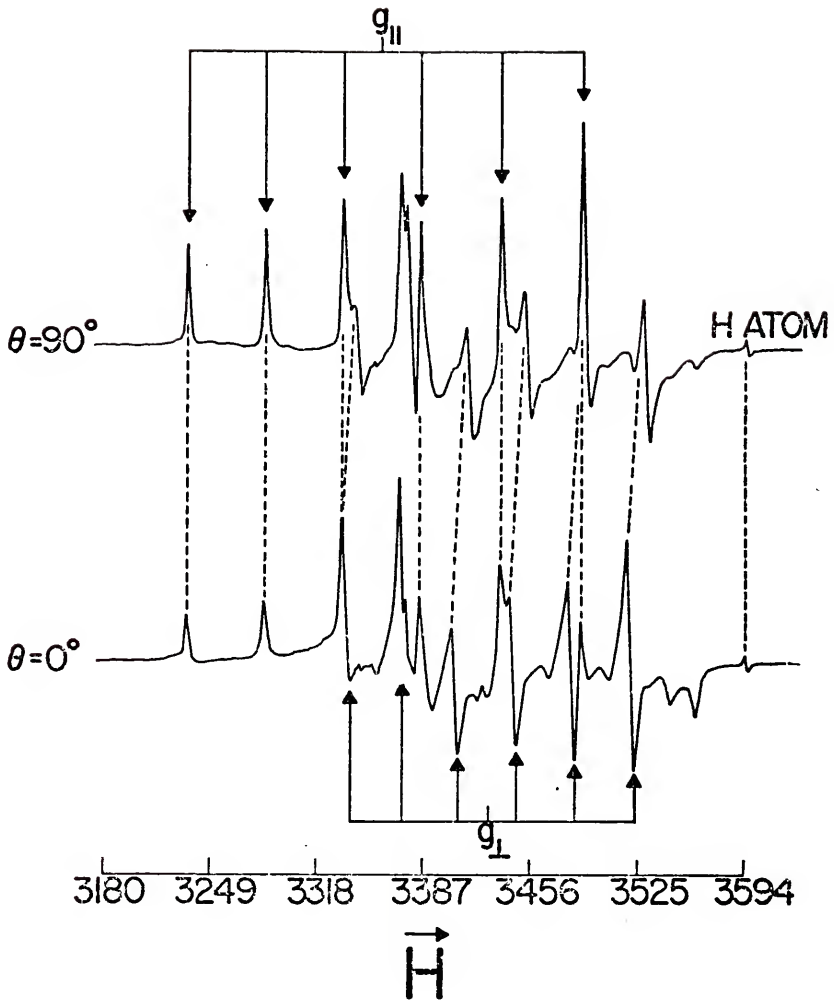
$g_{\parallel}$
θ=90°
H ATOM
θ=0°
$g_{\perp}$
3180 3249 3318 3387 3456 3525 3594
H

III-5 g values, ^{27}Al (I = 5/2) hyperfine values (with estimated uncertainties in parentheses) and linewidths are listed separately for all analyzed sites. For convenience, the g shifts $\Delta g = g - 2.0023$, the isotropic hyperfine coupling constants $A_{iso} = (A_{11} + 2A_{\perp})/3$, and the axial hyperfine anisotropies $A_{11} - A_{\perp}$ are also listed. The sign of $A_{\perp}$ has been chosen to be positive in reference 13; this choice, together with the observation that very diluted matrices gave strong aluminum atom UV absorption but no ESR signals, led the above authors to the conclusion that the magnetic parameters could not be satisfactorily ascribed to matrix-isolated Al atoms. If the sign of $A_{\perp}$ is chosen to be negative (Table III-5), the assignment of the hyperfine parameters is consistent for matrix-isolated Al atoms, a point to be discussed later. Further, the fact that unusually high metal concentrations are necessary for obtaining reasonable ESR spectra can be explained by the large linewidths.

The data for Al in Kr, site 3 in Table III-5, correspond to the spectrum referred to as Kr-AlX in reference 13. This spectrum is stable at low temperatures only and shows hyperfine structure in the parallel lines, attributable to the 11.55% natural abundance of ^{83}Kr with I = 9/2. Comparison of the observed pattern (such as shown in reference 13, Figure 11) with calculated intensity distributions for given numbers of equivalent interacting krypton atoms leads to the conclusion that 5 ±1 equivalent krypton atoms surrounding the Al impurity are compatible with the obtained spectrum.

Gallium atoms

Although attempts were made to study Ga atoms in all four rare gas matrices by ESR, complete data could be obtained only for argon and

and krypton. The magnetic parameters measured at 4.2° K are collected in Table III-6. Spectra of Ga atoms in the three heavier rare gas matrices are shown in Figures III-5, III-6 and III-7.

Natural gallium consists of 60.4% ^{69}Ga and 39.6% ^{71}Ga; both nuclei are magnetic with a spin of 3/2, the ratio of the magnetic moments being $\mu_{71}/\mu_{69} = 1.270$. The usual second order equations[13] for the ESR analysis reproduced the observed ^{69}Ga line positions in all matrices accurately. The interaction of the electric quadrupole moments of both Ga nuclei with the field gradient were found to be smaller than the experimental uncertainty, as expected from the known quadrupole coupling constant in the gas phase.[19]

As could be expected from a comparison of the atomic spin orbit ($\zeta_{np} = 74.9$ cm^{-1} for Al and 550.8 cm^{-1} for Ga) and hyperfine coupling constants,[19] the (negative) g shifts and the hyperfine values are both substantially larger for ^{69}Ga than for ^{27}Al. Table III-6 illustrates that the magnetic parameters are strongly matrix dependent, that there are different sites, and that the perpendicular lines are some seven times broader than the parallel ones. $g_\perp$ shows the strongest matrix dependence; the trends are the same for Al, i.e., the g values increase with atomic weight of the rare gas.

Annealing experiments (short warming of the matrix to temperatures corresponding roughly to 1/3 of the melting temperature followed by rapid recooling to 4.2° K) reduced the ESR linewidths substantially; however, they did not cause measurable changes in the values of the magnetic parameters, the intensity ratios of different sites or the effects of preferential orientation which will be discussed below.

Table III-6. ESR data for matrix-isolated Ga atoms[a]

Matrix	Site No.	g Tensor	A Tensor[b]	Linewidth[c] (gauss)
Argon 4.2°K	1	$g_{\parallel}$ = 1.9396(3)	$A_{\parallel}$ = 144.97(0.15)	$\parallel$: 1.5
		$g_{\perp}$ = 1.5805(10)	$A_{\perp}$ = -200.62(0.50)	$\perp$: 10
		$\Delta g_{\parallel}$ = -0.0627(3)	$A_{\parallel}-A_{\perp}$ = 345.59(0.65)	
		$\Delta g_{\perp}$ = -0.4218(10)	A_{iso} = - 85.42(0.20)	
Argon 4.2°K	2	$g_{\parallel}$ = 1.9456(3)	$A_{\parallel}$ = +144.13(0.15)	$\parallel$: 1.5
		$g_{\perp}$ = 1.6015(10)	$A_{\perp}$ = -198.02(0.50)	$\perp$: 10
		$\Delta g_{\parallel}$ = -0.0567(3)	$A_{\parallel}-A_{\perp}$ = 342.15(0.65)	
		$\Delta g_{\perp}$ = -0.4008(10)	A_{iso} = - 83.97(0.20)	
Krypton 4.2°K	1	$g_{\parallel}$ = 1.9522(6)	$A_{\parallel}$ = +131.85(0.30)	$\parallel$: 3.2
		$g_{\perp}$ = 1.6751(20)	$A_{\perp}$ = -180.79(0.90)	$\perp$: 22
		$\Delta g_{\parallel}$ = -0.0501(6)	$A_{\parallel}-A_{\perp}$ = 312.64(1.20)	
		$\Delta g_{\perp}$ = -0.3272(20)	A_{iso} = - 76.58(0.30)	
Krypton 4.2°K	2	$g_{\parallel}$ = 1.9602(6)	$A_{\parallel}$ = +130.86(0.30)	$\parallel$: 3.2
		$g_{\perp}$ = 1.7014(20)	$A_{\perp}$ = -177.03(0.90)	$\perp$: 22
		$\Delta g_{\parallel}$ = -0.0421(6)	$A_{\parallel}-A_{\perp}$ = 307.89(1.20)	
		$\Delta g_{\perp}$ = -0.3009(20)	A_{iso} = - 74.40(0.30)	
Xenon[d] 4.2°K	1	$g_{\parallel}$ = 1.968(3)	$A_{\parallel}$ = +114.0(2.0)	$\parallel$: 20
		$\Delta g_{\parallel}$ = - 0.034(3)		$\perp$: >> 20

[a] This work.

[b] ^{69}Ga hfs tensor in units of 10^{-4} cm^{-1}, choice of sign, see text.

[c] The tabulated values correspond to annealed matrices; linewidths of unannealed matrices are larger.

[d] No perpendicular lines observed, see text.

Argon and krypton matrices. Typical ESR spectra of Ga in Ar and Kr which were taken immediately after matrix deposition are shown in Figure III-5. Parallel and perpendicular lines originating from the two gallium isotopes are marked by arrows; the weak signals from hydrogen atoms, formyl radical and methyl radical, which are well known and could always be observed whenever the carbon cells were not carefully outgassed, are also indicated.

The effect of annealing on the ESR spectra was very similar in both matrices and can be seen by comparing Figure III-5 with Figure III-6. Figure III-6(a) shows the Ga:Ar spectrum of Figure III-5(a) after annealing; evidently the heat treatment of the matrices results in a substantial sharpening of the formerly very broad perpendicular lines but also in a significant loss of over-all intensity of the original spectrum and in a buildup of new signals around $g \approx 2.0$. These observations indicate that metal atoms which were not sufficiently well isolated from neighboring metal atoms or other impurities by the matrix underwent chemical reaction during the thermal treatment.

In both annealed and unannealed argon and krypton matrices two distinct spectra were found, both attributable to gallium in axially symmetric sites. When the sapphire rod holding the matrix was rotated in the magnetic field, the same puzzling orientation behavior was observed as for Al in argon.[13] Again the perpendicular lines of the predominant site (1 in Table III-6) are associated with the larger $|\Delta g_{\perp}|$ value and appear more strongly at $\theta = 90^{\circ}$ (flat sapphire rod surface perpendicular to the magnetic field. A comparison of the unannealed spectra of Ga:Ar at $\theta = 0^{\circ}$ is shown in Figure III-5(a); the shift of the perpendicular lines of site 2 relative to the corresponding lines of site 1 can be seen

easily. In the annealed spectrum at $\theta = 90^{o}$ the last ^{69}Ga hyperfine line of site 2 is barely visible and marked with an arrow in Figure III-6(a). At intermediate angles both sets of perpendicular lines show similar intensities. In contrast to the aluminum case, the two gallium sites could also be distinguished in the parallel lines because the Δg_{11} values are no longer close to zero. This is apparent already in Figure III-5(a) but can be seen much better in Figures III-6(b) and III-6(c) where the first parallel lines of each gallium isotope [at the low field end of Figure III-6(a)] are shown at an expanded scale for two different orientations. At $\theta = 90^{o}$ [Figure III-6(b)] the peaks of site 2 are hardly visible; at $\theta = 0^{o}$ [Figure III-6(c)] both sites show similar intensities.

As in the case of aluminum, the perpendicular lines of the gallium spectra were strongly temperature-dependent; negative $\Delta g_{\perp}$ shifts of over 10% and negative $A_{\perp}$ shifts of over 5% were measured for both sites in argon and krypton when the matrices were allowed to gradually warm. Corresponding shifts of the parallel lines were much smaller and therefore more difficult to measure accurately. No significant increase in linewidth or any other changes in the appearance of the two spectra were noticed during warming until rapid diffusion set in and the signals of both sites disappeared irreversibly at the same time. At this point the formerly colorless or light green matrices turned red-brown, almost certainly because of gallium cluster formation. In Table III-7 the total temperature shifts of the magnetic parameters (from 4.2^{o} K up to the point at which the last measurements could be taken) are listed. The pronounced differences in linewidth (Table III-6) at 4.2^{o} K seem to correlate with the differences in matrix and temperature-sensitivity of the parallel vs perpendicular lines. This together with the observation that the ESR

Figure III-5(a). ESR spectra of matrix-isolated gallium atoms in an argon matrix at 4.2°K prior to annealing.

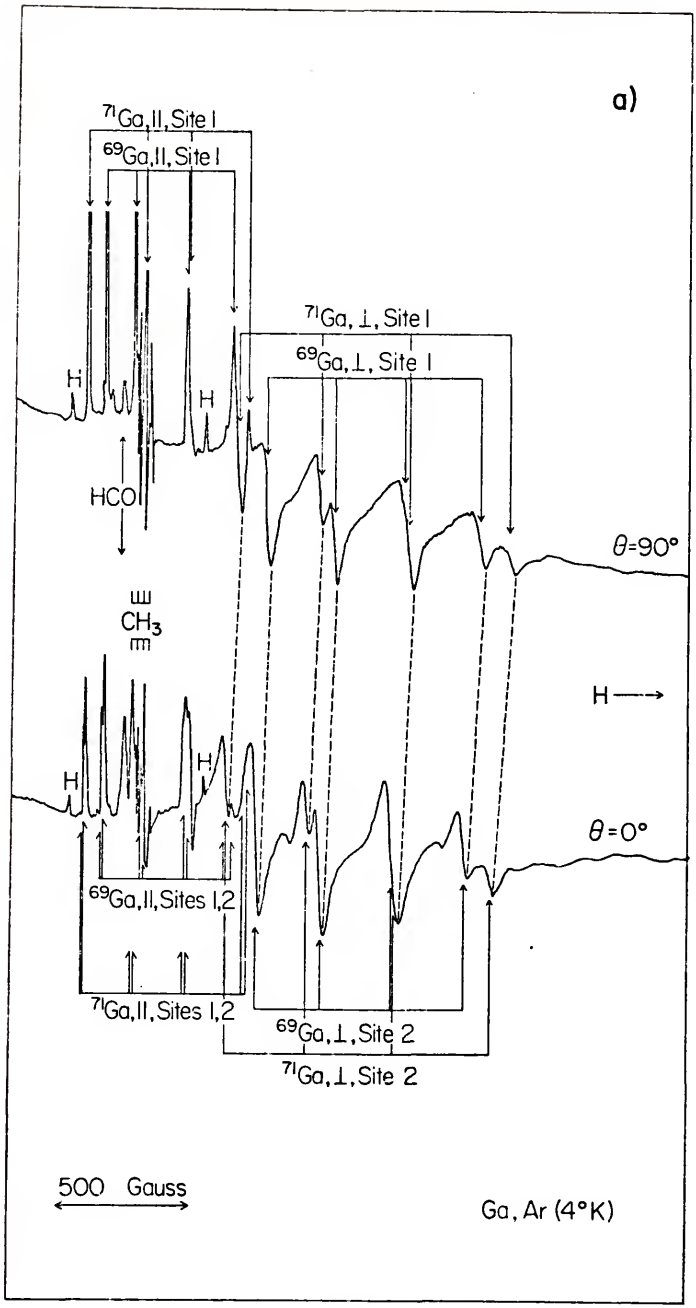
a)
^{71}Ga, II, Site I
^{69}Ga, II, Site I
^{71}Ga, ⊥, Site I
^{69}Ga, ⊥, Site I
H
H
HCO
θ=90°
CH$_3$
H ⟶
H
H
θ=0°
^{69}Ga, II, Sites 1,2
^{71}Ga, II, Sites 1,2
^{69}Ga, ⊥, Site 2
^{71}Ga, ⊥, Site 2
500 Gauss
Ga, Ar (4°K)

Figure III-5(b). ESR spectrum of matrix-isolated gallium atoms in a krypton matrix at 4.2°K prior to annealing.

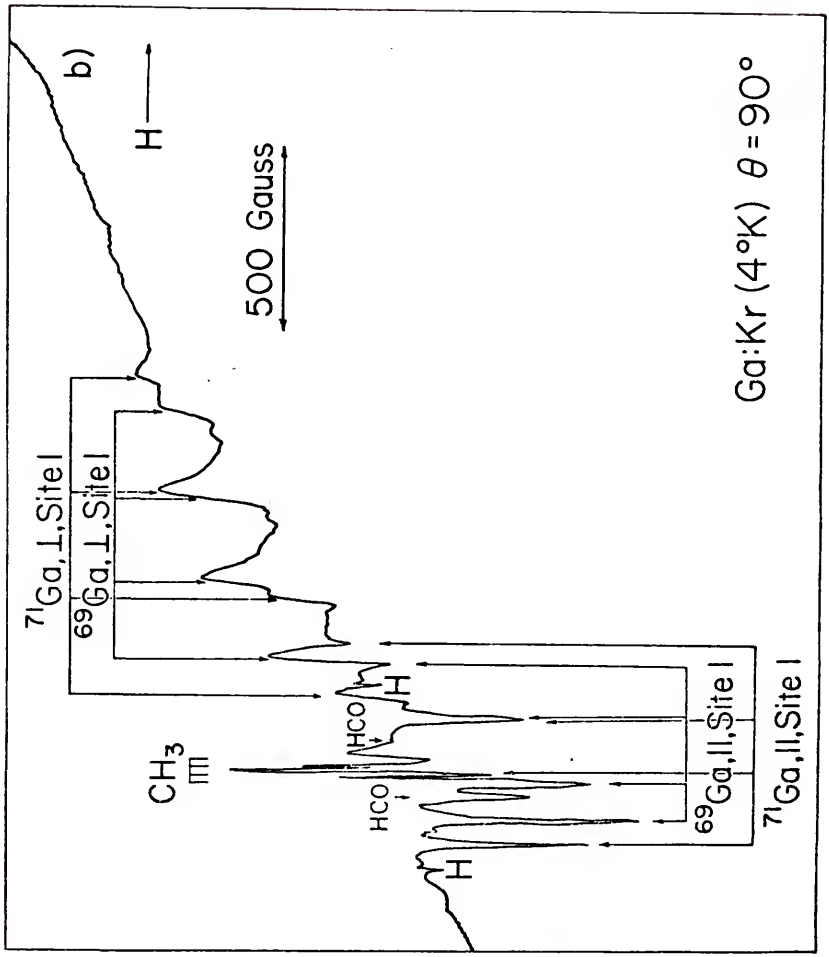
b)
H
500 Gauss
Ga:Kr (4°K) θ = 90°
^{71}Ga,⊥,Site I
^{69}Ga,⊥,Site I
CH$_3$
HCO
H
HCO
H
^{69}Ga,II,Site I
^{71}Ga,II,Site I

Figure III-6(a). ESR spectrum of matrix-isolated gallium atoms in argon at 4.2°K after annealing.

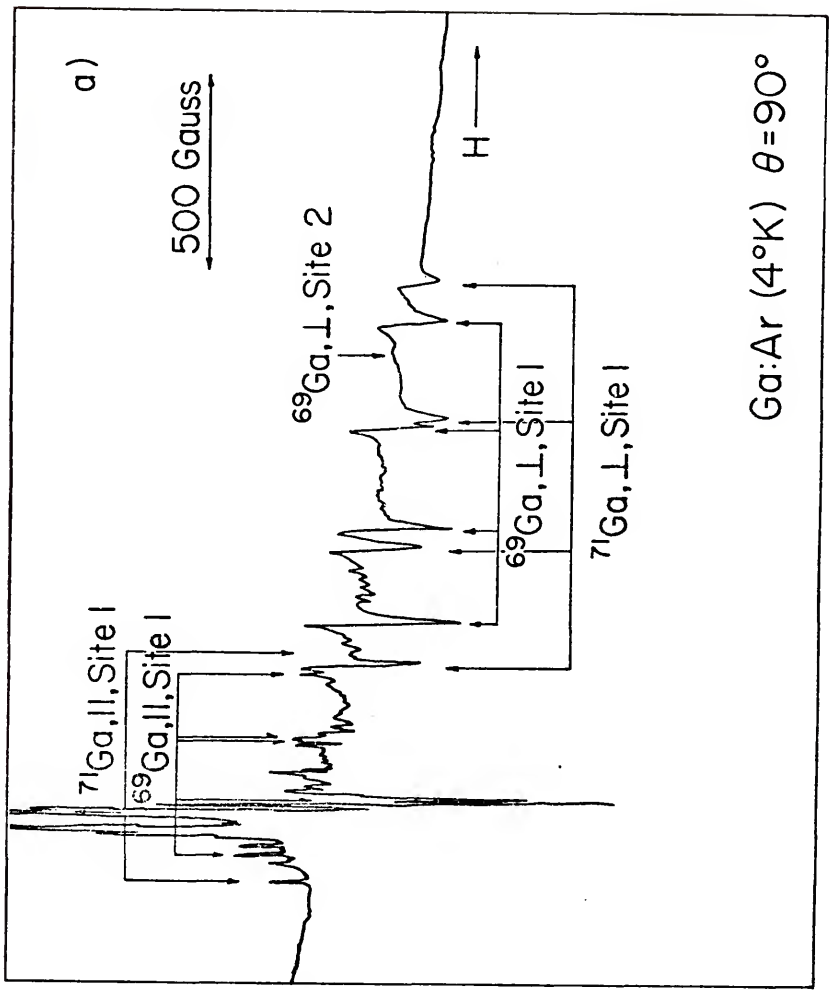
a)
500 Gauss
^{71}Ga,II,Site I
^{69}Ga,II,Site I
^{69}Ga,⊥,Site 2
^{69}Ga,⊥,Site I
^{71}Ga,⊥,Site I
H
Ga:Ar (4°K) θ=90°

Figure III-6(b). ESR spectrum of low field parallel lines of gallium in argon at 4.2°K after annealing. The rod surface is perpendicular to the magnetic field direction.

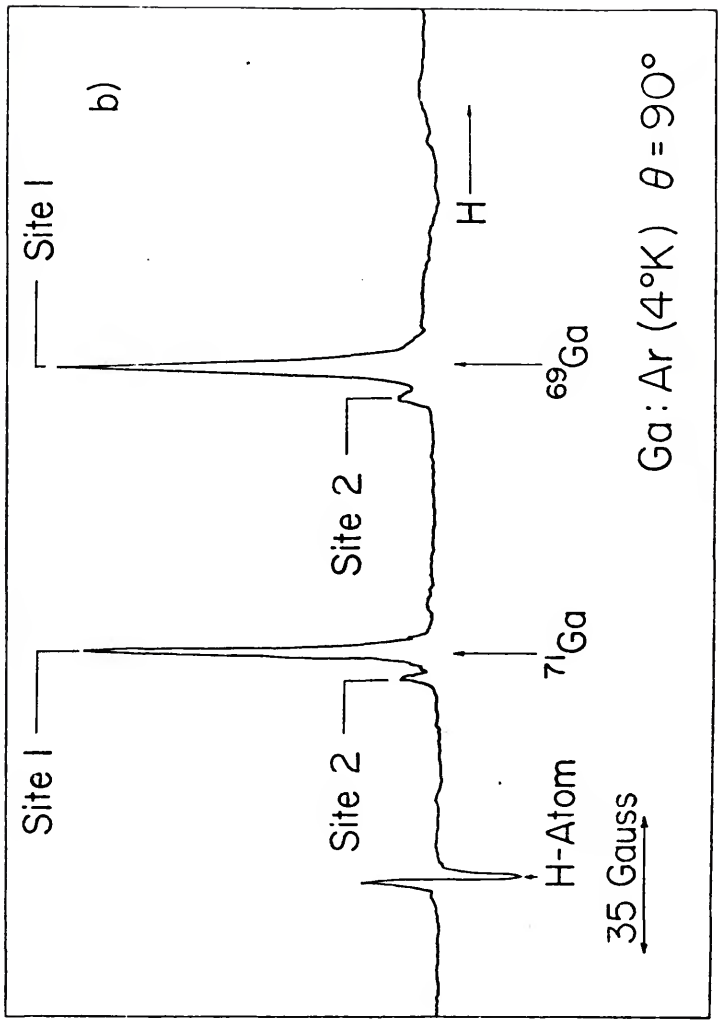
b)
Site I
Site I
Site 2
Site 2
H
^{69}Ga
^{71}Ga
H-Atom
35 Gauss
Ga:Ar (4°K) θ = 90°

Figure III-6(c). ESR spectrum of low field parallel lines of gallium in argon at 4.2°K after annealing. The rod is parallel to the magnetic field.

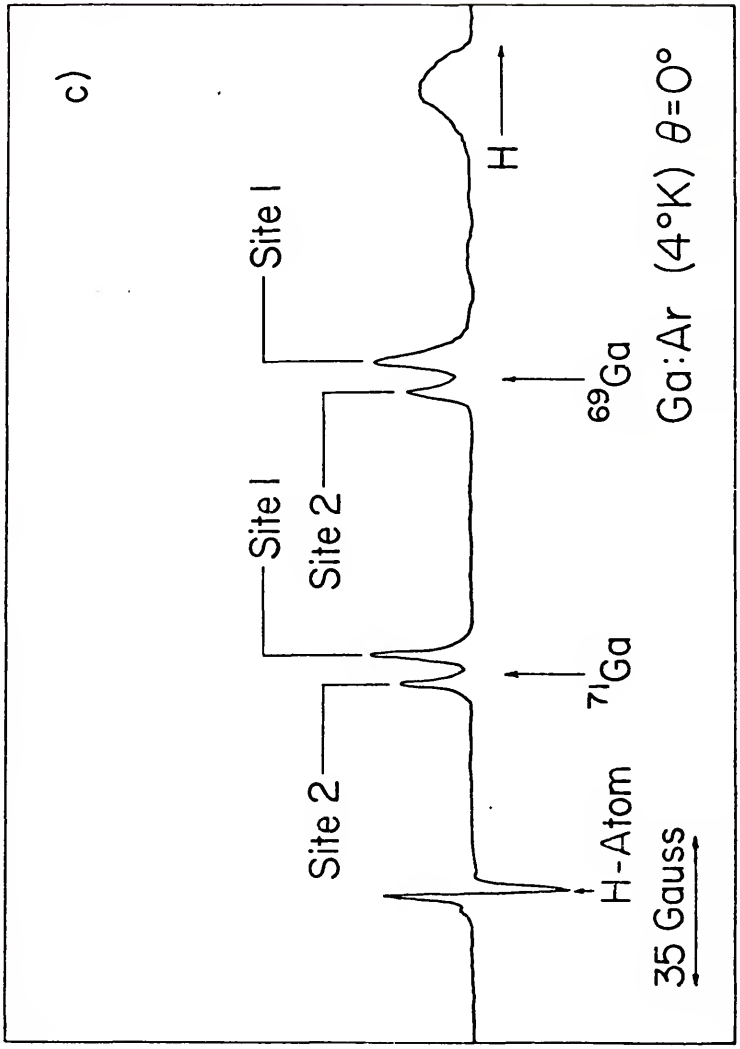
c)
Site 1
Site 1
Site 2
Site 2
H
^{69}Ga
^{71}Ga
H-Atom
35 Gauss
Ga:Ar (4°K) θ=0°

Table III-7. Temperature shifts of the magnetic parameters[a]

Atom	Matrix	Site No.[b]	$\delta g_{\parallel}$	$\delta g_{\perp}$	$\delta A_{\parallel}$[c]	$\delta A_{\perp}$[c]	T_{max}[d]
^{27}Al[e]	Ar	1	-0.000(1)	-0.0085(10)	+0.0(0.3)	-0.5(0.3)	25
		2	-0.000(1)	-0.0085(10)	+0.0(0.3)	-0.5(0.3)	± 10
^{69}Ga	Ar	1	-0.006(2)	-0.0506(15)	+5.2(2.0)	-11.4(1.0)	30
		2	-0.006(2)	-0.0455(30)	+4.6(2.0)	-10.0(2.0)	± 10
^{69}Ga	Kr	1	-0.005(2)	-0.0485(20)	+5.7(2.0)	-12.4(1.0)	40
		2	-0.005(2)	-0.0430(40)	+4.9(2.0)	-10.5(2.0)	± 10

[a] Total shifts of the magnetic constants from 4.2°K up to the temperature T_{max}, after which the atomic spectra disappeared irreversibly.

[b] Correspond to the site numbers in Tables III-5 and III-6.

[c] In units of 10^{-4} cm^{-1}.

[d] Estimate of the temperature, at which the tabulated data were measured, just before rapid loss of the ESR signals due to diffusion was noticed, in °K.

[e] From Ref. 13.

linewidths were almost independent of temperature indicates that the linewidths are determined by random lattice inhomogeneities and not by the spin-lattice relaxation time.

No conclusive evidence was found for a gallium spectrum analogous to Kr-AlX (Al in Kr, site 3 in Table III-5), although several weak additional ESR signals, possibly attributable to gallium atoms in a third site, appeared at higher fields in both krypton and argon matrices after annealing. All the 16 lines required for a complete ^{71}Ga-^{69}Ga spectrum could not be detected; either most of these lines were hidden under the more intense peaks of the dominant sites, or else this possible third site does not exhibit axial symmetry, causing a further decrease in resolution of the broad perpendicular lines. The possibility that the two axial sites analyzed by ESR constitute only a fraction of the total number of metal atoms in these matrices cannot be ruled out; in fact, the appearance of the optical spectra (Figures III-1 and III-2) does not suggest the presence of two dominant well-defined axially symmetric sites. Of course optical spectra can always contain additional contributions from diamagnetic impurities (such as dimers) which do not produce ESR signals at all.

Xenon matrix. The difficulties encountered earlier in the analysis of the ESR spectra of aluminum in xenon[13] reappeared in the present gallium investigation. Due to the excessive line widths (Figure III-7), no reliable assignment of the perpendicular lines was possible; however, the results for the parallel lines (Table III-6) left little doubt that the observed spectrum had to be attributed to matrix-isolated Ga atoms.

Figure III-7. ESR spectrum of gallium atoms in xenon at 4.2°K.

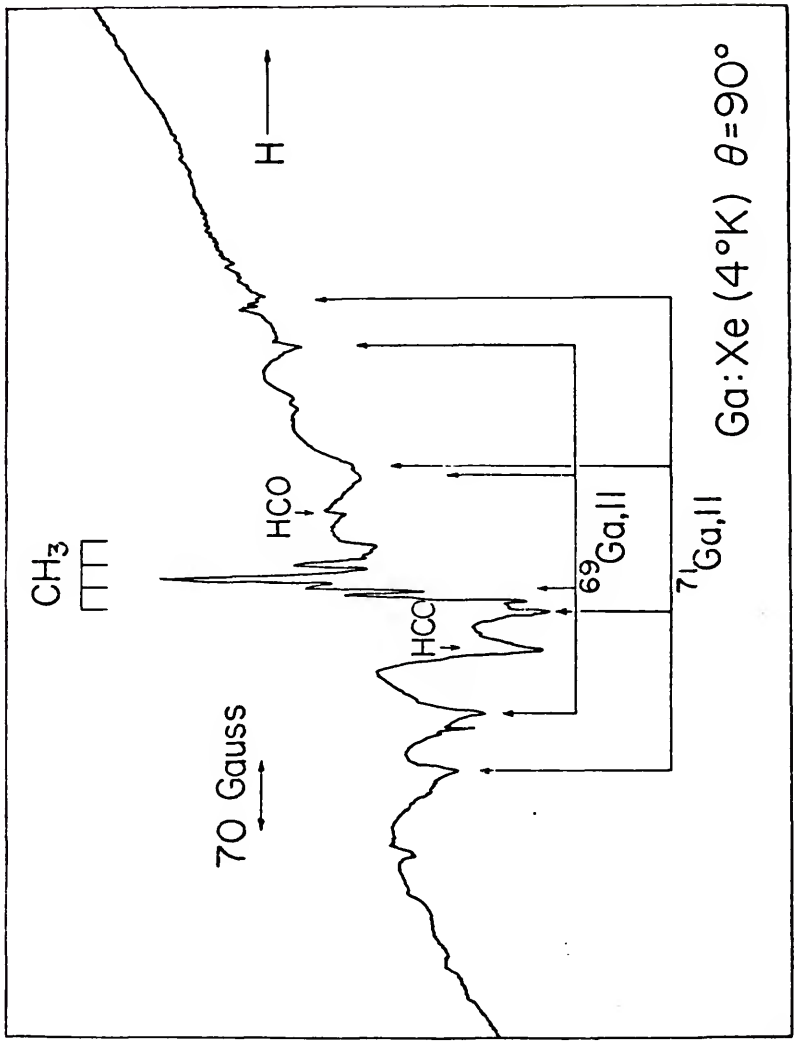
Ga:Xe (4°K) θ=90°
H
HCO
HCO
^{69}Ga,II
^{71}Ga,II
CH_3
70 Gauss

The large linewidths are probably caused by the combined effect of multiple sites and complex hyperfine interactions with a large number of inequivalent xenon nuclei.

Neon matrix. In contrast to the aluminum case, all attempts to obtain an ESR spectrum of gallium atoms isolated in a neon matrix failed. Although in concentrated matrices at least two different spectra exhibiting gallium hyperfine structure could be identified, none of them could be attributed to isolated Ga atoms. The fact that depositions performed under the same conditions as for the successful argon, krypton and xenon experiments invariably resulted in a dark red matrix indicates that recombination of metal atoms took place. On the other hand, more diluted colorless matrices (as used for the optical experiments) did not produce ESR signals of measurable intensity.

Discussion: The Crystal Field Model

The Group III metal atoms, characterized by a single unpaired electron in a p orbital outside closed shells, have a ^2P electronic ground state; spin-orbit coupling splits the spatially triply degenerate ground term, leaving the $^2P_{1/2}$ ground level $3\zeta_{np}/2$ lower in energy than the $^2P_{3/2}$ excited level (see Figure III-3). The g values of all the free gaseous Group III atoms in their Kramers degenerate $^2P_{1/2}$ ground level are approximately equal to 2/3.[19] From a $^2P_{1/2}$ atom isolated in a rare gas matrix, an isotropic ESR spectrum with a g value of ~2/3 could still be expected if the metal atom occupied a site of perfect octahedral symmetry, since cubic fields do not split ^2P states. In order to produce an ESR spectrum

with a pronounced axial anisotropy, as found for matrix-isolated Ga and Al in this work, noncubic matrix potentials must be operative which are at least of the same order of magnitude as the spin-orbit coupling energy, ζ_{np}.

The simplest way of trying to rationalize the observed ESR spectra is to assume that the matrix environment can be simulated by a static axial crystal field acting on the isolated $^2P_{1/2}$ atoms, leading to a partial quenching of the orbital angular momentum. This problem can be solved in analytical form using a procedure similar to the one used by Brailsford, Morton and Vannotti[20,21] in their ESR investigation of the $^2P_{3/2}$ impurity centers $^{17}O^-$ and $^{33}S^-$ in alkali halide crystals.

In the case of axial symmetry the crystal field can be expressed by a single parameter Δ, and the resulting expressions for the wavefunctions and the magnetic parameters of interest are determined completely by the ratio $x = \Delta/\zeta$. After choosing a convenient basis set, the wavefunctions and energies of the ^2P term can be determined from the operators $\mathcal{H}_{so}$ and $\mathcal{H}_{cf}$, the spin-orbit and crystal field Hamiltonians. $\mathcal{H}_{cf}$ can be factored into octahedral and tetragonal terms; as mentioned above, cubic fields do not remove the degeneracy of p orbitals thus

$$\mathcal{H}_{cf} = \mathcal{H}_{ax} . \tag{1}$$

The spin-orbit operator is defined as

$$\mathcal{H}_{so} = \zeta[L_z S_z + 1/2(L_+S_- + L_-S_+)] . \tag{2}$$

The effects of the general raising and lowering operators (I_+ and I_-) on the function u(I,m) are well known and are as shown:

$$I_+[u(I,m)] = [I(I+1) - m(m+1)]^{1/2}\, u(I,m+1)\ ,$$

$$I_-[u(I,m)] = [I(I+1) - m(m-1)]^{1/2}\, u(I,m-1).$$

$\mathcal{H}_{cf}$ and $\mathcal{H}_{so}$ can be applied to the following set of complex functions

$$\{\Phi_m{}^{\sigma}\} = \{\Phi_{-1}{}^{+},\ \Phi_o{}^{+},\ \Phi_1{}^{+};\ \Phi_{-1}{}^{-},\ \Phi_o{}^{-},\ \Phi_1{}^{-}\}$$

where σ (+,-) and m (-1,0,+1) denote the spin and orbital angular momentum quantum numbers along the crystal field axis. Following Wertz and Bolton,[22] the effect of a distortion of the crystal field along the z-axis is given by

$$\langle\Phi_o|\,\mathcal{H}_{ax}|\Phi_o\rangle = -\Delta\ ,$$

$$\langle\Phi_1|\,\mathcal{H}_{ax}|\Phi_1\rangle = \Delta/2\ ,\ \text{etc.}$$

The spin-orbit operator gives

$$\langle\Phi_o|\,\mathcal{H}_{so}|\Phi_o\rangle = 0\ ,$$

$$\langle\Phi_1{}^{\pm}|\,\mathcal{H}_{so}|\Phi_1{}^{\pm}\rangle = \pm\zeta/2\ ,\ \text{etc.}$$

The non-zero matrix elements of $\langle\Phi|\,\mathcal{H}_{so} + \mathcal{H}_{ax}|\Phi\rangle$ are given in Table III-8. The matrix can be factored into two 1 x 1 and two 2 x 2 matrices, each pair being equivalent. Solving the secular equations gives the energies:

$$E(^2\Sigma^+) = -1/4[\zeta + \Delta + 3(\zeta^2 + \Delta^2 - (2/3)\zeta\Delta)^{1/2}]\ ,$$

$$E(^2\Pi_{1/2}) = -1/4[\zeta + \Delta - 3(\zeta^2 + \Delta^2 - (2/3)\zeta\Delta)^{1/2}]\ , \qquad (3)$$

$$E(^2\Pi_{3/2}) = +1/2(\zeta + \Delta)$$

The matrix (Table III-8) shows that spin-orbit coupling mixes $\Phi_o{}^+$ and $\Phi_1{}^-$ and mixes $\Phi_o{}^-$ and $\Phi_{-1}{}^+$. The following Kramers doublets (each pair

Table III-8. Non-zero matrix elements of $\mathcal{H}_{so} + \mathcal{H}_{ax}$ applied to the six-dimensional complex basis.

	Φ_1^+	Φ_o^+	Φ_1^-	Φ_{-1}^+	Φ_o^-	Φ_{-1}^-
Φ_1^+	$\frac{\Delta}{2} + \frac{\zeta}{2}$					
Φ_o^+		$-\Delta$	$\frac{\zeta}{\sqrt{2}}$			
Φ_1^-		$\frac{\zeta}{\sqrt{2}}$	$\frac{\Delta}{2} - \frac{\zeta}{2}$			
Φ_{-1}^+				$\frac{\Delta}{2} - \frac{\zeta}{2}$	$\frac{\zeta}{\sqrt{2}}$	
Φ_o^-				$\frac{\zeta}{\sqrt{2}}$	$-\Delta$	
Φ_{-1}^-						$\frac{\Delta}{2} + \frac{\zeta}{2}$

degenerate in the absence of a static magnetic field) correspond to the above three energy levels:

$$\Psi^{\pm}(^2\Sigma^+) = a\Phi_o^{\pm} - b\Phi_{\pm 1}^{\mp} ,$$

$$\Psi(^2\Pi_{1/2}) = b\Phi_o^{\pm} + a\Phi_{\pm 1}^{\mp} , \tag{4}$$

$$\Psi(^2\Pi_{3/2}) = \Phi_{\pm 1}^{\pm} .$$

The coefficients of the wavefunctions (4) are given by

$$a = \{1 + 1/4[5 - 6x + 9x^2 + 3(1 - 3x)$$

$$(x^2 - 2/3x + 1)^{1/2}]\}^{-1/2} , \tag{5}$$

$$b = (1 - a^2)^{1/2} .$$

The energies in equation (3) are plotted against x in Figure III-8. For a $^2P_{1/2}$ atom, $^2\Sigma$ will lie at lowest energy for positive values of Δ ($^2\Pi_{1/2}$ will lie lowest for negative Δ). For $^2P_{3/2}$ atoms, this is inverted.

The g tensor can be calculated for $\Psi^{\pm}$ by the Zeeman operator

$$\mathcal{H}_z = 2[L_z + g_e S_z + 1/2(L_+ + L_- + g_e S_+ + g_e S_-)] ,$$

where $g_e = 2.0023$.

$$g_{11} = \langle \Psi^+(^2\Sigma) | \mathcal{H}_z | \Psi^+(^2\Sigma) \rangle$$

$$= g_e(1 - 2b^2) + 2b^2 \simeq 2 - 2b^2 ,$$

$$g_{\perp} = \langle \Psi^+(^2\Sigma) | \mathcal{H}_z | \Psi^-(^2\Sigma) \rangle \tag{6}$$

$$= g_e(1 - b^2) - 2\sqrt{2}ab \simeq 2 - 2b^2 - 2\sqrt{2}ab .$$

Figure III-8. Energy levels of an $(np)^1$ atom in an axial crystal field with $\Delta > 0$. Δ is the axial field parameter and ζ is the spin-orbit parameter. For an $(np)^5$ atom the diagram is inverted.

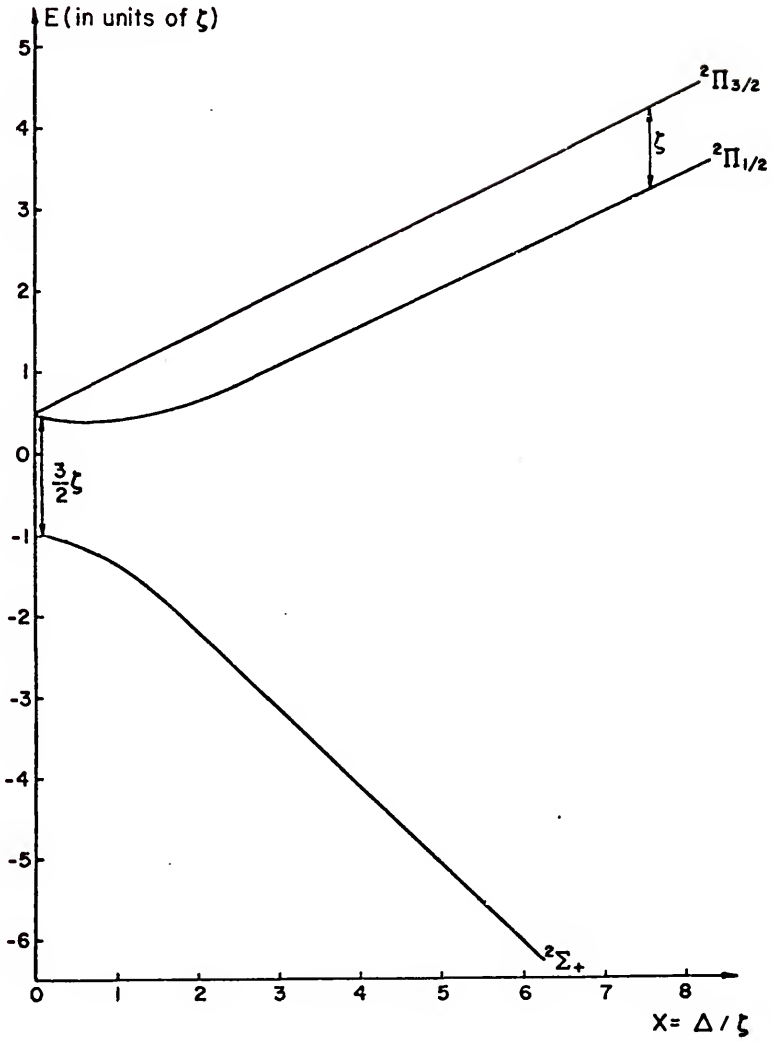
E (in units of ζ)
5
4
3
2
1
0
-1
-2
-3
-4
-5
-6
$^2\Pi_{3/2}$
$^2\Pi_{1/2}$
ζ
$\frac{3}{2}\zeta$
$^2\Sigma_+$
0
1
2
3
4
5
6
7
8
X= Δ / ζ

The g tensor for $\Psi^{\pm}(^2\Pi_{1/2})$ can be obtained by replacing a with b and b with a in equations (6). The dependence of the g values on the Δ/ζ ratio is shown in Figure III-9 for the $^2\Sigma$ and the $^2\Pi_{1/2}$ states.

The g tensor for the $^2\Pi_{3/2}$ state is independent of x and can be calculated using $\mathcal{H}_z$ to give

$$g_{11}(^2\Pi_{3/2}) = 2 + g_e \sim 4,$$

$$g_{\perp}(^2\Pi_{3/2}) = 0 \ . \qquad (7)$$

Because of its vanishing $g_{\perp}$ value, this state does not show an ESR spectrum, but the $^2\Pi_{3/2}$ state is not the most stable one for either sign of Δ. In the case of $\Delta > 0$ (dominant matrix repulsion perpendicular to the symmetry axis) the $^2\Sigma^+$ state is lowest; in the strong field limit ($\Delta \gg \zeta$, $b \to 0$) the unpaired electron is localized completely in $\Phi_o = -z \cdot f(r)$ (i.e., in the p_z orbital), and the g values approach the free spin value g_e (solid lines in Figure III-9). In the case of $\Delta < 0$ (dominant matrix repulsion along the symmetry axis) the $^2\Pi_{1/2}$ state is lowest; in the strong field limit the unpaired electron is confined completely to $\Phi_1 = \frac{1}{\sqrt{2}}(x + iy)f(r)$ (i.e., to a symmetric linear combination of the p_x and p_y orbitals), and the g values go towards zero asymptotically (dashed lines in Figure III-9).

In the case of atoms in $^2P_{3/2}$ ground states (np^5 systems such as the halogen atoms[3] or the chalcogenide anions[20,21] the energy diagram (Figure III-8) is inverted; $^2\Sigma^+$ is the ground level for negative Δ's (and $^2\Pi_{3/2}$ for positive Δ's). The dotted lines in Figure III-9 show the x dependence of the g values of the $^2\Sigma^+$ state; for the $^2\Pi_{3/2}$ state, again the expressions (7) are valid.

Figure III-9. g tensor of ^2P atoms in an axial crystal field. Solid line: $^2\Sigma$ ground state of a $^2P_{1/2}$ atom for $\Delta > 0$; dashed line: $^2\Pi_{1/2}$ ground state of a $^2P_{1/2}$ atom for $\Delta < 0$; dotted line: $^2\Sigma$ ground state of a $^2P_{3/2}$ atom for $\Delta < 0$. The experimental g values found for gallium are indicated by arrows and connected by solid lines.

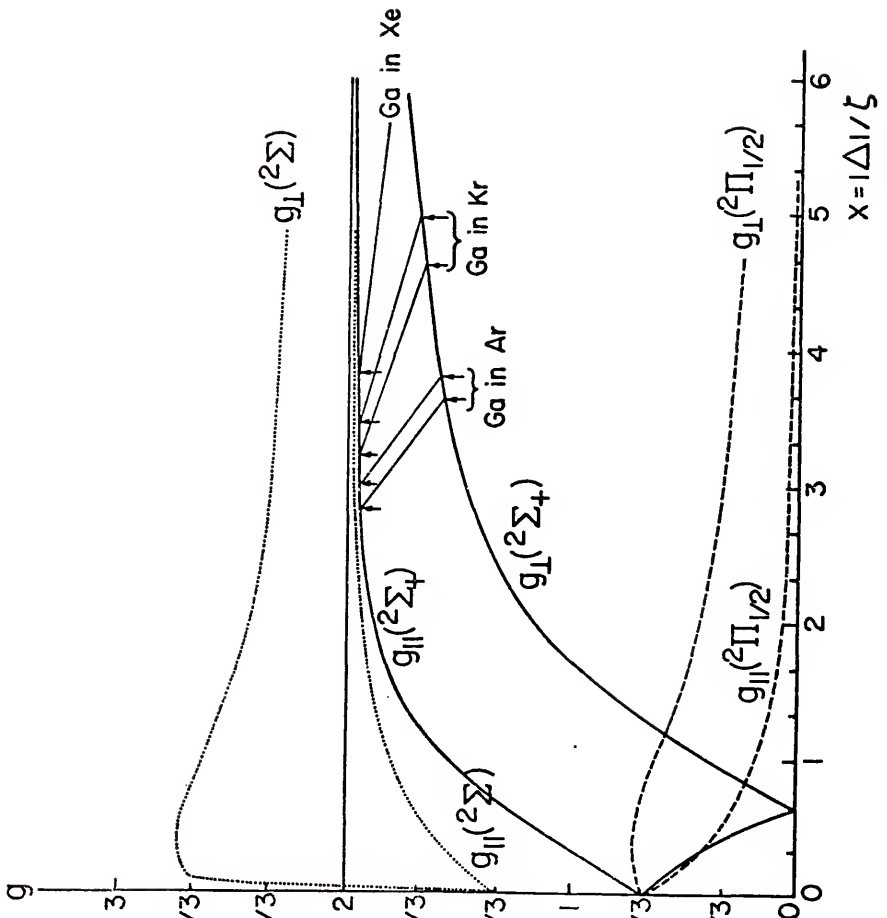
g
3
8/3
7/3
2
5/3
4/3
1
2/3
1/3
0
0
1
2
3
4
5
6
x=|Δ|/ζ
$g_\perp(^2\Sigma)$
$g_\perp(^2\Sigma_+)$
$g_{\parallel}(^2\Sigma_+)$
$g_{\parallel}(^2\Sigma)$
$g_\perp(^2\Pi_{1/2})$
$g_{\parallel}(^2\Pi_{1/2})$
Ga in Xe
Ga in Kr
Ga in Ar

In the strong field case ($\Delta >> \zeta$) only the $^2\Sigma$ states have a chance of being detectable by ESR; the $^2\Pi_{1/2}$ states have very small transition probabilities and require very high magnetic fields. $^2\Sigma$ ground states are formed in matrix sites which stabilize the p_z orbital relative to the p_x and p_y orbitals in the case of $^2P_{1/2}$ atoms; the opposite is true for $^2P_{3/2}$ atoms, where a stabilization of the inplane p orbitals relative to the p_z orbital is necessary. The crystal field parameter Δ can be calculated from the g values of the trapped metal atoms; in fact the problem is overdetermined, as both g values depend on one single parameter b only. In principle b can be calculated from either g_{11} or $g_{\perp}$; x in turn can be obtained from b and $a = (1 - b^2)^{1/2}$ from the following equations:

$$x = (\Delta/\zeta) = 4/3\ C^{-1} - C/6 + 1/3,$$
$$C = 2\sqrt{2}\ (b/a)\ . \tag{8}$$

Δ then follows from x and the known atomic ζ_{np} parameter mentioned earlier in the text.

In the case of Al the b^2 terms in equations (6) are smaller than the experimental uncertainty; $\Delta g_{11} \simeq 0$, and therefore the first of equations (6) cannot be used as a consistency check for the crystal field model. To a very close approximation

$$C = 2\sqrt{2}\ b = -\Delta g_{\perp}\ . \tag{9}$$

Substituting this expression for C into the first of equations (8) and realizing that the second and third terms on the right-hand side are negligible compared to the first term gives the following approximation:

$$\Delta g_{\perp} = -4/3x = -(4\zeta)/(3\Delta)\ . \tag{10}$$

The results of the Al crystal field analysis (equation 10) are given in Table III-9 as calculated from $\Delta g_{\perp}$ and $\zeta_{3p}(Al)$.

As could have been expected, the calculated Δ values increase with increasing matrix polarizability, but the numerical results for the heavier rare gases seem excessively high. The Δ value for site 2 in krypton corresponds to a p-orbital splitting energy

$$\Delta E_p = E(p_x, p_y) - E(p_z) = (3/2)\Delta ,$$

of more than 10,000 wavenumbers, and the positive $\Delta g_{\perp}$ value of Al in xenon, if correct, cannot be explained by the crystal field model at all. Furthermore the g tensor of site 3 in krypton (Kr - AlX) is not compatible with equations (6); b calculated from Δg_{11} is more than three times larger than if calculated from $\Delta g_{\perp}$.

The situation is quite different in the case of the gallium atoms. Due to the larger spin-orbit coupling constant of Ga ($\zeta_{Ga}/\zeta_{Al} = 7.35$) the second order terms are no longer negligible, and the Δg_{11} values are large enough to permit an accurate experimental determination. This implies that the consistency of the crystal field model can be checked by means of equations (6). In Table III-10 the x and Δ values, calculated from both g_{11} and $g_{\perp}$ via equations (6) and (8) are listed and compared in the last column.

The results show that the Δ values calculated from $g_{\perp}$ are substantially larger than if calculated from g_{11}, as was the case for Al in Kr, site 3. The discrepancy is largest for the heaviest rare gases. In Figure III-9 the experimental values for g_{11} and $g_{\perp}$ are marked by arrows and connected by solid lines. If the measured g_{11} and $g_{\perp}$ were compatible with the crystal field equations (6), these connecting lines would be

Table III-9 Crystal field analysis of the ESR data of matrix-isolated ^{27}Al atoms.[a]

Matrix	Site No.[b]	$x = \Delta/\zeta$[c]	$\Delta(10^3\ cm^{-1})$
Neon	1	17.6(0.2)	1.32
Neon	2	18.0(0.2)	1.35
Argon	1	26.6(0.5)	1.99
Argon	2	29.4(0.5)	2.20
Krypton	1	100.6(7.0)	7.54
Krypton	2	--	--
Krypton	3[d]	33.1(0.7)	2.48
Xenon	1	∞	∞

[a] Used $\zeta = 74.93\ cm^{-1}$ (from Ref. 17).

[b] Correspond to site numbers in Table III-5.

[c] Calculated from $\Delta g_{\perp}$.

[d] If x and Δ are calculated from $\Delta g_{\parallel}$, x = 9.37 and $\Delta = 700\ cm^{-1}$

Table III-10. Crystal field analysis of the g values of matrix-isolated gallium atoms.

Matrix	Site no.[a]	$x_{\parallel}$[b]	$\Delta_{\parallel}$ (10^3 cm^{-1})[c]	$x_{\perp}$[d]	$\Delta_{\perp}$ (10^3 cm^{-1})[e]	$\Delta_{\perp} / \Delta_{\parallel}$
Argon	1	2.869(14)	1.580	3.669(10)	2.021	1.279
Argon	2	3.008(15)	1.657	3.842(10)	2.116	1.277
Krypton	1	3.199(40)	1.762	4.616(25)	2.542	1.443
Krypton	2	3.479(45)	1.916	4.982(25)	2.744	1.432
Xenon	1	3.85(35)	2.12	6.27[f]	3.46[f]	1.63[f]

[a] Correspond to site numbers in Table III-6.

[b] $x = \Delta/\zeta$ calculated from $g_{\parallel}$.

[c] Δ calculated from $x_{\parallel}$ using $\zeta = 550.8$ cm^{-1}.

[d] $x = \Delta/\zeta$ calculated from $g_{\perp}$.

[e] Δ calculated from $x_{\perp}$ using $\zeta = 550.8$ cm^{-1}.

[f] Extrapolated values.

vertical. The gallium Δ values calculated from $\Delta g_{\perp}$ are very similar to the corresponding numbers for aluminum. This is an additional piece of evidence for the hypothesis stated earlier that these two strikingly similar atoms occupy almost identical matrix sites. The differences in the ESR spectra seem to originate almost exclusively from the differences in the atomic fine-structure and hf constants.

In the paper[13] on Al-X, $A_{\perp}$ was assigned to be positive and the calculated values of $A_{dip} = (A_{11} - A_{\perp})/3$ (see reference 23) were found to be very small, around 5×10^{-4} cm^{-1}, in comparison to $A_{dip} \simeq 26 \times 10^{-4}$ cm^{-1} for the free aluminum atom.[24] This would indicate a drastic reduction of $\langle r^{-3} \rangle_{3p}$ and for this reason the authors believed the species under examination could not be the free Al atom. In this work the assignment of $A_{\perp}$ to be negative gives values of $A_{dip} \simeq 27 \times 10^{-4}$ cm^{-1}, close to that of the free atom, and the values obtained change only slightly with the rare gas matrix (see Table III-5). Thus the negative sign of $A_{\perp}$ is consistent with matrix-isolated Al atoms.

The free Al atom[25] has $A_{iso} = 915 \times 10^{-4}$ cm^{-1}. The values for matrix-isolated Al ($A_{iso} \simeq -8 \times 10^{-4}$ cm^{-1}) indicates an extremely small s contribution to the odd-electron wavefunction. The fact that A_{iso} is negative can be explained in terms of spin polarization;[26] the unpaired electron causes a slight unpairing of the core electrons. This effect can be explained by the Pauli principle whereby the unpaired electron can be considered to attract electrons of the same spin and repel those of opposite spin. The spin density at the nucleus can be from either α or β spin depending upon the radial distribution functions of the electrons: if an s orbital lies outside of the unpaired electron (of β spin), the α electron will be repelled away from the nucleus leaving net electron

density due to β spin; if the unpaired electron lies mainly outside of an s orbital, the α electron will be directed toward the nucleus with a subsequent increase in α spin density. The sign of A_{iso} depends upon the net spin density at the nucleus (either net α or net β spin).

The same general trends of A_{iso} and A_{dip} described above for aluminum also hold for gallium atoms (Table III-6).

Conclusions

This investigation of Group III metal atoms constitutes the first successful ESR analysis of matrix-isolated atoms in an orbitally degenerate ground state. The ESR spectra of aluminum atoms in all four rare gas matrices had been observed previously in this laboratory by Knight, Easley and Weltner,[12,13] and had been ascribed first to the AlO molecule[12] and later to a molecular complex, Al-X.[13] The ESR spectra of the two different metal atoms showed extremely similar behavior, as did their ultraviolet spectra. In all matrices permitting sufficient resolution, spectra from two closely related, partially oriented, axially symmetric sites exhibiting the same matrix and temperature dependence were found. The two g values $g_{||}$ and $g_{\perp}$ have been analyzed in terms of a crystal field model. This simple crystal field treatment demonstrated that the basic features of the observed spectra can be understood if the matrix environment is approximated by an axial electrostatic field Δ acting on the single unpaired p electron of the isolated metal atom, characterized by its spin-orbit parameter ζ_{np}. In this approximation the magnetic parameters depend only on the spin-orbit and hf constants of the free atom and the single matrix parameter Δ. The analysis showed that the main difference between aluminum and gallium spectra could be explained

solely by the differences in the atomic constants and that Δ increased strongly in the series Ne < Ar < Kr < Xe. The p-orbital splitting energies are very similar for Al and Ga in the same matrices. However these energies, calculated from $\Delta g_{\perp}$, tend to reach unphysically high values in the case of the heavier rare gas matrices, especially for aluminum. The $g_{\perp}$ value (greater than 2.0023) for Al in Xe cannot be understood from this model. The proximity of the experimental g values to free spin for both metals indicates that the unpaired electron occupies an almost unperturbed p_z orbital. Thus the orbital angular momentum of the corresponding free $^2P_{1/2}$ atoms is strongly quenched in the matrix.

Optical absorption studies allowed reliable assignment of the $^2S \leftarrow {}^2P$ transition. The frequency shift to the blue of the gaseous line which increases from Xe to Ne is consistent with orbital expansion in going from np to (n + 1) s. Lattice expansion at higher temperatures would account for the (reversible) red shift upon warming the matrix. Likewise, warming would decrease the observed g values as predicted by the model.

It has been noted that the values of Δ calculated from Δg_{11} and $\Delta g_{\perp}$ (from the Ga data) differ somewhat. Inspection of equations (6) gives evidence toward the origin of the inconsistency of the observed g values with the crystal field model. In the relation

$$\Delta g_{11} = -2g_e b^2 + 2b^2$$

the sign of the orbital angular momentum matrix element ($+2b^2$) is positive and opposes the sign of the dominant spin matrix element ($-2g_e b^2$), whereas in the expression

$$\Delta g_{\perp} = -g_e b^2 - 2\sqrt{2}ab$$

both signs are negative. The fact that the reduction of either one or both of the orbital angular momentum matrix elements in these equations would improve the agreement with experiment suggests that in addition to the quenching effect of the crystal field (by splitting of the orbital degeneracy) some mechanism leading to a reduction of the orbital angular momentum around the metal nuclei must be operative. The present situation is somewhat related to the well-known case of transition metal ions in ionic lattices, where the simple field picture also leads to an overestimate of the g shifts, and where (i) the quenching effect of the orbital angular momentum and (ii) the effect of ligand spin-orbit coupling from the small covalent ligand valence orbital admixtures into the free metal ion wavefunction have to be taken into account.[27] The theories of Adrian[28] and Smith[29] demonstrate that the matrix shifts of the g values of S-state atoms originate from the matrix-atom orbital admixtures into the impurity center wavefunction (resulting from the process of orthogonalizing the impurity wavefunction to the wavefunction of the matrix environment). As has been pointed out by Baylis[30] in a paper dealing with semiempirical calculations on alkali-rare gas complexes, the p^1 electron configuration is well suited for the formation of strong van der Waals complexes with the rare gas atoms. Thus a refined model would require orthogonalization of the metal p orbitals to the valence orbitals of the surrounding rare gas atoms.[31]

A few points remain unexplained in this work. One is the origin of the two different sites observed for Al and Ga in some of the matrices. Second, discussed below, is the lack of ESR spectra from either boron

atoms or indium atoms or from gallium in neon.

No signals for B atoms were detected in the ESR investigation of BC by Easley and Weltner[32] though substantial concentrations of B atoms must have been produced in this experiment. Using experimental conditions which gave strong ESR signals for Al and Ga in Ar and Kr failed to give ESR signals for In in these matrices. The large spin-orbit coupling constant (ζ_{np} = 1608 cm^{-1}) of In would resist the quenching effect of the rare gas crystal potential. As shown in Figure III-9, the g values are very sensitive to small changes in the axial field in the vicinity of the free atom limit. Slight perturbations, present as lattice inhomogeneities, could cause severe broadening of the signals to the point where they would no longer be recognizable. B, with smaller atomic radius (Table III-3), may occupy a matrix site in which no tetragonal distortion occurs. Again the free atom case would apply.

References

1. For a recent review of optical work see Meyer, B., Science 168, 783 (1970) or Meyer, B., Low Temperature Spectroscopy, American Elsevier, New York, 1971.

2. McCarty, M., and Robinson, G. W., Mol. Phys. 2, 415 (1959).

3. Jen, C. K., Foner, S. N., Cochran, E. L., and Bowers, V. A., Phys. Rev. 112, 1169 (1958); J. Chem. Phys. 32, 963 (1959).

4. Brewer, L., and Chang, C. A., J. Chem. Phys. 56, 1728 (1972).

5. Jen, C. K., Bowers, V. A., Cochran, E. L., and Foner, S. N., Phys. Rev. 126, 1749 (1962).

6. Goldsborough, J. P., and Koehler, T. R., Phys. Rev. 133, A135 (1964).

7. Jackel, G. S., Nelson, W. H., and Gordy, W., Phys. Rev. 176, 453 (1968).

8. Kasai, P. H., and McLeod, P., Jr., J. Chem. Phys. 55, 1566 (1971).

9. Kasai, P. H., Phys. Rev. Lett. 21, 67 (1968).

10. Clementi, E., IBM J. Res. Suppl. 9, 2 (1965).

11. Froese-Fischer, C., Tabulation of Hartree-Foch Results, University of British Columbia, 1968 (unpublished).

12. Knight, L. B., Jr., Easley, W. C., and Weltner, W., Jr., J. Chem. Phys. 52, 1607 (1970).

13. Knight, L. B., Jr., and Weltner, W., Jr., J. Chem. Phys. 55, 5066 (1971).

14. Kasai, P. H., Whipple, E. B., and Weltner, W., Jr., J. Chem. Phys. 44, 2581 (1966).

15. Easley, W. C., and Weltner, W., Jr., J. Chem. Phys. 52, 197 (1970).

16. Knight, L. B., Jr., Ph.D. dissertation, 1970.

17. Moore, C. E., Circ. U. S. Natl. Bur. Stand. 467, 1 (1949).

18. Corliss, C. H., and Bozman, W. R., Monogr. U. S. Natl. Bur. Stand. 53, XXX (1962).

19. Kopfermann, H., Nuclear Moments, Academic, New York, 1958.

20. Vannotti, L. E., and Morton, J. R., Phys. Rev. 174, 448 (1968).

21. Brailsford, J. R., Morton, J. R., and Vannotti, L. E., J. Chem. Phys. 49, 2237 (1968).

22. Wertz, J. E., and Bolton, J. R., Electron Spin Resonance: Elementary Theory and Practical Applications, p. 270. McGraw-Hill, New York, 1972.

23. A_{iso} is proportional to the spin density at the nucleus; A_{dip} is proportional to $\langle r^{-3} \rangle_{np}$.

24. Ammeter, J. H., private communication.

25. Ayscough, P. B., Electron Spin Resonance in Chemistry, p. 438. Methuen, London, 1967.

26. Abragam, A., and Bleaney, B., Electron Paramagnetic Resonance of Transition Ions, chapter 17. Clarendon, Oxford, 1970.

27. Misetich, A. A., and Watson, R E., Phys. Rev. 143, 335 (1966).

28. Adrian, F. J., J. Chem. Phys. 32, 972 (1960).

29. Smith, D. Y., Phys. Rev. 131, 2056 (1963); Phys. Rev. 133, A1087 (1964).

30. Baylis, W. E., J. Chem. Phys. 51, 2665 (1969).

31. Ammeter, J. H., and Schlosnagle, D. C., J. Chem. Phys. 59, 4784 (1973).

32. Easley, W. C., and Weltner, W., Jr., J. Chem. Phys. 52, 1489 (1970).

BIOGRAPHICAL SKETCH

David Carl Schlosnagle was born May 22, 1948, in Rochester, Minnesota and is the son of Mr. and Mrs. Marvin V. Schlosnagle. He was graduated from John Marshall High School in Rochester, Minnesota in June of 1966. He received the Associate of Arts from Rochester State Junior College in June of 1968 and the Bachelor of Arts in chemistry, magna cum laude, from Augsburg College in May of 1970. He worked as a graduate research assistant at the University of Florida from June of 1970 to December of 1974. He is married to the former Sara Ann Davidson.

I certify that I have read this study and that in my opinion it conforms to acceptable standards of scholarly presentation and is fully adequate in scope and quality, as a dissertation for the degree of Doctor of Philosophy.

W. Weltner, Jr., Chairman
Professor of Chemistry

I certify that I have read this study and that in my opinion it conforms to acceptable standards of scholarly presentation and is fully adequate, in scope and quality, as a dissertation for the degree of Doctor of Philosophy.

W. S. Brey
Professor of Chemistry

I certify that I have read this study and that in my opinion it conforms to acceptable standards of scholarly presentation and is fully adequate, in scope and quality, as a dissertation for the degree of Doctor of Philosophy.

W. B. Person
Professor of Chemistry

I certify that I have read this study and that in my opinion it conforms to acceptable standards of scholarly presentation and is fully adequate, in scope and quality, as a dissertation for the degree of Doctor of Philosophy.

R. C. Stoufer
Associate Professor of Chemistry

I certify that I have read this study and that in my opinion it conforms to acceptable standards of scholarly presentation and is fully adequate, in scope and quality, as a dissertation for the degree of Doctor of Philosophy.

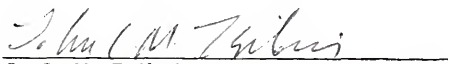

J. C. M. Tsibris
Assistant Professor of Biochemistry

This dissertation was submitted to the Department of Chemistry in the College of Arts and Sciences and to the Graduate Council, and was accepted as partial fulfillment of the requirements for the degree of Doctor of Philosophy.

December, 1975

Dean, Graduate School

UNIVERSITY OF FLORIDA
3 1262 08553 0276